Supporting information for

Surfactant-free colloidal syntheses of gold-based nanomaterials in alkaline water and mono-alcohol mixtures

Jonathan Quinson,[a,b,*] Olivia Aalling-Frederiksen,[a] Waynah L. Dacayan,[c] Joachim D. Bjerregaard,[a] Kim D. Jensen,[a] Mads R. V. Jørgensen,[d,e] Innokenty Kantor,[e,f] Daniel R. Sørensen,[d,e] Luise Theil Kuhn,[c] Matthew S. Johnson,[a] María Escudero-Escribano,[a,g,h] Søren B. Simonsen,[c] Kirsten M. Ø. Jensen[a,*]

a) Department of Chemistry, Copenhagen University, Universitetsparken 5, DK-2100 Copenhagen Ø, Denmark
b) Biochemical and Chemical Engineering Department, Aarhus University, Åbogade 40, DK-8200 Aarhus, Denmark
c) Department of Energy Conversion and Storage, Technical University of Denmark, Fysikvej Bldg. 310, DK-2800 Kgs. Lyngby, Denmark
d) Department of Chemistry & iNANO, Aarhus University, Langelandsgade 140, DK-8000 Aarhus C, Denmark
e) MAX IV Laboratory, Lund University, Fotongatan 2, SE-224 84 Lund, Sweden
f) Department of Physics, The Technical University of Denmark, Fysikvej Bldg. 311, DK-2800 Kgs. Lyngby, Denmark
g) Catalan Institute of Nanoscience and Nanotechnology (ICN2), CSIC and BIST, UAB Campus, 08193 Bellaterra, Barcelona, Spain
h) ICREA, Passeig de Lluís Companys, 23, 08010 Barcelona, Spain

Corresponding authors: jquinson@bce.au.dk, kirsten@chem.ku.dk

Note to the reader:

The proposed *Supporting Information* is relatively detailed. This is a preferred format to:

- ⇨ Document thoroughly the results that support claims that cannot be detailed in the manuscript to keep the manuscript relatively short. For each experimental parameter studied, typically *only* a picture, a Table and a short discussion of the influence of the experimental parameters are given. Since several parameters are investigated, and different characterization techniques used, this adds to the length of this document.
- ⇨ Comply with the FAIR principles https://publish.acs.org/publish/data_policy
- ⇨ Address to our best the general challenges of reproducibility in nanomaterial synthesis.[1,2] We reproduced the synthesis presented in 3 different laboratories. Based on this experience we hope that the details provided here will help the community to reproduce and best exploits the results.

Table of contents - Sections

Abbreviations and definitions

A_{spr}:	Absorption intensity at the surface plasmon resonance evaluated by UV-vis
A_{380}:	Absorption intensity at 380 nm evaluated by UV-vis
A_{400}:	Absorption intensity at 400 nm evaluated by UV-vis
A_{450}:	Absorption intensity at 450 nm evaluated by UV-vis
A_{650}:	Absorption intensity at 650 nm evaluated by UV-vis
A_{800}:	Absorption intensity at 800 nm evaluated by UV-vis
Δλ:	width of the plasmon peak, evaluated by UV-vis at 0.9 x A_{spr}
d_N:	Number weighted size (diameter) evaluated by TEM, Feret mean diameter defined as: $$d_N = \frac{\sum d_i}{N}$$
d_S:	Surface weighted size (diameter) evaluated by TEM, Sauter mean diameter defined as: $$d_S = \frac{\sum {d_i}^3}{\sum {d_i}^2}$$
d_V:	Volume weighted size (diameter) evaluated by TEM, De Brouckere mean diameter defined as: $$d_V = \frac{\sum {d_i}^4}{\sum {d_i}^3}$$
σ:	standard deviation related to d_N
PdI:	polydispersity index defined as $(\frac{\sigma}{d_N})^2$
DMF:	N,N-dimethylformamide
CA:	chronoamperometry
CV:	cyclic voltammogram
CTAB:	cetyltrimethylammonium bromide
ECSA:	electrochemically active surface area
EG:	ethylene glycol
EGOR:	ethylene glycol oxidation reaction
EOR:	ethanol oxidation reaction
EtOH:	ethanol
Li_3Ct:	trilithium citrate
MeOH:	methanol
Na_3Ct:	trisodium citrate
NM:	nanomaterial
NP:	nanoparticle
PDF:	pair distribution function
PM:	precious metal
PP:	polypropylene
PVP:	polyvinylpyrrolidone
RHE:	relative hydrogen electrode
ROH:	(mono)alcohol(s)
RT:	room temperature, ca. 22 °C
SA:	specific activity
SCE:	saturated calomel electrode
S/N:	signal-to-noise
SurFree:	surfactant-free
spr:	surface plasmon resonance
TEM:	transmission electron microscope/microscopy
TS:	total scattering
XPS:	X-ray photoelectron spectroscopy
XRD:	X-ray diffraction
X:	In Tables, this means that no stable colloids were obtained, and no further characterization was performed.
-:	In Tables, this means that the characterization could not be performed and/or the data is not available

SA. Synthesis of Au NPs using ROH

There is to date and to the best of our knowledge, no surfactant-free synthesis method as simple and user-friendly as the Turkevich-Frens synthesis. Such a synthesis is much needed for both fundamental and applied research and development as well as industrial applications.[3] RT-syntheses are promising in this respect. A range of syntheses can be performed at RT, but are typically performed in water and in the presence of strong reducing agents and/or surfactants.[4] The potential of using low boiling point solvents as both solvents and reducing agents in surfactant-free RT-synthesis, while it seems promising, has not yet been fully investigated and exploited.

Table S1. Examples of studies using ROHs in alkaline conditions as reducing agent, focus on RT and surfactant-free syntheses.

Ref	**Date**	**Glycerol v.%** in water	**Au** mM	**NaOH** mM	**NaOH/Au** molar ratio	**PVP**	**T** °C	**Order of addition**	**Size** nm (if no PVP)
[5]	2012	0.005-22	0.50 ($AuCl_3$)	100	200	10 g L^{-1}	RT	ROH+NaOH to Au	
[6]	2013	100	0.10-0.75 ($HAuCl_4$)	0.5-1 (with PVP)	5-10	0.05-0.1% w/v	RT	Not defined	
[7]	2014	100	0.10-0.75 ($AuCl_3$)	pH: 9-13	-	0.04-10 g L^{-1}	25, 0	ROH+NaOH to Au	
[8]	2016	0.7, 1.5, 2.2	0.315 ($HAuCl_4$)	100-400	315-1270	0.03-1% w/v	RT	ROH+NaOH to Au	
[6]	2013	20	0.75 ($HAuCl_4$)	1	1.3	none	RT	Not defined	8
		50	0.75 ($HAuCl_4$)	1	1.3				20
		80	0.75 ($HAuCl_4$)	1	1.3				25
		100	0.50 ($HAuCl_4$)	1	2				30
		100	0.10-0.75 ($HAuCl_4$)	0.5	1.3-10				-
[9]	2019	65.7	0.75 ($HAuCl_4$)	200	266	none	RT	Au last	7.0 ± 1.7
		49.3		200	266		RT		7.0 ± 2.2
		32.8		200	266		RT		8.1 ± 3.0
		16.4		200	266		RT		-
		65.7		200	266		10		6.0 ± 1.5
		65.7		200	266		40		-
		65.7		200	266		60		-
		65.7		10	13		RT		-
		65.7		50	68		RT		-
		65.7		100	133		RT		-
		65.7		200	266		RT		-
		65.7		300	400		RT		-
		100		200	266		RT		9.2 ± 2.0
Ref	**Date**	**Ethanol v.%** in water	**$HAuCl_4$ mM**	**NaOH** mM	**NaOH/Au molar ratio**	**PVP**	**T**	**Order of addition**	**Size** nm if no PVP
[10]	2013	10, 50, 100	10, 25, 50, 100 (?) 0.10, 0.25, 0.50, 1 (?)	?	?	none	RT	NaOH last	10-20

SB. Experimental section

Chemicals

All chemicals were used as received: $HAuCl_4 \cdot 3H_2O$ (Sigma Aldrich); $PdCl_2$ (anhydrous, 60% Pd basis, Aldrich); $H_2PtCl_6 \cdot 6H_2O$ (99.9% Alfa Aesar); $OsCl_3$ (Premion®, 99.99% metals basis, Alfa Aesar); H_2IrCl_6 (99.9%, Alfa Aesar); $RuCl_3 \cdot xH_2O$ (99.9%, Alfa Aesar); LiOH (98%, Alfa Aesar); NaOH (Puriss., Sigma-Aldrich); KOH (ACS reagent, Sigma-Aldrich); CsOH (99.95%, Aldrich); water (Milli-Q, Millipore, resistivity of >18.2MΩ·cm, total organic carbon (TOC) < 5 ppb); methanol (MeOH, 99.8%, VWR); ethanol (EtOH, absolute, VWR); ethylene glycol (99+%, Sigma-Aldrich); glycerol (bi-distilled, 99.5% VWR); tert-butanol (ACS, 99.0%); Snaps (Havblik, Klar, 32v.%) LiCl (ReagentPlus, +99%); NaCl (ReagentPlus, +99%); cetrimmonium bromide (CTAB, AnalaR Normapur, VWR); trisodium citrate dehydrate (Na_3Ct, 99%, Alfa Aesar); lithium citrate tribasic tetrahydrate (Li_3Ct, 99.5%, Sigma Aldrich); polyvinylpyrrolidone (PVP, Alfa Aesar, MW: 58 000); TiO_2 (nanopowder, Sigma Aldrich); MnO_2 (activated, < 10 µm, Sigma Aldrich); Al_2O_3 (Puralox SBa 200 Sasol); Carbon (XC72R, Cabot); H_2SO_4 (96%, Merck, Suprapur); HCl (37%, 37%, EMSURE® ACS, ISO, Reag. Ph Eur); HNO_3 (67%, Normatom® VWR).

Supported nanomaterials

The supported Au NPs were obtained in two different ways. In a first approach, supported Au NPs were obtained by directly performing the synthesis in presence of a support with the desired Au:Support mass ratio. Examples of support are oxides materials such as MnO_2, Al_2O_3, TiO_2, CeO_2, etc. typically used in heterogeneous catalysis or carbon supports typically used in electrocatalysis. Experiments were performed for example with a total volume of 13 or 50 mL, a LiOH/$HAuCl_4$ molar ratio of 4 at ambient light and temperature in PP containers (50 mL) left under stirring for 24 hours. After synthesis the dispersion was centrifuged (and no colored supernatant was observed in most cases) and washed with water. Alternatively, supported Au NPs were also obtained by mixing the required amount of colloidal synthesized Au NPs and a support material. The solvent was left to evaporate overnight under stirring at RT. The collected powder was then washed with water. It is worth stressing that for some support like Al_2O_3 the colloidal NPs spontaneously interact with the support and by simply mixing the colloids and the support a clear supernatant is obtained after centrifugation. Therefore, the evaporation step is not needed to obtain supported Au NPs in this case.

Characterization

The size reported correspond to the average diameter size and the related deviation (Feret diameter), in addition the Sauter mean diameter (d_S, surface weighted) and the De Brouckere mean diameter (d_V, volume weighted) are indicated. The estimated polydispersity index (PdI) is also reported. The PdI is considered to be low for values lower than 0.05 for surfactant-free Au NPs.[9] As a comparison, NPs produced by the Turkevich method are typically characterized by a PdI value around 0.010-0.015 due to the use of surfactants.[11]

Upon TEM analysis, different types of structures were observed. If no indication is given, it means that the NPs are spherical. A note 'Network', 'Worm', 'Chunks' means that the structures look as per the classification proposed in **Figure S1**.

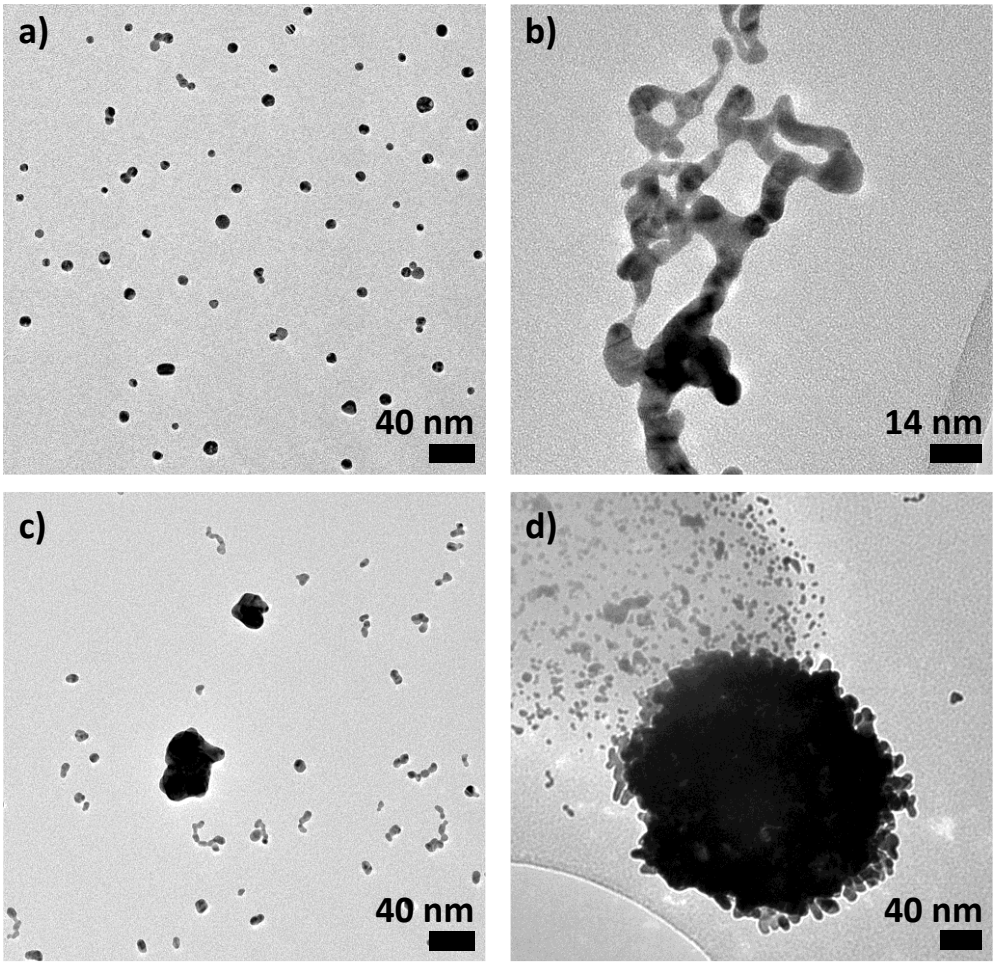

Figure S1. TEM micrographs of representative (a) NPs, (b) 'Network', (c) 'Worm' and (d) 'Chunks' structures observed.

X-ray photo-electron spectroscopy (XPS).

XPS measurements on the Au_xPd_y NPs prepared at RT were performed with a focus on the Au4*f*, Au4*d* and Pd3*d* peaks to evaluate elemental composition (Pd:Au ratios) and to some extend the chemical state of Au and Pd. However, XPS is not straightforward for the small size NMs due to the generally low signals originating from adsorption of oxygen and carbon species on the high surface area NPs. This absorption significantly lowers the sensitivity of the signal recorded. The NPs were placed on cleaned Cu foils (MaTecK, 99.99%) to improve the electric contact with the NPs. However, the Pd NP samples were consistently prone to charging, even when employing charge neutralization tools (flood gun: 0.5 µA, 1 keV at 1.1×10^{-7} mbar Ar (N6)). It was challenging to get a high signal-to-noise (S/N) ratio for the Pd NPs, despite using several approaches and loadings. We suspect that the carbophilic nature of Pd combined with the solvent used in the synthesis, may have formed a non-conductive ligand layer around the NPs, possibly upon drying for sample preparation, making Pd NPs prone to charging. Herein, we only present work on samples on which no noticeable charging was detected. This was confirmed by verifying the C1*s* peak position around the expected 284.7 eV [NIST XPS Database][a], **Figure S2**.

[a] https://srdata.nist.gov/xps/main_search_menu.aspx

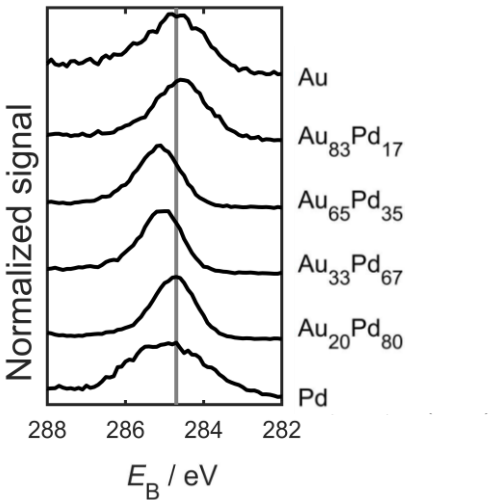

Figure S2. Normalized XPS C1*s* signal for the Au_xPd_y NPs synthesized at RT.

The C1*s* signal, **Figure S2**, is generally weaker on Pd containing samples, suggesting some increase in the C-O relative signal compared to the Au containing samples. Due to the strong overlap of Au*4d* and Pd*3d* peaks the Au4*f* intensity was used to evaluate more accurately the Au:Pd ratio derived from the Au4*d* and Pd3*d* peaks. The relatively low S/N prohibited any conclusive identification of Pd or Au chemical state. To conduct the analysis, we employed the peak information derived from NIST XPS database and the *CasaXPS* software library.

Electrochemical measurements: ***Drying***. In the case of NPs obtained in EG or glycerol, the solvent did not dry at RT. It took few minutes to evaporate the solvent at RT when the solvent was mixtures of MeOH or EtOH and water, but several days when the solvent was a mixture of EG and glycerol and water. A heat treatment at 70 °C for few hours could speed the drying process if EG and water were used as solvent, but this treatment had to be longer for the case where glycerol and water was used and was even unsuccessful to evaporate most of the glycerol even after 48 hours. The synthesis performed using the polyols (EG and glycerol) was therefore considered disadvantageous for the preparation of electrocatalysts. This is in line with results from the literature where a support is directly used during the synthesis in order to develop electrocatalyst when glycerol is the solvent and reducing agent (the colloidal NPs cannot easily be used further).[9]

SC. Effect of mono-alcohol, mono-alcohol content and cation

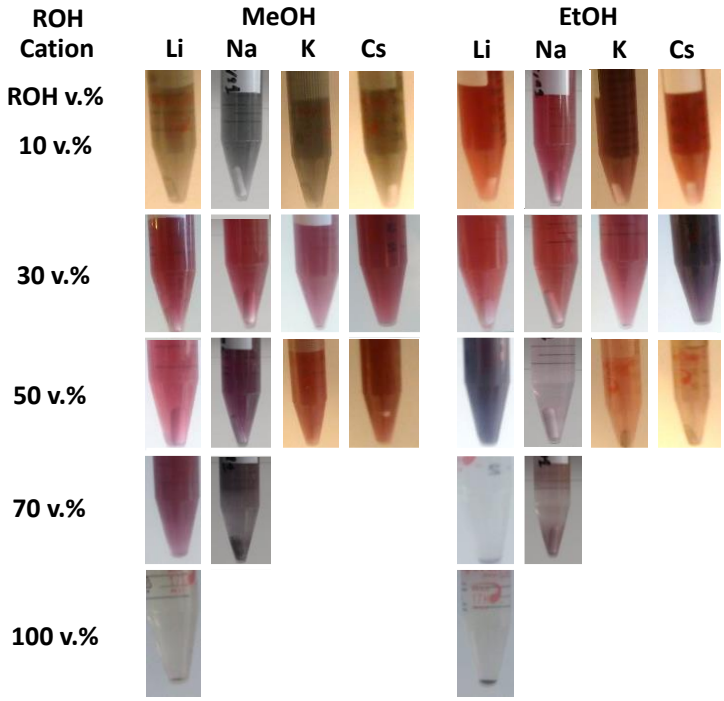

Figure S3. Pictures of the colloidal dispersions obtained for 0.5 mM $HAuCl_4$ and 2 mM of base (molar ratio Base/Au of 4) for different ROH, ROH contents and cations in the base, as indicated. The different colors of the background correspond to different days of synthesis.

Table S2. Physical characteristics of the Au NPs obtained using different water contents and cations when (A) EtOH or (B) MeOH are used as reducing agents.

Table S2A. Using EtOH as reducing agent.

ROH	H_2O v.%*	ROH v.%*	$HAuCl_4$ mM*	Base	Base mM*	V mL*	T °C	t h	Base/Au molar ratio	λ_{spr} ($\Delta\lambda/\lambda_{spr}$) nm	A_{spr}/A_{450}	Relative yield **	A_{650}/A_{spr}	A_{380}/A_{800}	d_N nm	d_S nm	d_V nm	PdI
EtOH	90	10	0.5	LiOH	2	13	RT	24	4	523 (6.9%)	1.61	1.00	0.09	32.0	7.5 ± 3.3	10.5	12.0	0.19
				NaOH						530 (7.0%)	1.75	0.98	0.20	8.20	9.1 ± 6.4	22.3	31.0	0.49
				KOH						536 (6.9%)	1.82	0.99	0.18	18.4	13.8 ± 5.7	18.2	19.9	0.17
				CsOH						523 (7.5%)	1.54	1.00	0.16	21.5	10.2 ± 3.8 + Network	X	X	0.14
	70	30		LiOH						515 (6.6%)	1.53	0.97	0.10	26.3	8.6 ± 2.0	9.5	10.0	0.05
				NaOH						518 (6.9%)	1.52	0.83	0.10	34.0	8.9 ± 2.2	10.0	10.5	0.06
				KOH						526 (6.5%)	1.68	0.97	0.16	19.3	13.1 ± 2.9	14.4	15.1	0.05
				CsOH						534 (12.0%)	1.46	1.00	0.60	2.5	7.6 ± 1.5	8.2	8.4	0.04
	50	50		LiOH						592 (18.9%)	1.62	1.00	0.92	1.2	> 50	X	X	X
				NaOH						X	X	X	X	X	X	X	X	X
				KOH						554 (15.0%)	1.58	0.3	0.77	1.2	> 50	X	X	X
				CsOH						X	X	X	X	X	X	X	X	X
	30	70		LiOH						X	X	X	X	X	X	X	X	X
				NaOH						X	X	X	X	X	X	X	X	X
	0	100		LiOH						X	X	X	X	X	X	X	X	X

* before volume contraction; ** evaluated as the ratio of A_{400} for the sample and the maximum values of A_{400} for the dataset at a given v.% of ROH.

The results in **Figure S3** and **Table S2A** show that without ROH, no NPs are formed. This suggests that ROH is the reducing agent in the synthesis. Using EtOH as reducing agent, the smallest NPs (considering size and distribution retrieved from TEM analysis) are obtained using 30 v.% ROH. Based on the UV-vis analysis, the most stable NPs with low A_{650}/A_{spr} and high A_{380}/A_{800} values are obtained using NaOH or LiOH. Across various v.% ROH, LiOH leads to the smallest and more stable NPs, followed by NaOH, KOH and CsOH. CsOH is the most expensive base in this study and was not considered further. The effect of cations is further discussed in **section SO. Cation and surfactant effect**.

The NPs obtained for a 30 v.% EtOH or less are around 10 nm in diameter.

Table S2B. Using MeOH as reducing agent.

ROH	H_2O v.%*	ROH v.%*	$HAuCl_4$ mM*	Base	Base mM*	V mL*	T °C	t h	Base/Au molar ratio	λ_{spr} ($\Delta\lambda/\lambda_{spr}$) nm	A_{spr}/A_{450}	Relative yield **	A_{650}/A_{spr}	A_{380}/A_{800}	d_N nm	d_S nm	d_V nm	PdI
MeOH	90	10	0.5	LiOH	2	13	RT	24	4	563 (x.x%)	1.05	0.72	0.95	1.4	11 + Network	X	X	X
				NaOH						570 (x.x%)	0.62	0.88	0.96	1.4	Network (15)	X	X	X
				KOH						556 (9.5%)	1.79	0.76	0.52	2.7	10.2 ± 6.8	21.5	30.8	0.44
				CsOH						569 (x.x%)	X	1.00	X	X	10 + Network	X	X	X
	70	30		LiOH						535 (7.1%)	1.87	0.94	0.25	9.4	20.1 ± 7.9	27.2	32.1	0.15
				NaOH						531 (6.3%)	1.84	0.98	0.17	14.3	21.2 ± 7.1	26.3	29.1	0.11
				KOH						539 (7.4%)	1.84	0.52	0.35	4.9	20.0 ± 9.0	28.1	33.5	0.20
				CsOH						523 (6.5%)	1.68	1.00	0.96	1.39	9.7 ± 4.4	13.8	15.8	0.21
	50	50		LiOH						526 (6.0%)	1.79	0.90	0.16	14.6	18.3 ± 5.4	21.7	22.6	0.09
				NaOH						542 (8.4%)	1.72	0.74	0.47	4.5	28.3 ± 11.1	39.3	41.7	0.15
				KOH						541 (7.7%)	1.85	0.7	0.33	12.9	8.4 ± 7.3	26.8	37.0	0.76
				CsOH						540 (7.2%)	1.91	1.0	0.15	12.0	20-40	X	X	X
	30	70		LiOH						536 (9.2%)	1.70	1.0	0.48	2.5	> 30	X	X	X
				NaOH						X	X	X	X	X	X	X	X	X
	0	100		LiOH						X	X	X	X	X	X	X	X	X

* before volume contraction; ** evaluated as the ratio of A_{400} for the sample and the maximum values of A_{400} for the dataset at a given v.% of ROH.

The results in **Figure S3** and **Table S2B** show that using MeOH as reducing agent, the smallest NPs overall are obtained using 30 v.% ROH. In MeOH-water mixtures with up to 50 v.% MeOH, NPs are still obtained, as opposed to the case of 50 v.% EtOH. Across various v.% ROH, LiOH and NaOH leads to the smallest and more stable NPs, followed by KOH and CsOH. CsOH is the most expensive base in this study and was not considered further. The effect of cations is further discussed in **section SO. Cation and surfactant effect**.

The NPs obtained for 30 v.% MeOH are around 20 nm in diameter.

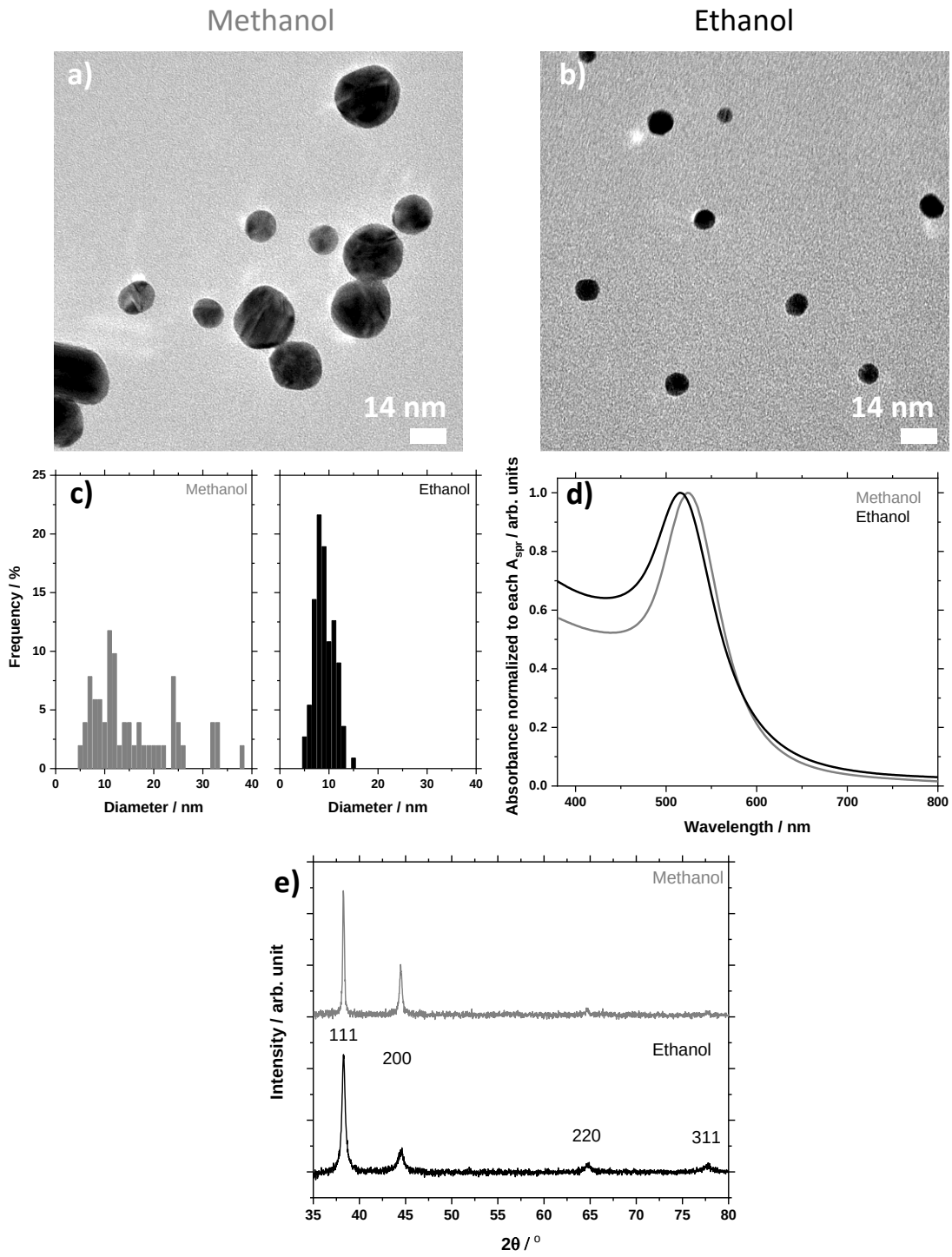

Figure S4. (a,b) Representative TEM micrographs of the Au NPs obtained using (a) MeOH, (b) EtOH for 30 v.% ROH using 0.5 mM $HAuCl_4$ and 2 mM LiOH (molar ratio LiOH/Au of 4) at RT. (c) is the resulting size distribution and (d) UV-vis characterization where each spectrum is normalized to the absorbance at the plasmon resonance wavelength. (e) XRD diffractograms of Au NPs. The expected peaks for the Au *fcc* structure are indexed,[5] with peaks at ca. 2θ = 38, 44, 65 and 77° corresponding to (111), (200), (220) and (311) planes.[12]

SD. Effect of experimental parameters: $HAuCl_4$ concentration, volume of solution, type of container used, light

Table S3. Physical characteristics of the Au NPs obtained using different experimental conditions such as volumes of solution, concentrations of reactants, ambient light or dark, glass or PP containers, with or without stirring. Unless otherwise specified, the synthesis was performed at RT and ambient light in PP containers with stirring.

Table S3. Using 30 v.% EtOH as reducing agent.

$HAuCl_4$ mM*	**Base**	**Base** mM*	**V** mL*	**T** °C	**t** h	**Base/Au** molar ratio	**Variable**			**λ_{spr}** ($\Delta\lambda/\lambda_{spr}$) nm	**A_{spr}/A_{450}**	**A_{650}/A_{spr}**	**A_{380}/A_{800}**	**d_N** nm	**d_S** nm	**d_V** nm	**PdI**
0.5	LiOH	2	25	RT	24	4	Volume			520 (6.7%)	1.55	0.13	16.4	8.4 ± 2.3	9.6	10.3	0.07
			6.5				Volume			521 (6.4%)	1.60	0.13	11.3	11.6 ± 2.5	12.6	13.2	0.05
0.1		0.4	13			4	Concentration			526 (6.4%)	1.48	0.24	8.3	7.4 ± 2.6	9.2	10.1	0.12
5		20				4	Concentration			533 (6.8%)	1.84	0.25	11.5	19.2 ± 9.7	31.0	40.6	0.26
10		40				4	Concentration			X	X	X	X	Network (>10)	X	X	X
5		2				30	Concentration			X	X	X	X	X	X	X	X
0.1		2				20	Concentration			X	X	X	X	X	X	X	X
0.5		20				40	Concentration			X	X	X	X	X	X	X	X
0.5		0.2				0.4	Concentration			X	X	X	X	X	X	X	X
100		20				0.2	Concentration			X	X	X	X	X	X	X	X
200		20				2	Concentration			X	X	X	X	X	X	X	X
							in	stirring	light								
0.5	LiOH	2	13	RT	24	4	PP	YES	LIGHT	516 (6.5%)	1.55	0.10	28.8	9.2 ± 2.4	10.4	11.1	0.07
							PP	YES	DARK	536 (11.4%)	1.49	0.49	3.6	5.8 ± 1.4	6.5	6.9	0.06
							GLASS	YES	LIGHT	519 (7.5%)	1.45	0.22	7.4	7.0 ± 2.3	8.5	9.5	0.11
							PP	NO	LIGHT	517 (6.6%)	1.51	0.11	18.6	7.4 ± 2.4	8.9	9.6	0.11
							GLASS	NO	DARK	525 (10.7%)	1.53	0.57	3.8	10.3 ± 2.6	11.7	12.5	0.06
				50-RT	1-23		PP	YES	DARK	523 (6.3%)	1.77	0.10	30.5	-	-	-	-
	NaOH			RT	24		PP	YES	LIGHT	517 (6.4%)	1.57	0.12	20.0	9.9 ± 2.3	11.0	11.5	0.05
							GLASS	YES	DARK	519 (6.4%)	1.63	0.13	22.5	10.3 ± 2.8	11.8	12.5	0.07

* before volume contraction.

Table S3. Using 30 v.% MeOH as reducing agent.

$HAuCl_4$ mM*	**Base**	**Base** mM*	**V** mL*	**T** °C	**t** h	**Base/Au** molar ratio	**Variable**			**λ_{spr}** ($\Delta\lambda/\lambda_{spr}$) nm	**A_{spr}/A_{450}**	**A_{650}/A_{spr}**	**A_{380}/A_{800}**	**d_N** nm	**d_S** nm	**d_V** nm	**PdI**
0.5	LiOH	2	25	RT	24	4	Volume			527 (5.9%)	1.53	0.14	17.2	14.5 ± 5.1	17.9	19.4	0.12
			6.5				Volume			534 (6.6%)	1.82	0.14	21.2	22.4 ± 6.6	26.3	28.2	0.09
0.1		0.4	13			4	Concentration			530 (9.6%)	1.52	0.73	1.1	11.1 ± 5.6	16.3	18.1	0.25
5		20				4	Concentration			549 (10.2%) + ca. 740	1.57	0.40	4.2	26.0 ± 12.3	38.7	46.0	0.22
5		2				30	Concentration			X	X	X	X	X	X	X	X
0.1		2				20	Concentration			X	X	X	X	X	X	X	X
0.5		20				40	Concentration			X	X	X	X	X	X	X	X
0.5		0.2				0.4	Concentration			X	X	X	X	X	X	X	X
10		40				4	Concentration			X	X	X	X	X	X	X	X
							in	**stirring**	**light**								
0.5	LiOH	2	13	RT	24	4	PP	YES	LIGHT	535 (7.1%)	1.87	0.25	9.4	20.1 ± 7.9	27.2	32.1	0.15
							PP	YES	DARK	529 (6.0%)	1.87	0.10	33.0	17.2 ± 8.9	26.7	32.2	0.27
							GLASS	YES	LIGHT	525 (5.9%)	1.82	0.09	25.6	13.2 ± 5.7	19.4	25.2	0.19
							GLASS	NO	DARK	541 (7.9%)	1.89	0.32	6.6	10.3 ± 4.5	14.9	18.4	0.19
				50-RT	1-23		PP	YES	DARK	536 (5.4%)	1.94	0.15	16.9	-	-	-	-
	NaOH			RT	24		PP	YES	LIGHT	534 (7.0%)	1.87	0.22	10.9	23.4 ± 6.8 + Chunks	X	X	0.08
							GLASS	YES	DARK	553 (17.9%)	1.23	0.80	1.6	Network (10)	X	X	X

* before volume contraction.

When EtOH is used a as reducing agent, **Table S3A**, the synthesis leads to Au NPs for a range of $HAuCl_4$ concentrations, although at higher concentrations (ca. from 10 mM $HAuCl_4$) the NPs tend to form gold nuggets rapidly or over time. A molar ratio of 4 between the base and $HAuCl_4$ favors the formation of small size and stable colloidal NPs, see also **section SH. Influence of base concentration**. Using a PP or glass container does not seem to influence the outcome of the synthesis (NPs are only slightly smaller using a glass container) as opposed to observation in previous reports.[13] However, the solution left to react in the dark shows very slow kinetics of formation although NPs are still formed, see also **section SF. Kinetics of the reduction**, as well as **section SJ. Influence of the order of addition of the chemicals** for further experimental evidence. Stirring does not seem to influence much the outcome of the synthesis, which is ultimately beneficial to develop cheaper synthesis methods, but also alleviate from potential contamination that could originate from cleaning procedures of the magnetic stir bars. The reactions are scalable to 1 L as detailed in **section SM. Scalability**.

Using MeOH as reducing agent, see **Table S3B**, the synthesis leads to Au NPs for a range of $HAuCl_4$ concentrations, although at higher concentrations the NPs tend to form gold nuggets rapidly or over time and larger NPs tend to form at higher $HAuCl_4$ concentrations. At lower concentration (e.g. 0.1 mM), smaller NPs (ca. 10 nm) can be obtained using MeOH but the NPs remained larger or about the size than those obtained using EtOH for higher $HAuCl_4$ concentrations (e.g. at 0.5 mM). Using a PP or glass container does not seem to influence much the outcome of the synthesis (NPs are only slightly smaller using glass container), however the solution left to react in the dark shows very slow kinetics of formation, although NPs are still formed.

As the light influences the kinetics of the reaction, and especially the reaction of $HAuCl_4$ with different species,[14] see also **section SF. Kinetics of the reduction**, and since this variable is relatively challenging to control (changes from day to day or even within a day), alternative syntheses at moderate temperature (< 100 °C) were performed to control better the reaction, see also **section SG. Influence of the temperature**. For instance, leaving the reaction to react at 1 hour at 50 °C and later on store the NPs in the dark clearly lead to a different UV-vis characterization of the NPs, see **Figure S5**. The interpretation of these results is further detailed in **section SF. Kinetics of the reduction**.

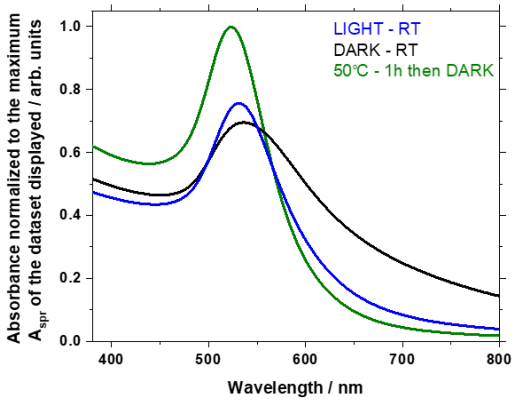

Figure S5. UV-vis spectra of Au NP colloidal dispersions obtained using 0.5 mM $HAuCl_4$, 2 mM LiOH (molar ratio LiOH/Au of 4) in PP tubes with stirring for (blue) 24 hours at RT and light, (black) 24 hours in the dark (dark conditions were achieved by covering the sample with aluminum foil) and (green) after heating up the samples at 50 °C for 1 hour and later on keep the sample in the dark for 23 hours.

SE. Effect of the nature of the alcohols

To the best of our knowledge, only glycerol was shown to be a suitable reducing agent for reproducible RT-synthesis of Au NPs.[9] While Tremiliosi-Filho and co-workers stressed that presence of PVP is preferred for the synthesis,[5,7,8,15] they showed together with others, that surfactants like PVP are not needed for the reaction to be completed and Au NPs obtained,[6,9] see also **Table S1**. It is often argued that the high viscosity of glycerol is key to stabilize the NPs. It is shown here, see **Table S4**, that less viscous ethylene glycol (EG) is also a suitable reducing agent and more interestingly, the even less viscous mono-alcohols MeOH and EtOH as well. However, the synthesis does not lead to colloids if isopropanol is used and to large size structures if tert-butanol is used, see also **Figure S6**.

Table S4. Physical characteristics of the Au NPs obtained using different ROH as reducing agents.

ROH	H_2O v.%*	ROH v.%*	$HAuCl_4$ mM*	Base	Base mM*	V mL*	T °C	t h	Base/Au molar ratio	λ_{spr} ($\Delta\lambda/\lambda_{spr}$) nm	A_{spr}/A_{450}	A_{650}/A_{spr}	A_{380}/A_{800}	d_N nm	d_S nm	d_V nm	PdI
MeOH	70	30	0.5	LiOH	2	13	RT	24	4	529 (5.8%)	1.89	0.11	32.3	21.8 ± 7.4	26.6	28.7	0.12
EtOH										515 (6.6%)	1.53	0.10	26.3	8.6 ± 2.0	9.5	10.0	0.05
Isopropanol										689 (26.7%)	1.45	1.27	1.9	-	-	-	-
tert-Butanol										557 (14.4%)	1.42	0.56	1.0	> 30	X	X	X
EG										528 (6.9%)	1.67	0.25	7.1	9.7 ± 3.2	11.8	12.8	0.11
Glycerol										535 (6.2%)	1.00	0.18	9.8	10.8 ± 4.5	15.0	17.7	0.17

* before volume contraction.

In previous reports, and to the best of our knowledge, an exclusive focus was given to NaOH as base, with only rare examples overall using KOH across the literature on Au NP synthesis.[16] The results presented below suggest that LiOH might lead to shape control given that significant amount of rods is here obtained using glycerol as reducing agent, **Figure S6d**. Unfortunately, the high viscosity of the polyols prevents the direct use of the NPs and requires washing steps before the NPs can be further considered in most applications. These extra steps and the related challenges as well as energy consumption and related waste generation are here alleviated using mono-alcohols, see **section SP. Electrochemical characterization**.

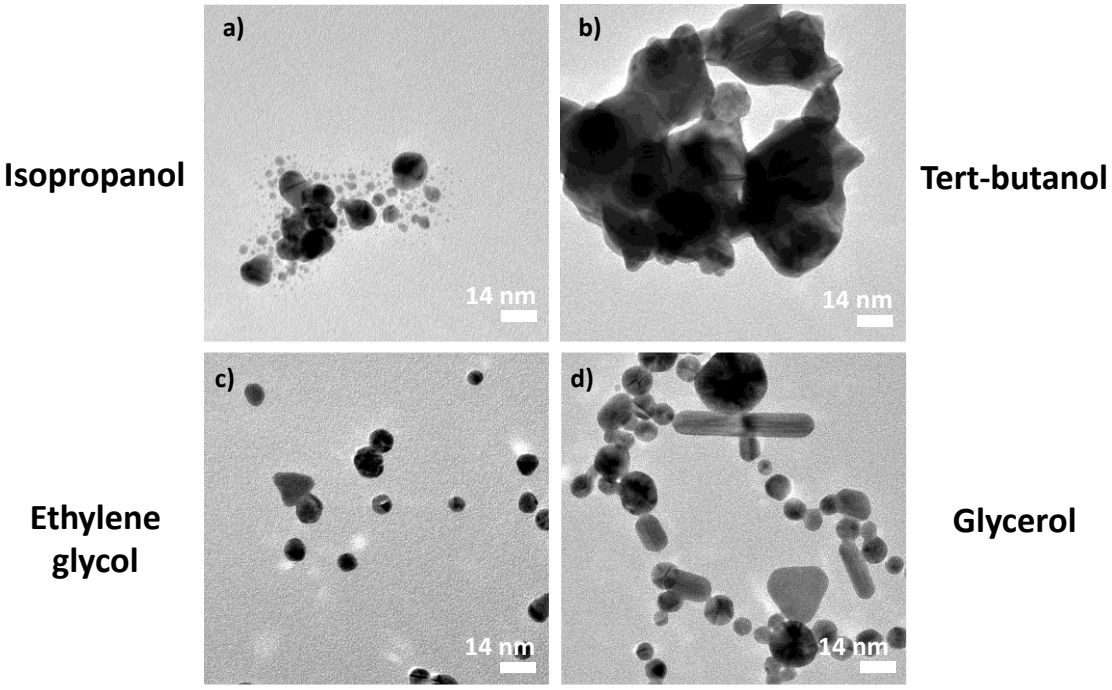

Figure S6. Representative TEM micrographs of the different NMs obtained using 0.5 mM $HAuCl_4$ and 2 mM LiOH (molar ratio LiOH/Au of 4) in 30 v.% ROH where ROH is (a) isopropanol, (b) tert-butanol, (c) ethylene glycol and (d) glycerol.

SF. Kinetics of the reduction

Table S5. Kinetics of the synthesis of Au NPs reaction followed by UV-vis. The reaction mixtures consisted of 0.5 mM $HAuCl_4$ and 2 mM LiOH left to react at RT and light without stirring. The $HAuCl_4$ was added last. Aliquots of 2-3 mL were sampled over time for UV-vis measurements. This data set correspond to data presented in Figure 1 of the main manuscript.

ROH	H_2O v.%*	ROH v.%*	$HAuCl_4$ mM*	Base	Base mM*	V mL*	T °C	t	Base/Au molar ratio	λ_{spr} ($\Delta\lambda/\lambda_{spr}$) nm	A_{spr}/A_{450}	Relative yield **	A_{650}/A_{spr}	A_{380}/A_{800}
EtOH	70	30	0.5	-	-	-	RT	0h00	-	(308)[x]	X	X	X	X
				LiOH	2	39	RT	0h05	4	X	X	X	X	2.0
								0h10		536 (broad)	0.95	0.62	0.73	1.6
								0h20		535 (broad)	1.08	0.83	0.59	1.8
								0h30		526 (13.1%)	1.21	0.94	0.58	2.7
								0h40		519 (7.9%)	1.43	0.97	0.43	15.4
								0h50		515 (7.0%)	1.47	0.99	0.18	21.0
								1h00		515 (6.8%)	1.48	1.00	0.13	18.0
								1h10		515 (6.8%)	1.49	1.00	0.13	21.0
								1h20		515 (6.8%)	1.49	1.00	0.13	18.0
								1h30		515 (6.8%)	1.49	1.00	0.13	18.0
								1h40		515 (6.8%)	1.49	1.00	0.12	21.0
								1h50		515 (6.8%)	1.49	1.00	0.12	21.0
								2h00		515 (6.8%)	1.49	1.00	0.13	20.8
								9 D		515 (6.6%)	1.52	0.94	0.11	19.8
								2 W		518 (6.6%)	1.51	0.93	0.12	19.7
								3M***		520 (6.3%)	1.58	0.89	0.09	28.3

* before volume contraction; ** evaluated as the ratio of A_{400} for the sample and the maximum values of A_{400} for the dataset at a given v.% of ROH; *** still stable after 3 months, left at RT and ambient light; [x] without base, the $HAuCl_4$ complex show a well-defined peak around 308-309 nm in 30 v.% EtOH.

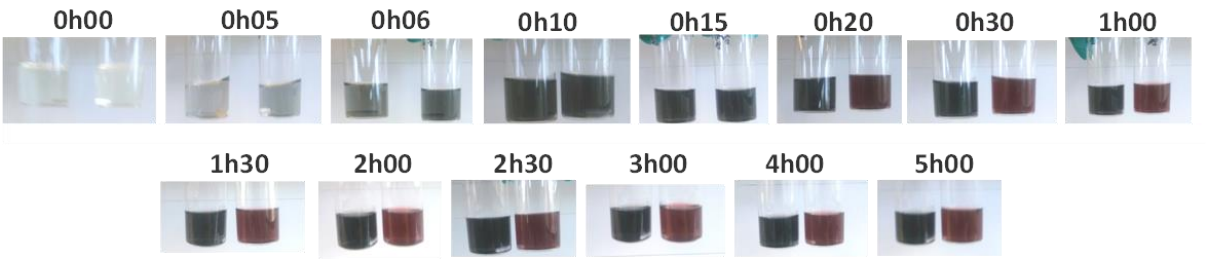

Figure S7. Pictures of solutions of 0.5 mM $HAuCl_4$, 2 mM LiOH (molar ratio LiOH/Au of 4) for 30 v.% ROH where the sample on the right is EtOH and the sample on the sample on the left is MeOH, for different times after adding $HAuCl_4$.

While the initial steps of the reaction are relatively fast in both MeOH and EtOH, the appearance of a red color is much faster in EtOH, see **Figure S7**. The TEM analysis of aliquots taken at different times of reaction for syntheses performed using EtOH and MeOH suggest the formation of network-like or worm-like structures, see **Figure S8**, discussed in the manuscript. Although the *in situ* PDF experiments were performed at a much higher $HAuCl_4$ concentration and using a different order of chemical addition, see **experimental section in the manuscript**, the NPs also form slower in MeOH than in EtOH, **Figure S Figure S10** and **Figure S11** as well as **Figure 1h**. It must be noted that eventually the NPs show a small crystal domain but agglomerate when a high $HAuCl_4$ concentration is used, **Figure S12**.

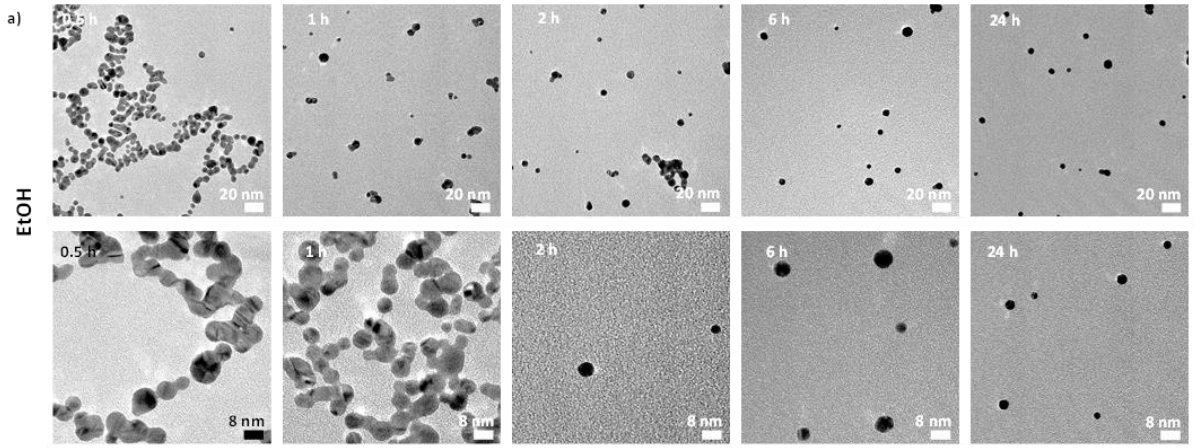

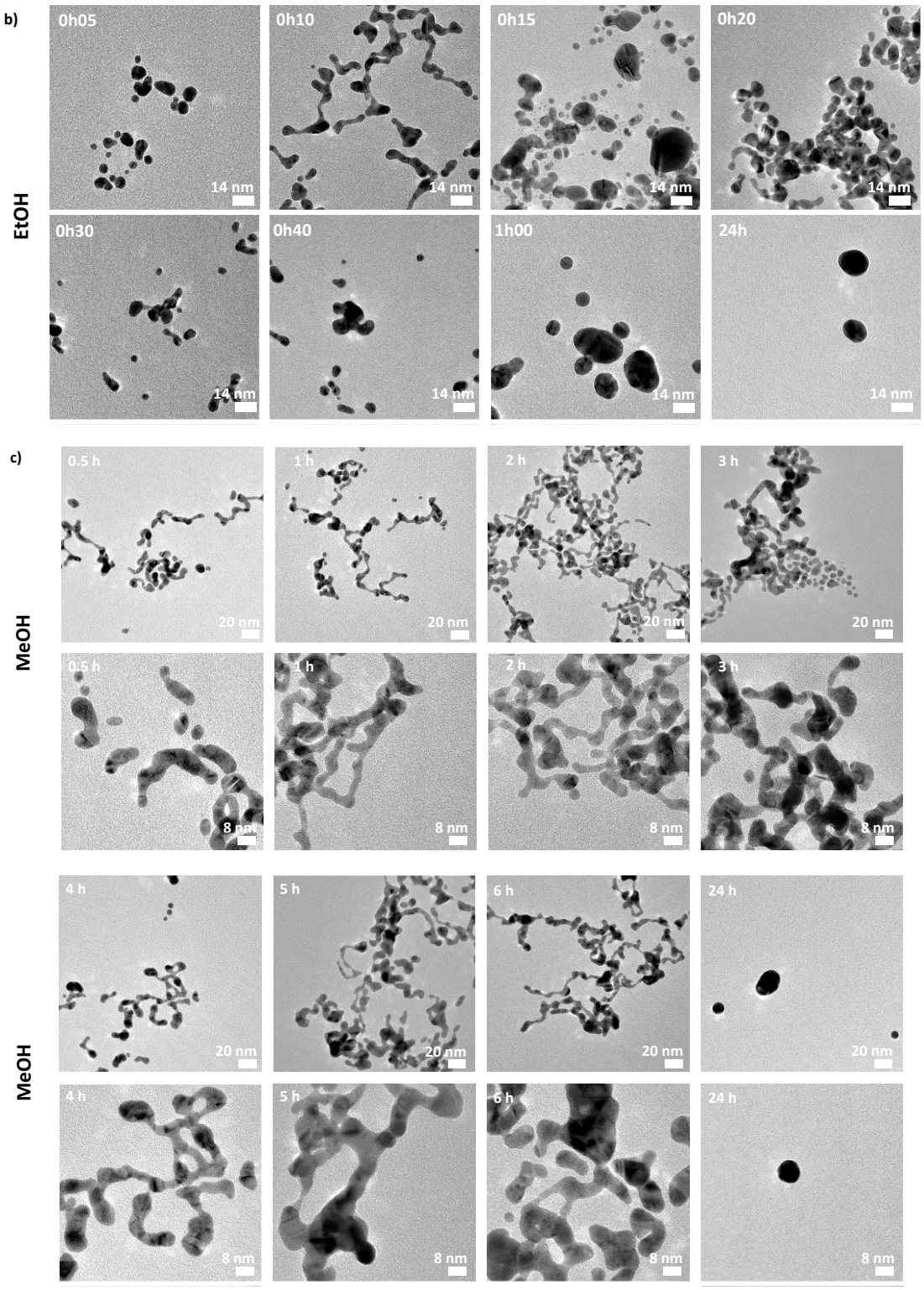

Figure S8. TEM micrographs of the samples from aliquots of a reaction mixture containing 0.5 mM $HAuCl_4$, 2 mM LiOH (molar ratio LiOH/Au of 4) in 30 v.% ROH with (a, b) EtOH and (c) MeOH, for different times of reaction after mixing all the reactants as indicated. (a) and (b) are two different experiments, the solutions (13 mL) were in glass containers under stirring.

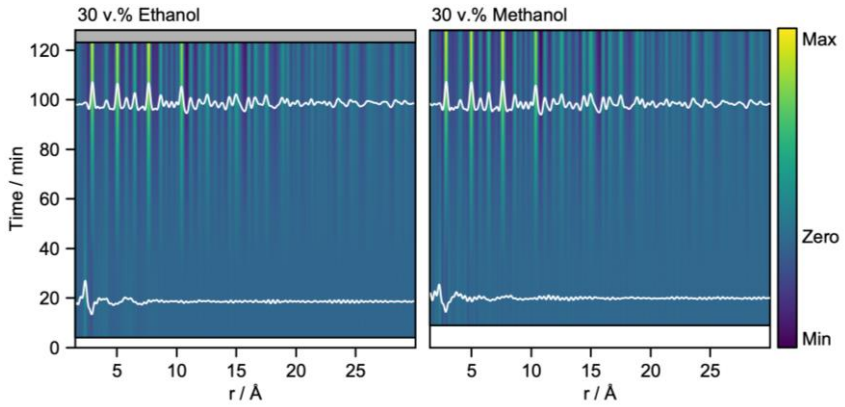

Figure S9. Time resolved PDFs obtained during the formation of Au NPs using 50 mM $HAuCl_4$, 150 mM LiOH and where either 30 v.% EtOH or MeOH was used and the alcohol added last.

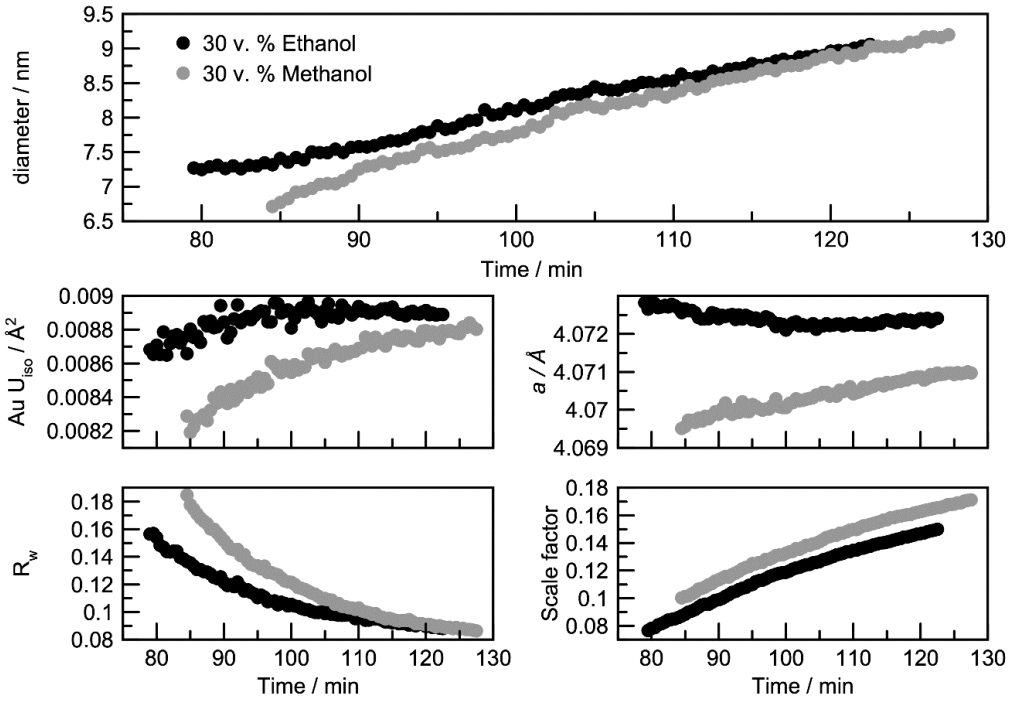

Figure S10. Spherical crystallite diameter retrieved from PDF analysis through sequential refinement of *in situ* X-ray data using the Au *fcc* structural model. The U_{iso}, R_w, lattice parameter *a* and scale factor from the refinements are also plotted. 50 mM $HAuCl_4$ and 150 mM LiOH were used in 30 v.% ROH in water and the ROH added last. The experiments were performed at RT.

Through sequential refinement, the refined crystalline domain size can be plotted as a function of time. In the early stages of the synthesis (before 75-80 min) a contribution from the precursor cluster indicated by the presence of the Au-Cl peak at 2.4 Å influence the refinement and no reliable size of the *fcc* NPs can be obtained. U_{iso} is the atomic displacement parameters and take into account the thermal vibration of the atoms, resulting in a broadening of the PDF peaks. R_w evaluates the fit quality and a lower value indicates an improved fit. The lattice parameter '*a*' corresponds to the dimensions of the unit cell. The scale factor relates to the scaling of the calculated PDF to fit the measured PDF. If the scaling increases throughout the experiment, it indicates that more particles with that structure forms.

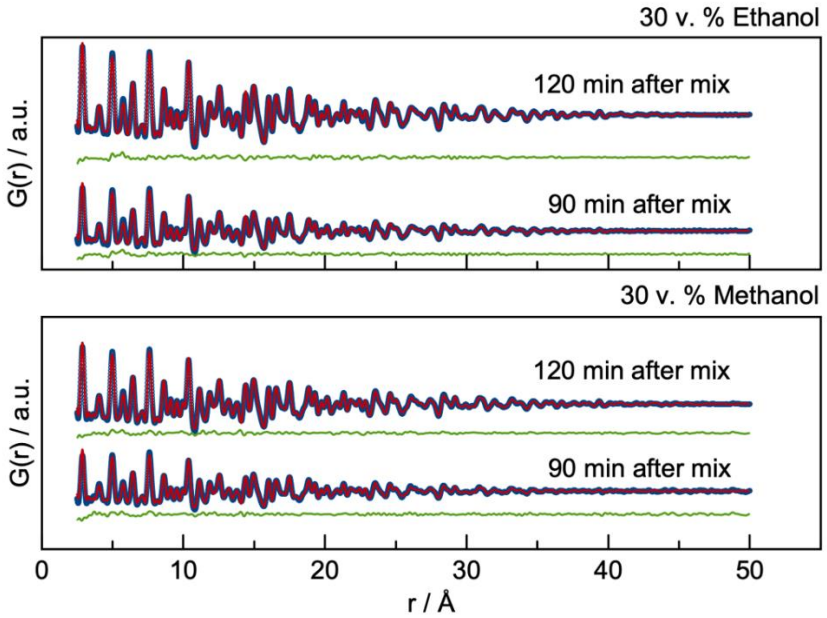

Figure S11. PDF analysis using the Au *fcc* structural model showing (blue) data, (red) fit and (green) difference between data and fit for the Au nanostructure obtained at the different time of synthesis. Refinement parameters are given in **Table S6**. 50 mM $HAuCl_4$ and 150 mM LiOH were used in 30 v.% ROH in water as indicated and the ROH added last. The experiments were performed at RT.

Table S6. Refinement parameters for PDF analysis of *in situ* studies performed at P02.1 beamline, DESY and presented in **Figure S11**.

	90 min 30 v.% EtOH	**120 min 30 v.% EtOH**	**90 min 30 v.% MeOH**	**120 min 30 v.% MeOH**
Scale Factor	0.099	0.15	0.11	0.16
Fit range	2.5 Å – 50 Å	2.5 Å – 50 Å	2.5 Å – 50 Å	2.5 Å – 50 Å
Number of refined parameters	5	5	5	5
R_w	0.12	0.090	0.15	0.091
Q_{damp} (Å^{-1})	0.049	0.049	0.049	0.049
Q_{broad} (Å^{-1})	0.016	0.016	0.016	0.016
Q_{max} (Å^{-1})	18.0	18.0	18.0	18.0
U_{iso} (Å^2)	0.0088	0.0089	0.0084	0.0088
Lattice par., *a* (Å)	4.07	4.07	4.07	4.07
δ_2 (Å^2)	3.58	3.66	3.41	3.86
Sp-diameter (Å)	75.8	89.6	72.5	89.1

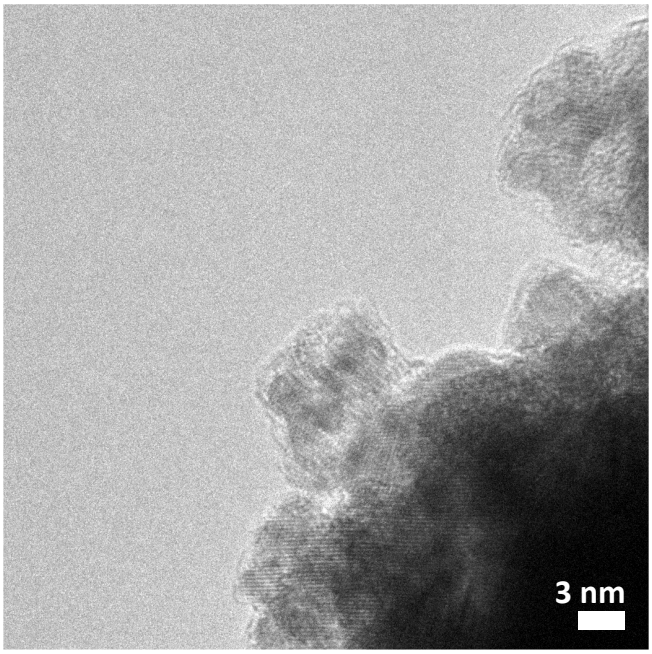

Figure S12. TEM micrograph for Au NMs obtained after 24 hours for the synthesis conditions used for PDF experiments. 50 mM $HAuCl_4$ and 150 mM LiOH were used in 30 v.% EtOH in water and the ROH added last. The experiment was performed at RT.

SG. Influence of the temperature

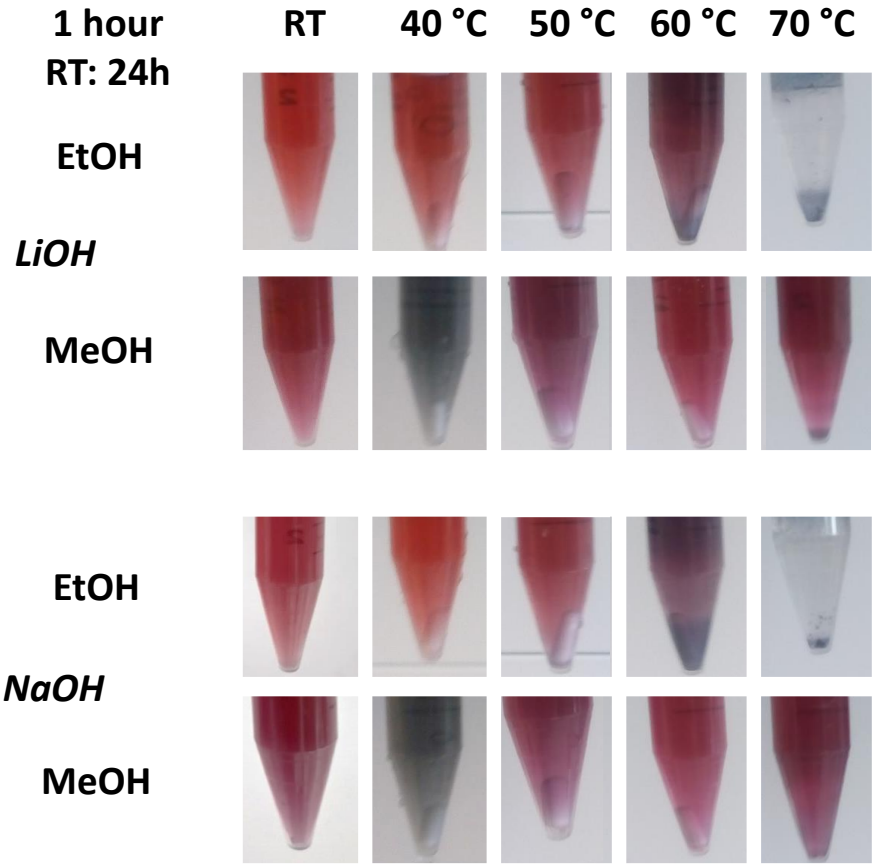

Figure S13. Pictures of Au NP dispersions obtained with 0.5 mM $HAuCl_4$ and 2 mM of base (molar ratio Base/Au of 4) in 30 v.% ROH, where the nature of ROH, base and temperature of the experiments is indicated. The samples were left 1 hour at the indicated temperature and then 23 hours at ambient light and RT, or 24 hours at RT. The pictures correspond to the sample after 1 hour at a given temperature, or after 24 hours in the case of the RT-synthesis.

Table S7. Physical characteristics of the Au NPs obtained using 1 hour treatment at moderate temperature. The syntheses were performed with 0.5 mM $HAuCl_4$ and 2 mM base (molar ratio Base/Au of 4).

ROH	H_2O v.%*	ROH v.%*	Base	V mL*	T °C	t h	λ_{spr} ($\Delta\lambda/\lambda_{spr}$) nm	A_{spr}/A_{450}	Relative yield **	A_{650}/A_{spr}	A_{380}/A_{800}	d_N nm	d_S nm	d_V nm	PdI
EtOH	70	30	LiOH	13	RT	24	516 (6.2%)	1.55	0.96	0.10	28.8	9.2 ± 2.4	10.4	11.1	0.07
					40-RT	1-23	516 (6.6%)	1.55	1.00	0.13	24.2	-	-	-	-
					50-RT	1-23	517 (6.6%)	1.55	1.00	0.17	12.0	9.2 ± 2.6	10.7	11.5	0.08
					60-RT	1-23	524 (9.0%)	1.45	0.70	0.49	3.7	10.3 ± 2.3	11.3	11.8	0.05
					70-RT	1-23	X	X	X	X	X	X	X	X	X
MeOH					RT	24	529 (5.5%)	1.89	0.97	0.11	32.3	21.8 ± 7.4	26.6	28.7	0.12
					40-RT	1-23	535 (6.9%)	1.92	0.92	0.18	13.3	-	-	-	-
					50-RT	1-23	533 (6.6%)	1.92	0.94	0.13	20.3	21.4 ± 9.5	29.6	33.5	0.20
					60-RT	1-23	530 (6.3%)	1.95	1.00	0.11	26.0	21.8 ± 8.5	27.7	30.0	0.15
					70-RT	1-23	530 (6.1%)	1.99	0.72	0.12	18.6	25.6 ± 10.0	33.9	38.0	0.15
EtOH			NaOH		RT	24	517 (6.4%)	1.57	0.72	0.12	20.0	9.9 ± 2.3	11.0	11.5	0.05
					40-RT	1-23	518 (6.2%)	1.61	0.96	0.09	35.67	11.0 ± 3.5	13.3	14.3	0.10
					50-RT	1-23	519 (6.6%)	1.57	1.00	0.16	18.50	9.5 ± 2.9	11.2	12.0	0.09
					60-RT	1-23	532 (19.0%)	1.39	0.59	0.78	1.68	13.0 ± 3.8 + Chunks	15.6	17.8	0.09
					70-RT	1-23	X	X	X	X	X	-	-	-	-
MeOH					RT	24	534 (7.0%)	1.87	1.00	0.22	10.9	23.4 ± 6.8 + Chunks	X	X	0.08
					40-RT	1-23	536 (7.1%)	1.91	0.95	0.21	9.6	27.4 ± 5.7	29.6	30.8	0.04
					50-RT	1-23	532 (6.5%)	1.92	0.99	0.13	20.2	28.6 ± 6.8	31.9	33.4	0.06
					60-RT	1-23	534 (6.6%)	1.93	0.98	0.14	19.8	23.2 ± 11.9	35.9	44.0	0.26
					70-RT	1-23	529 (5.7%)	1.90	0.72	0.21	5.4	25.2 ± 10.5	34.3	39.7	0.17

* before volume contraction; ** evaluated as the ratio of A_{400} for the sample and the maximum values of A_{400} for the dataset at a given v.% of ROH.

Background. In order to develop on the one hand faster syntheses and on the other hand syntheses less dependent to light, the effect of temperature was investigated, see **Figure S13** and **Table S7**. Consistent with the results gathered in the previous **Tables**, Au NPs synthesized using EtOH are smaller than those obtained using MeOH, the former being around 10 nm in diameter and the later around 20 nm.

Results. Using EtOH, for temperatures up to 60 °C the synthesis leads to colloidal dispersions, whereas at 70 °C no colloids are obtained any more, instead larger black materials that are not stable are observed that were not investigated further, see **Figure S13**. Note that there was no incentive for this study and at this stage to optimize the time spent at a given temperature to obtain stable colloidal Au NPs. The time required to observe the formation of the red dispersions of colloidal Au NPs becomes shorter as the temperature increases. While it takes between ca. 1.5 hours to 2 hours to observe this red color at RT, this happens in ca. 5-10 min at 50 °C, both using NaOH and LiOH. However, when the synthesis is performed at 60 °C, while relatively more stable NPs were obtained using LiOH, the overall colloidal stability was poor as characterized by higher A_{650}/A_{spr} and lower A_{380}/A_{800} values. It was concluded that with EtOH as reducing agent, a maximum temperature of 50 °C is to be preferred to speed up the reaction.

Using MeOH, the reaction also proceeds faster as the temperature increases. A difference is that the synthesis using MeOH still leads to colloids up to 70 °C (which is above the theoretical boiling point of MeOH in the closed PP container) and the size of the NPs (especially the size distribution) tends to increase as the temperature increases. This makes MeOH a more robust reducing agent in the sense that a larger parameter space successfully leads to Au NPs, in terms of water content, see **section SC. Effect of mono-alcohol, mono-alcohol content and cation**, and in terms of temperature range. However, the NPs obtained are relatively large using MeOH, ca. 20 nm in diameter.

Conclusion. There is a correlation between the resulting size of the NPs and the kinetics of the reaction since the smallest NPs are obtained using EtOH where the reaction happens faster than when MeOH is used, for comparable reaction conditions, see also **section SF. Kinetics of the reduction**. However, while a higher temperature considerably reduces the time needed to form the NPs, it provides a relatively poor size control on the NPs formed. Importantly for later discussion and achievements, the NP size is more controlled by the nature of the reducing agent than the temperature.

SH. Influence of base concentration

Background. Since temperature, see **section SG. Influence of the temperature**, does not lead to efficient size control we now turn to the effect of 'pH'. Since we here have alcohols-water mixture where pH is not a well-defined variable, we prefer to quote the expected experimental concentration of base and therefore the Base/Au molar ratio, see **Figure S14** and **Table S8**.

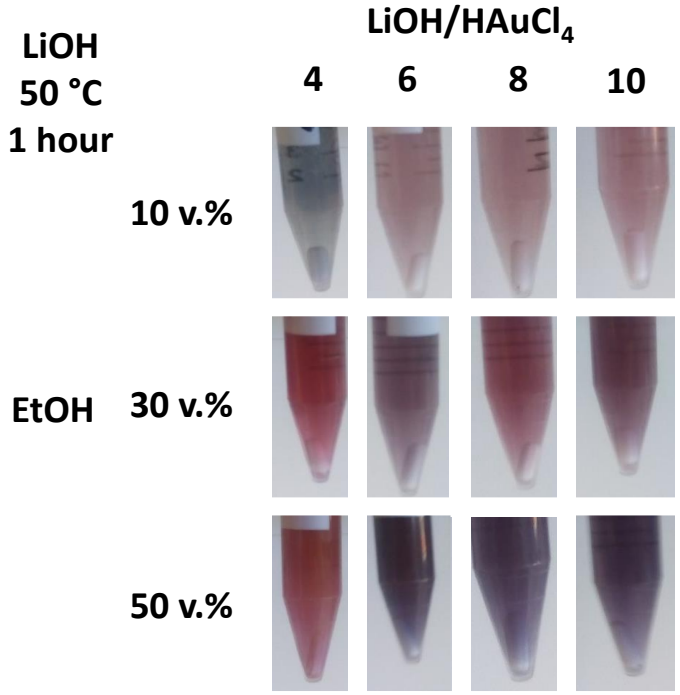

Figure S14. Pictures of Au NP dispersions obtained with 0.5 mM $HAuCl_4$ with EtOH and LiOH, for different EtOH contents and 1 hour treatment at 50 °C. The samples were left for 1 hour at the indicated temperature and then 23 hours at ambient light and RT.

Table S8. Physical characteristics of the Au NPs obtained using 1 hour treatment at 50 °C for different EtOH v.% ratios and Base/$HAuCl_4$ molar ratios. The synthesis was performed using 30 v.% EtOH with 0.5 mM $HAuCl_4$ and LiOH as base.

Table S8A. Data for 10 - 30 v.% EtOH.

ROH v.%*	**H_2O** v.%*	**ROH** v.%*	**LiOH** mM*	**V** mL*	**T** °C	**t** h	**LiOH/Au** molar ratio	**λ_{spr}** ($\Delta\lambda/\lambda_{spr}$) nm	**A_{spr}/A_{450}**	**Relative yield** **	**A_{650}/A_{spr}**	**A_{380}/A_{800}**	**d_N** nm	**d_S** nm	**d_V** nm	**PdI**
EOH	90	10	2	13	50-RT	1-23	4	548 (9.5 %)	1.65	1.00	0.50	2.7	-	-	-	-
			3				6	538 (13.0 %)	1.29	0.41	0.70	1.4	-	-	-	-
			4				8	532 (11.3 %)	1.26	0.39	0.64	1.5	-	-	-	-
			5				10	553 (13.6 %)	1.43	0.49	0.79	1.2	-	-	-	-
	80	20	1				2	544 (6.5 %)	1.98	0.54	0.29	3.3	> 40	-	-	-
			2				4	518 (6.2 %)	1.63	1.00	0.08	36.3	10.1 ± 2.7	11.5	12.2	0.07
			3				6	543 (13.4 %)	1.37	0.68	0.70	1.7	5.9 ± 1.7 + > 50	X	X	0.08
			4				8	536 (10.8 %)	1.40	0.54	0.50	2.8	5.4 ± 4.9 + > 50	X	X	0.82
			5				10	533 (10.3 %)	1.37	0.45	0.41	2.9	5.0 ± 1.5 + > 100	X	X	0.09
	70	30	1				2	542 (6.6 %)	2.02	0.52	0.19	20.9	> 100	X	X	X
			1.5				3	539 (8.0 %)	1.84	1.00	0.17	18.6	> 40	X	X	X
			1.75				3.5	523 (6.4 %)	1.69	0.90	0.09	35.4	11.7 ± 3.5	13.9	15.2	0.09
			2				4	523 (6.5 %)	1.63	0.85	0.17	29.4	9.3 ± 2.8	11.02	11.9	0.09
								517 (6.6%)	1.55	0.88	0.17	12.0	9.2 ± 2.6	10.7	11.5	0.08
								522 (6.7 %)	1.65	0.76	0.17	16.6	8.5 ± 2.1	9.5	9.9	0.06
			2.25				4.5	539 (12.2 %)	1.48	0.50	0.52	4.6	7.6 ± 2.6 Not spherical	9.5	10.4	0.12
			2.5				5	543 (12.2 %)	1.48	0.44	0.48	4.9	7.6 ± 3.9 Not spherical	13.5	18.7	0.26
			2.75				5.5	535 (10.2%)	1.46	0.38	0.36	4.3	7.0 ± 4.6 Not spherical	17.8	30.0	0.43
			3				6	549 (15.6%)	1.39	0.49	0.68	1.9	8.5 ± 2.3 + > 100 Not all spherical	X	X	0.07
			4				8	537 (11.4%)	1.41	0.60	0.50	2.5	7.9 ± 2.7 + > 100 Not spherical	X	X	0.12
			5				10	557 (17.2%)	1.44	0.69	0.77	1.8	7.0 ± 2.6 + > 100	X	X	0.14

* before volume contraction; ** evaluated as the ratio of A_{400} for the sample and the maximum values of A_{400} for the dataset at a given v.% of ROH.

Table S8B. Data for 50 - 70 v.% EtOH.

ROH v.%*	**H_2O** v.%*	**ROH** v.%*	**LiOH** mM*	**V** mL*	**T** °C	**t** h	**LiOH/Au** molar ratio	**λ_{spr}** ($\Delta\lambda/\lambda_{spr}$) nm	**A_{spr}/A_{450}**	**Relative yield** **	**A_{650}/A_{spr}**	**A_{380}/A_{800}**	**d_N** nm	**d_S** nm	**d_V** nm	**PdI**
EtOH	50	50	2	13	50-RT	1-23	4	560 (9.8%)	1.81	0.24	0.53	1.8	> 70	X	X	X
			3				6	604 (14.1%)	1.80	1.00	0.88	2.4	10 + > 85	X	X	X
			4				8	592 (15.4%)	1.64	1.00	0.84	2.5	9.8 ± 4.7 + Worm + > 50	X	X	0.23
			5				10	572 (18.2%)	1.46	0.75	0.81	2.2	11.6 ± 4.8 Elongated + > 100	X	X	0.17
	30	70	2				4	546 (15.6%)	1.38	0.33	0.85	1.0	> 100	X	X	X
			3				6	594 (18.9%)	1.50	1.00	0.91	1.3	20 + > 100	X	X	X
			4				8	568 (18.4%)	1.41	0.82	0.85	1.2	20 + > 100	X	X	X
			5				10	553 (15.0%)	1.41	0.61	0.83	1.1	> 20	X	X	X

* before volume contraction; ** evaluated as the ratio of A_{400} for the sample and the maximum values of A_{400} for the dataset at a given v.% of ROH.

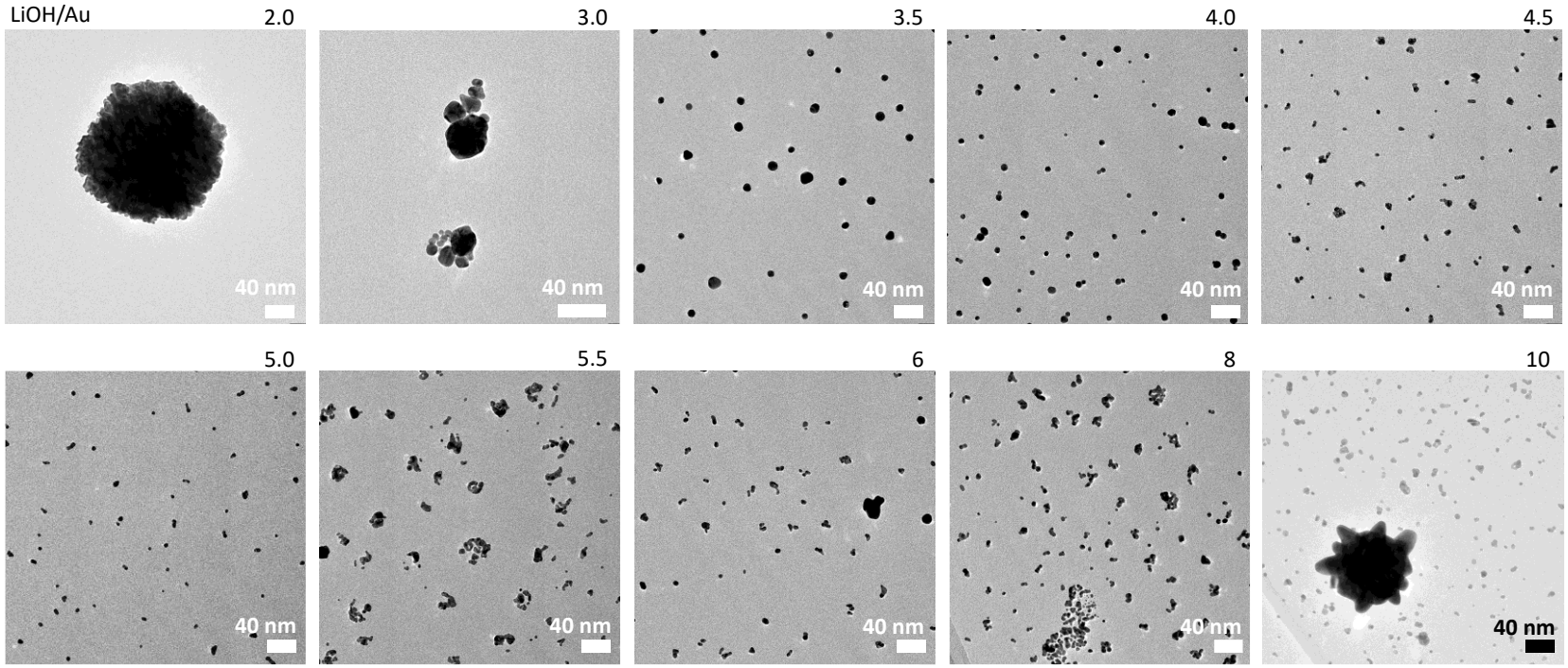

Figure S15. TEM micrographs of Au NPs obtained using 0.5 mM $HAuCl_4$, 30 v.% EtOH for different LiOH/Au molar ratio as indicated. The synthesis was performed with a 1 hour step at 50 °C followed by 23 hours at RT and ambient light.

Table S9. Physical characteristics of the Au NPs obtained using RT conditions or 1 hour treatment at 50 °C for different EtOH or MeOH v.% ratio and base/$HAuCl_4$ molar ratios. The synthesis was performed using 30 v.% ROH with 0.5 mM $HAuCl_4$ and LiOH as base.

ROH	**H_2O** v.%*	**ROH** v.%*	**Base** mM*	**V** mL*	**T** °C	**t** h	**LiOH/Au** molar ratio	**λ_{spr}** ($\Delta\lambda/\lambda_{spr}$) nm	**A_{spr}/A_{450}**	**Relative yield** **	**A_{650}/A_{spr}**	**A_{380}/A_{800}**	**d_N** nm	**d_S** nm	**d_V** nm	**PdI**
EtOH	70	30	1	13	RT	24	2	542 (6.5%)	2.02	0.54	0.20	11.14	-	-	-	-
			2				4	523 (7.5%)	1.64	0.48	0.17	12.60	15.8 ± 3.9	17.7	18.7	0.06
			2.5				5	527 (11.0%)	1.51	0.94	0.37	7.69	8.2 ± 4.0	12.7	15.3	0.24
			3				6	559 (21.6%)	1.34	1.00	0.84	1.68	Network (15)	X	X	X
			4				8	560 (28.0%)	1.29	0.67	0.93	1.24	Network (10-20) + >100	X	X	X
			5				10	678 (xx%)	1.37	0.59	0.99	0.88	10 + > 1000	X	X	X
MeOH	70	30	1	13	RT	24	2	X	X	X	X	X	-	-	-	-
			2				4	534 (6.9%)	0.85	1.00	0.24	8.62	-	-	-	-
			3				6	523 (8.1%)	0.69	0.64	0.33	3.23	-	-	-	-
			4				8	528 (10.8%)	1.38	0.34	0.51	2.18	-	-	-	-
			5				10	528 (11.6%)	1.33	0.27	0.58	1.88	-	-	-	-
MeOH	70	30	1	13	50-RT	1-23	2	X	X	X	X	X	-	-	-	-
			2				4	534 (6.6%)	1.92	1.00	0.15	19.8	-	-	-	-
			3				6	536 (11.9%)	1.42	0.56	0.54	2.2	-	-	-	-
			4				8	545 (15.0%)	1.36	0.30	0.71	1.7	-	-	-	-
			5				10	537 (14.5%)	1.30	0.19	0.65	1.8	-	-	-	-

* before volume contraction; ** evaluated as the ratio of A_{400} for the sample and the maximum values of A_{400} for the dataset at a given v.% of ROH.

The influence of the base concentration was also investigated using MeOH with a temperature treatment at 50 °C and using MeOH at RT, as well as by using EtOH for a RT-synthesis with a 30 v.% ROH content, see **Table S9**. An optimal LiOH/Au molar ratio is also found to be around 4-5 if EtOH is used (at lower and higher ratios no stable colloids are formed). The effect of the base concentration in MeOH seems less pronounced (based on the value of λ_{spr} and the lack of its variation with 'pH'). This further suggests that MeOH is a more robust reducing agent leading to the same NP size of around 20 nm over a wide range of experimental conditions. This is probably related to the relatively slow kinetics of the reaction regardless of the experimental conditions.

Table S10. Physical characteristics of the Au NPs obtained using 1 hour treatment at 50 °C and KOH.

ROH	H_2O v.%*	ROH v.%*	$HAuCl_4$ mM*	Base	Base mM*	V mL*	T °C	t h	Base/Au molar ratio	λ_{spr} ($\Delta\lambda/\lambda_{spr}$) nm	A_{spr}/A_{450}	Relative Yield **	A_{650}/A_{spr}	A_{380}/A_{800}	d_N nm	d_S nm	d_V nm	PdI
EtOH	70	30	0.5	KOH	1	13	50-RT	1-23	2	601 (25%)	1.59	0.4	0.97	1.1	99.5 ± 38.5	127.3	139.5	0.15
					2				4	521 (6.3%)	1.67	1.00	0.12	25.6	12.8 ± 3.4	14.6	15.5	0.07
					3				6	540 (10.2%)	1.50	0.69	0.48	3.7	7.4 ± 2.3	X	X	0.10
					4				8	536 (10.8%)	1.42	0.54	0.41	4.1	7.3 ± 2.8 + > 50	X	X	0.15
					5				10	542 (16.1%)	1.29	0.54	0.78	1.3	6.4 ± 2.8 > 50	X	X	0.1

* before volume contraction; ** evaluated as the ratio of A_{400} for the sample and the maximum values of A_{400} for the dataset at a given v.% of ROH.

To confirm the effect of the Base/Au molar ratio and illustrate further the influence of the base cation, a different base was used: KOH, see **Table S10** and **Figure S16**. The same trends were observed. There seems to be an optimal concentration of base at around 2 mM to obtain stable colloidal Au NPs when 0.5 mM $HAuCl_4$ is used (KOH/Au molar ratio of 4). A KOH concentration of 3 mM (KOH/Au molar ratio of 6) leads to smaller NPs, but the colloids were less stable, as reflected by the higher A_{650}/A_{spr} and lower A_{380}/A_{800} values. In the case of KOH used as base, agglomeration and/or presence of large structure > 100 nm in size was especially clear as the concentration of base increases. The colloidal dispersions prepared with KOH were also only stable for few days as opposed to dispersions prepared with LiOH or NaOH. This observation is in line with previous studies on the effects of cation on surfactant-free PM (Pt) NPs.[17]

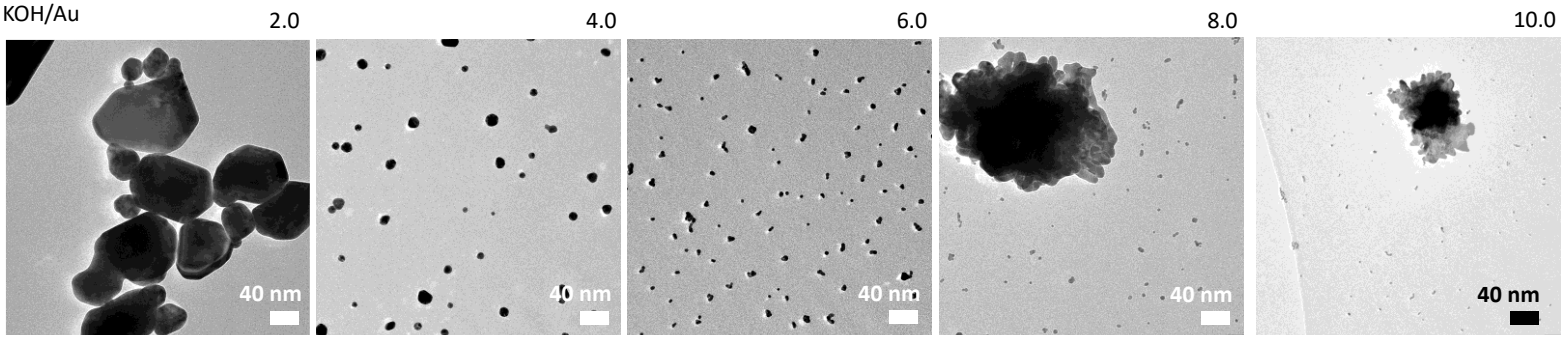

Figure S16. TEM micrographs of Au NPs obtained using 0.5 mM $HAuCl_4$, 30 v.% EtOH for different KOH/Au molar ratio as indicated. The syntheses were performed with a 1 hour step at 50 °C followed by 23 hours at RT and ambient light.

SI. Influence of gas atmosphere

Background. Gas atmosphere is often reported to influence the outcome of NP syntheses. In the following, the effect of using N_2 to degas the solution was investigated. For the synthesis at RT, the mixtures of water, ROH and base were left with a stream of N_2 to bubble under stirring for 15 minutes before $HAuCl_4$ was added, still under stirring. The flow of N_2 was maintained for 2 hours in the case of EtOH and 6 hours in the case of MeOH used as reducing agents, before the N_2 flow was stopped and the containers were capped with the dedicated cap of the centrifuge tube (15 mL) used as containers and further sealed with Parafilm®. Stirring was pursued for a total reaction time of 24 hours at RT and ambient light.

For the synthesis at 50 °C, the mixtures of water, ROH and base were left with a stream of N_2 to bubble under stirring for 15 minutes at RT and a further 15 minutes at 50 °C, before $HAuCl_4$ was added at 50 °C, still under stirring. The flow of N_2 was maintained for 15 minutes in the case of EtOH and MeOH used as reducing agents, before the N_2 flow was stopped and the containers were capped with the dedicated cap of the centrifuge tubes (15 mL) that were used as containers and further sealed with Parafilm®. Stirring was pursued for 15 minutes at 50 °C in the case of EtOH and 45 minutes in the case of MeOH used as reducing agents, and then the samples were left at RT and ambient light for a total synthesis time of 24 hours before further characterization. The total time at 50 °C was then 30 minutes when EtOH was used and 1 hour when MeOH was used.

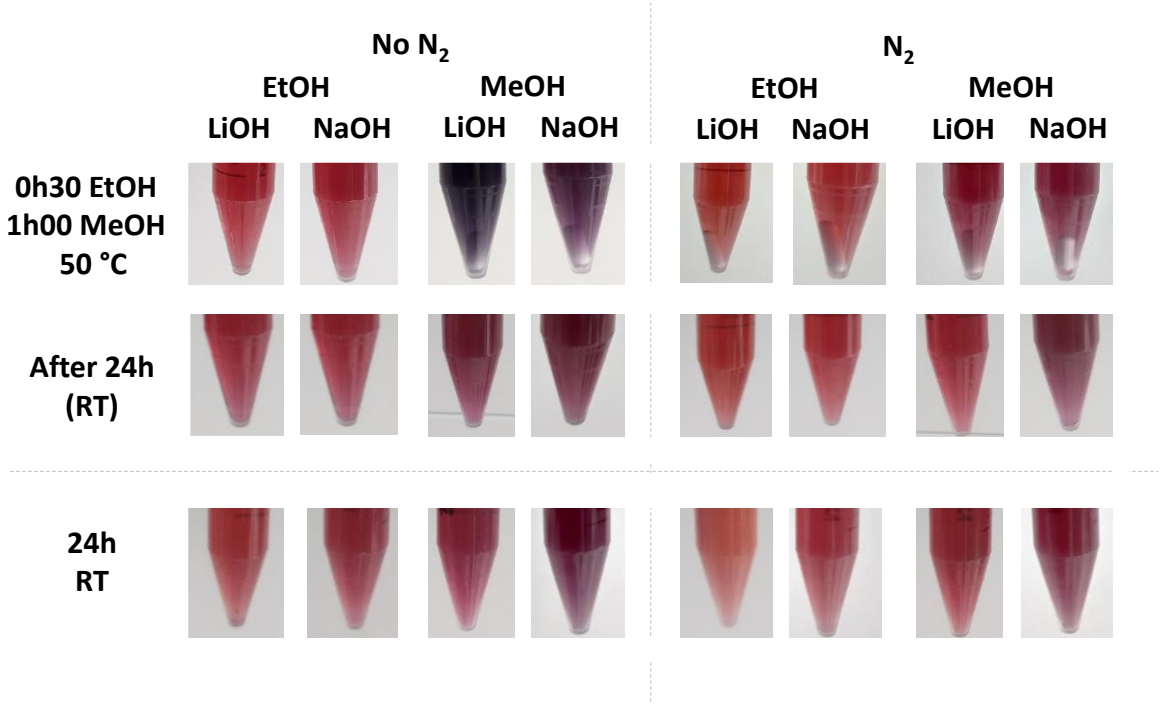

Figure S17. Pictures of colloidal Au NP dispersions obtained for different experimental conditions as indicated from 0.5 mM $HAuCl_4$ and 2 mM of base (Base/Au molar ratio of 4) in 30 v.% ROH. The influence of using N_2 in the reaction is investigated. The first two rows correspond to the pictures of the same dispersion after 30 minutes at 50 °C for EtOH used as reducing agent and 1 hour for MeOH used as reducing agent (1^{st} row), and after being left a day at RT and light (2^{nd} row). The last row corresponds to experiments performed at RT, after 24 hours of reaction.

Table S11. Physical characteristics of the Au NPs obtained using no gas or N_2 for 30 v.% ROH, 0.5 mM $HAuCl_4$ and 2 mM of base.

ROH	**Base**	**V** mL*	**T** °C	**t** h	**Base/Au** molar ratio	**N_2**	**λ_{spr}** ($\Delta\lambda/\lambda_{spr}$) nm	**A_{spr}/A_{450}**	**Relative yield** **	**A_{650}/A_{spr}**	**A_{380}/A_{800}**	**d_N** nm	**d_S** nm	**d_V** nm	**PdI**
EtOH	LiOH	6.5	RT	24	4	NO	521 (6.4%)	1.60	0.78	0.13	11.3	11.6 ± 2.5	12.6	13.2	0.05
						YES (2 h)	**529 (10.2%)**	1.36	0.74	0.70	1.7	7.5 ± 1.5	8.1	8.4	0.04
	NaOH					NO	524 (6.8%)	1.60	0.86	0.21	6.2	15.3 ± 4.4	18.3	20.5	0.08
						YES (2 h)	522 (6.9)	1.55	0.95	0.16	12.3	10.0 ± 2.0	10.8	11.2	0.04
MeOH	LiOH					NO	534 (6.6%)	1.82	0.89	0.14	21.2	22.4 ± 6.6	26.3	28.2	0.09
						YES (6 h)	522 (6.2%)	1.66	0.98	0.11	27.8	13.2 ± 3.6	15.4	17.0	0.08
	NaOH					NO	540 (8.1%)	1.79	0.92	0.24	14.6	19.4 ± 7.9	26.2	30.0	0.17
						YES (6 h)	537 (7.4%)	1.76	0.94	0.23	13.3	14.4 ± 5.0	18.6	21.8	0.12
EtOH	LiOH	6.5	50-RT	0.5-23.5	4	NO	523 (6.4%)	1.69	0.99	0.10	32.3	10.0 ± 3.9	13.2	14.7	0.16
						YES (0.25 h)	516 (6.6%)	1.49	0.99	0.09	26.0	7.3 ± 1.6	8.0	8.4	0.05
	NaOH					NO	524 (6.0%)	1.75	1.00	0.09	25.8	16.3 ± 3.9	18.1	19.0	0.06
						YES (0.25 h)	521 (6.4%)	1.58	1.00	0.09	32.5	11.0 ± 2.8	12.4	12.9	0.07
MeOH	LiOH					NO	533 (7.2%)	1.82	1.00	0.17	23.7	15.2 ± 10.7	32.2	40.9	0.50
						YES (0.25 h)	524 (6.2%)	1.82	0.99	0.11	28.4	11.5 ± 3.1	13.1	14.0	0.07
	NaOH					NO	540 (8.1%)	1.79	0.93	0.26	10.2	21.7 ± 7.6	26.7	28.9	0.12
						YES (0.25 h)	542 (7.7%)	1.82	0.99	0.29	9.3	14.6 ± 5.5	19.7	24.0	0.14
EtOH	LiOH	6.5	50-RT	0.5-23.5	4	YES (0.5 h)	515 (6.8%)	1.44	1.00	0.10	26.8	6.8 ± 1.7	7.6	8.0	0.06

* before volume contraction; ** evaluated as the ratio of A_{400} for the sample and the maximum values of A_{400} for the dataset at a given v.% of ROH. The sample highlighted in bold show a different optical behavior in absorption and transmission.

Results. From this dataset, it is further confirmed that smaller NPs are obtained in EtOH *versus* MeOH, see **Figure S17** and **Table S11**. At RT and without N_2, the combination LiOH/EtOH gives smaller NPs than NaOH/EtOH. However, NaOH/MeOH gives smaller NPs than LiOH/MeOH. This corresponds well to the kinetics of the reaction observed where the time needed to observe a color change increased as EtOH/LiOH < EtOH/NaOH < MeOH/NaOH < MeOH/LiOH.

At RT, the effect of N_2 is to lead to smaller NPs. This is especially clear when MeOH is used. The effect of N_2 purge is even more pronounced at 50 °C especially when LiOH is used. The solution turned to red much faster than at RT in agreement with results presented in **section SG. Influence of the temperature**. This points towards the effect of N_2 at the beginning of the reaction only. The NPs characterized by the lowest λ_{spr} in this study were obtained using LiOH and EtOH using a step at 50 °C with N_2. A control experiments using LiOH and EtOH 30 v.% was performed with 30 minutes of N_2 and similar results obtained as for only 15 minutes of N_2 during the synthesis, which suggests that the effect of N_2 is key in the first step(s) only of the reaction. The sample obtained at RT in LiOH/EtOH in presence of N_2 show an interesting optical behavior similar to what will be discussed in section **SJ. Influence of the order of addition of the chemicals**.

Conclusion. While using N_2 leads to a relative size control towards smaller NP sizes, especially at 50 °C and using LiOH and EtOH, this is not a convenient route to achieve size control since it requires a relatively complex set up using gases, ultimately impairing a simple scale up and large-scale production due to the related costs. However, it seems that N_2 is needed mainly at the beginning of the reaction which may allow designing protocols requiring little amount of gas. A focus is given below to syntheses without the need for any gas due to the simplicity (and cost-efficiency) of this approach.

SJ. Influence of the order of addition of the chemicals

There is no report to our knowledge on the influence of the order of addition for alcohol-based synthesis, see **Table S1**. We here investigated the effect of the order of addition of the chemicals.

SJ-A. Effect of the order of addition on the colloidal Au NPs

The outcome of the synthesis strongly depends on the order of addition of the chemicals for experiments performed at 50 °C, see **Figure S18**, at RT, see **Figure S19**, and using different ROH, see **Figure SFigure S20**.

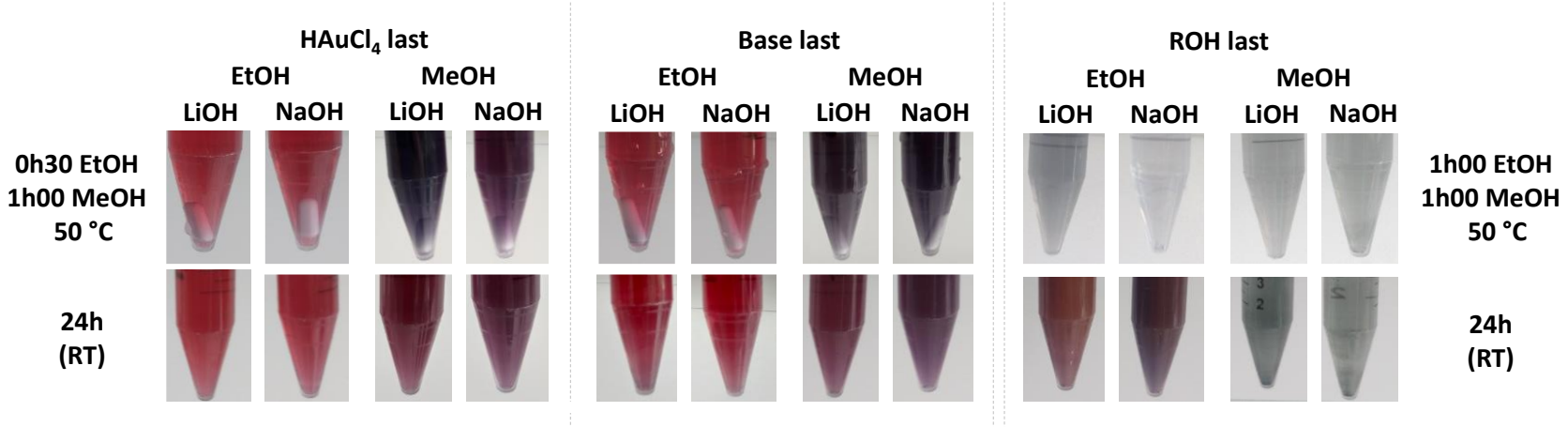

Figure S18. Pictures of colloidal Au NP dispersions obtained for different experimental conditions as indicated from 0.5 mM $HAuCl_4$ and 2 mM of base (Base/Au molar ratio of 4) in 30 v.% ROH. The influence of the order of addition of the chemicals is investigated. The left panel corresponds to a case where $HAuCl_4$ was added last. The middle panel corresponds to a case where the Base was added last. The right panel correspond to a case where the ROH was added last. The first row corresponds to pictures of the dispersions after 30 minutes at 50 °C for EtOH used as reducing agent when $HAuCl_4$ or the base was added last (left and middle panel) and 1 hour for MeOH used as reducing agent. On the right panel the reaction was left to react for 1 hour for both EtOH and MeOH. The second row corresponds to the same experiments left then for a day at RT and ambient light.

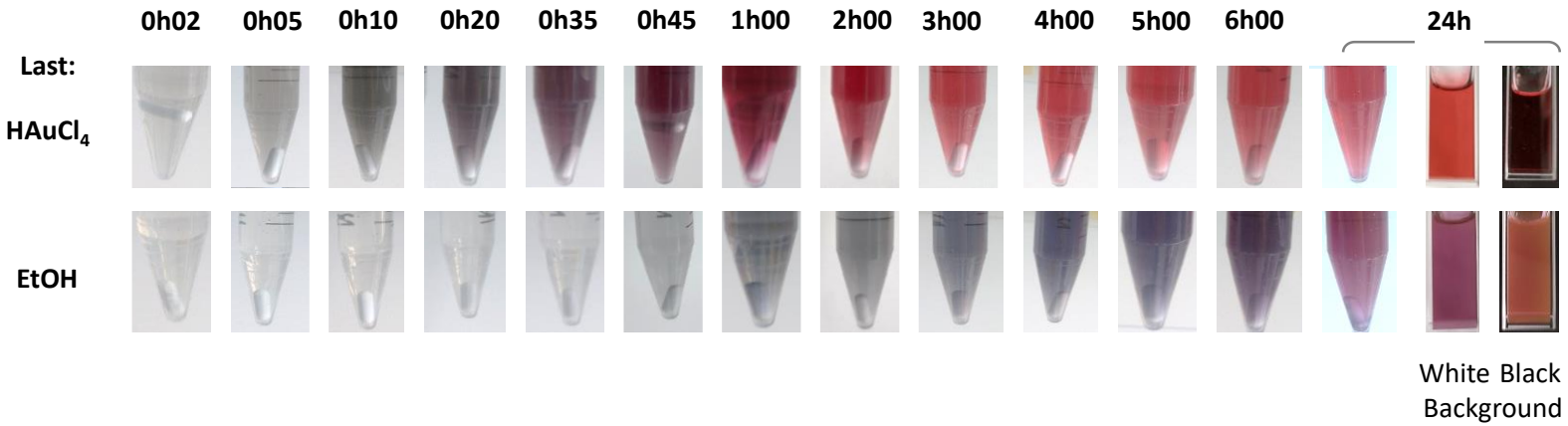

Figure S19. Pictures of colloidal Au NP dispersions obtained for different experimental conditions as indicated from 0.5 mM $HAuCl_4$ and 2 mM LiOH (molar ratio LiOH/Au of 4) in 30 v.% EtOH at RT. The influence of the order of addition of the chemicals is investigated. The pictures were taken at different times of the synthesis. In the panel corresponding to 24 hours the last 2 rows correspond to the colloid in UV-vis cuvettes (1 cm width) where a white or a black background, as indicated, were used for the pictures.

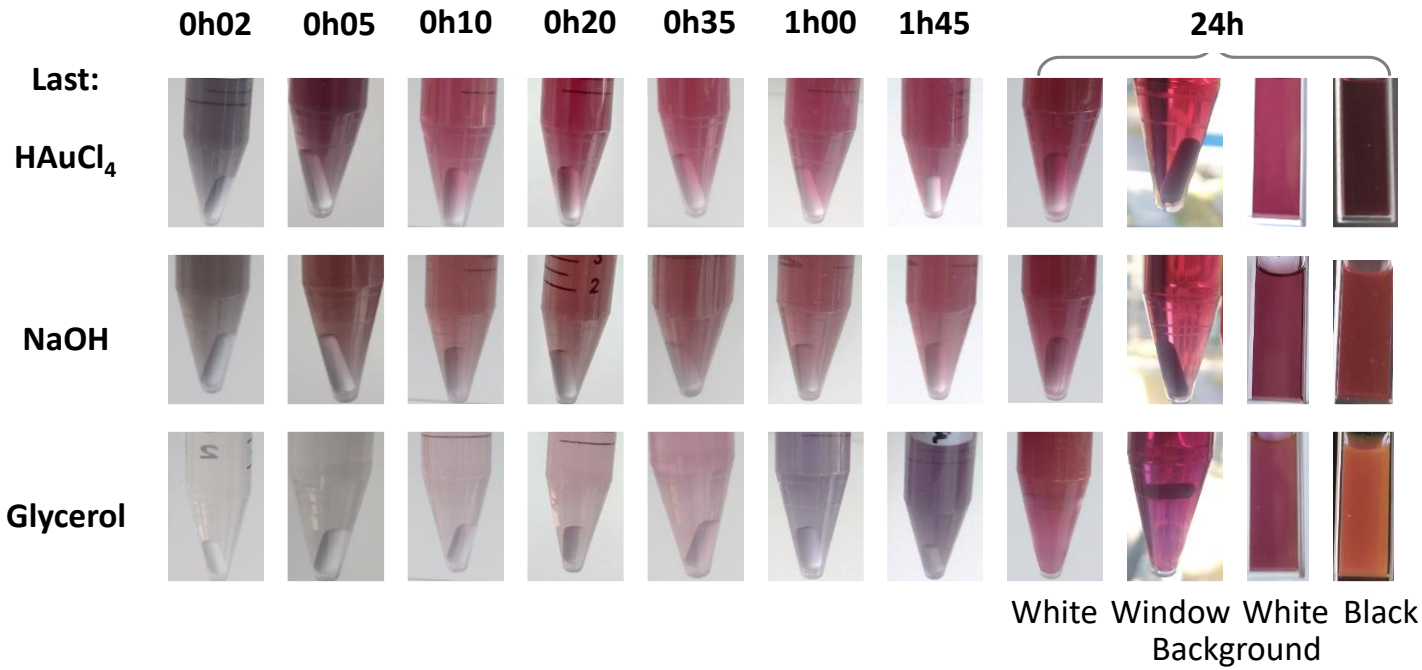

Figure S20. Pictures of colloidal Au NP dispersions obtained for different experimental conditions as indicated from 0.5 mM $HAuCl_4$ and 2 mM NaOH (NaOH/Au molar ratio of 4) in 30 v.% glycerol at RT. The influence of the order of addition of the chemicals is investigated. The pictures were taken at different times of the synthesis. In the panel corresponding to 24 hours different backgrounds were used for the pictures and the last two rows correspond to the colloids in UV-vis cuvettes (1 cm path length).

Table S12. Physical characteristics of the Au NPs obtained for different order of addition of the chemicals. 30 v.% ROH, 0.5 mM $HAuCl_4$ and 2 mM of base were used.

ROH	Base	V mL*	T °C	t h	Base/Au molar ratio	Added last	λ_{spr} ($\Delta\lambda/\lambda_{spr}$) nm	A_{spr}/A_{450}	Relative Yield **	A_{650}/A_{spr}	A_{380}/A_{800}	d_N nm	d_S nm	d_V nm	PdI
EtOH	LiOH	6.5	50-RT	0.5-23.5	4	$HAuCl_4$	523 (6.4%)	1.69	0.98	0.10	32.3	10.0 ± 3.9	13.2	14.7	0.16
						LiOH	525 (6.7%)	1.72	0.89	0.11	29.5	15.4 ± 4.3	17.9	19.4	0.08
						ROH	**547 (10.7%)**	1.62	0.89	0.61	1.6	> 50	X	X	X
	NaOH					$HAuCl_4$	524 (6.0%)	1.75	0.98	0.09	25.8	16.3 ± 3.9	18.1	19.0	0.06
						NaOH	525 (6.2%)	1.78	0.98	0.08	43.3	19.0 ± 6.9	23.8	26.0	0.13
						ROH	**553 (13.7%)**	1.65	1.00	0.65	2.4	> 50	X	X	X
MeOH	LiOH					$HAuCl_4$	533 (7.2%)	1.82	1.00	0.17	23.7	15.2 ± 10.7	32.2	40.9	0.50
						LiOH	537 (7.7%)	1.74	0.92	0.29	4.2	25.7 ± 7.0	29.6	31.8	0.08
						ROH	-	-	-	-	-	Fractal (20-50)	X	X	X
	NaOH					$HAuCl_4$	540 (8.1%)	1.79	0.93	0.26	10.2	21.7 ± 7.6	26.7	28.9	0.12
						LiOH	545 (8.8%)	1.77	0.93	0.41	5.1	26.9 ± 9.9	33.8	36.9	0.14
						ROH	-	-	-	-	-	Fractal (20-60)	X	X	X
EtOH	LiOH	6.5	RT	24	4	$HAuCl_4$	521 (6.5%)	1.62	0.88	0.09	23.2	12.3 ± 2.7	13.5	14.0	0.05
						ROH	540 (8.0%)	1.84	0.65	0.34	4.1	> 50	X	X	X
	NaOH					$HAuCl_4$	524 (6.8%)	1.60	0.85	0.21	6.2	15.3 ± 4.4	18.3	20.5	0.08
						ROH	550 (9.9%)	1.76	0.47	0.56	2.1	> 50	X	X	X
Glycerol	NaOH	6.5	RT	24	4	$HAuCl_4$	524 (6.9%)	1.64	1.00	0.17	26.6	11.9 ± 3.6	14.1	15.4	0.10
						NaOH	527 (7.4%)	1.56	0.84	0.26	6.2	10.4 ± 3.8	13.3	15.1	0.13
						ROH	**552 (7.2%)**	2.16	0.91	0.27	7.4	> 50	X	X	X

* before volume contraction; ** evaluated as the ratio of A_{400} for the sample and the maximum values of A_{400} for the dataset at a given v.% of ROH. The sample highlighted in bold show a different optical behavior in absorption and transmission.

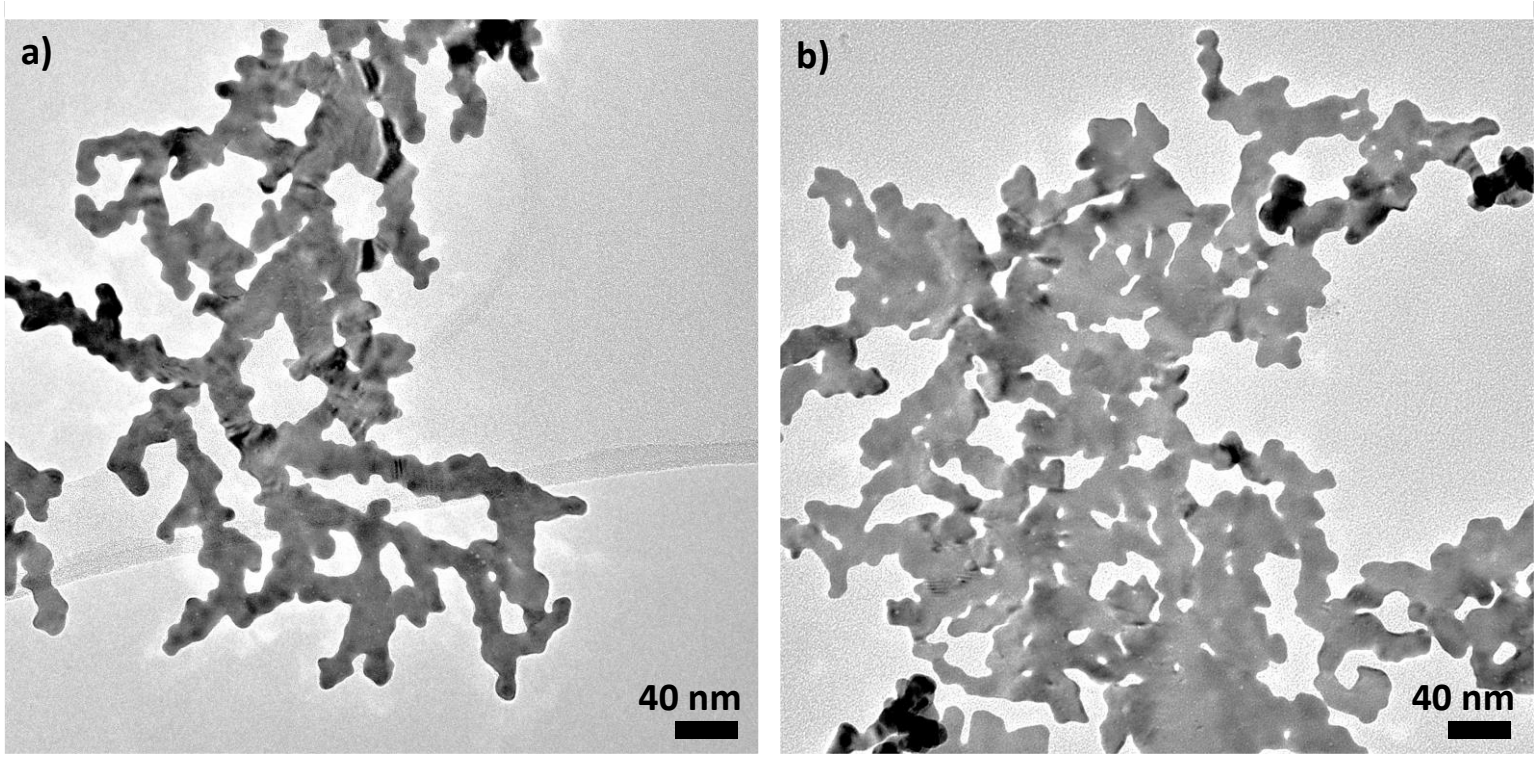

Figure S21. TEM micrographs of Au NMs obtained from 0.5 mM $HAuCl_4$ and 2 mM Base (Base/Au molar ratio of 4) in 30 v.% MeOH using a 1 hour step at 50 °C and adding the ROH last using (a) LiOH and (b) NaOH.

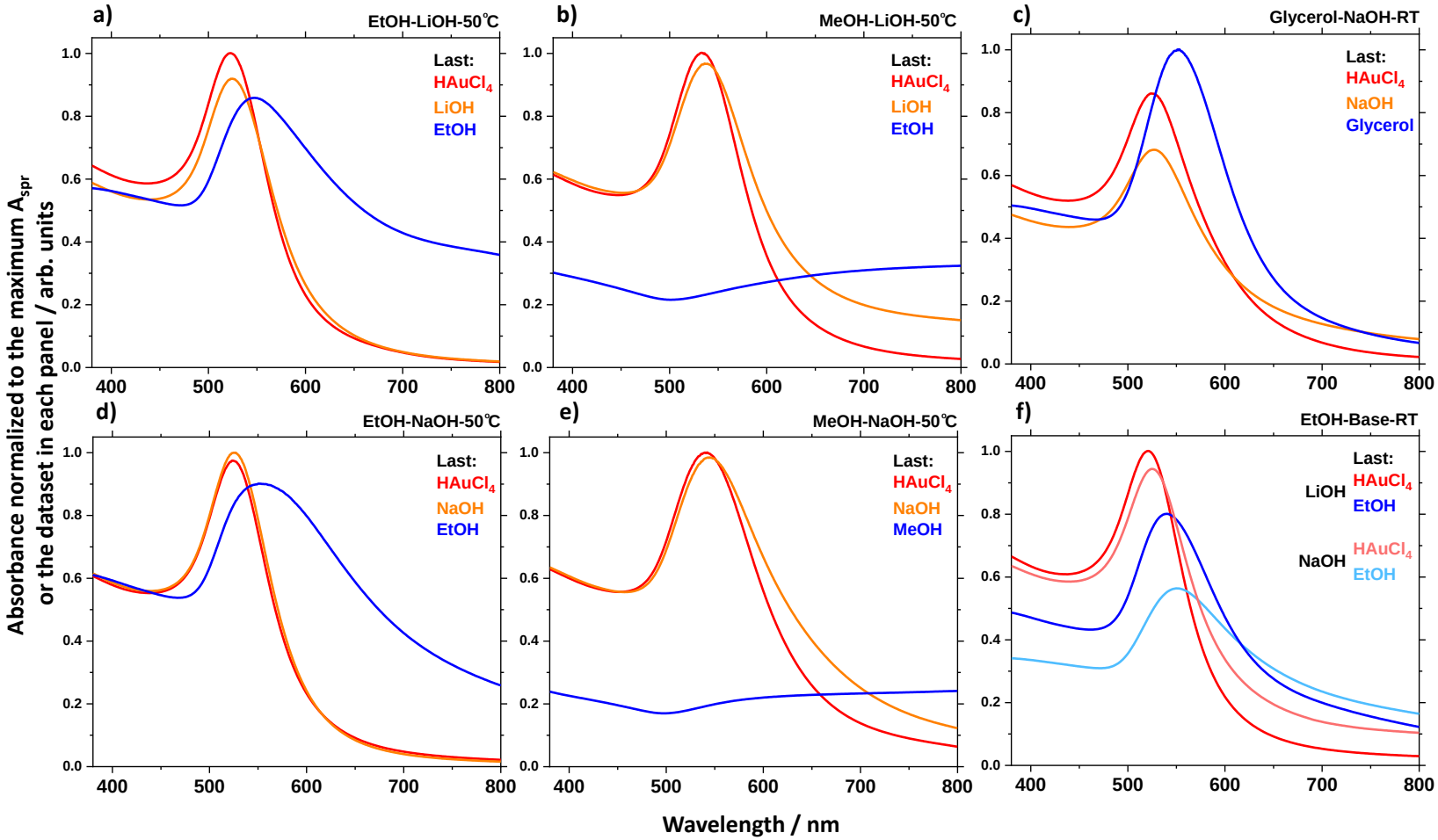

Figure S22. UV-vis spectra for Au colloidal dispersions obtained for different conditions as indicated. See experimental details in **Table S12**.

Results. Regardless of the temperatures used (RT or 50 °C) and regardless of the ROH and base used for the experiments, the NP size increases as the last chemical added is $HAuCl_4$ < Base << ROH, see **Table S12** and **Figure S22**. This is also the order of the time needed to observe a color change from fastest to slowest: $HAuCl_4$ < Base << ROH. While this approach that consists in changing the order of addition of the chemicals is a significant step forward to control the size of the NPs without using a different amount of a given chemical, it has not been reported for the glycerol synthesis,[9] see **Table S1**. We therefore made sure this approach leads to NP of different sizes in glycerol, see **Figure S20**. We confirmed that this effect is also observable at RT using EtOH, see **Figure S19**.

In the case where the ROH is added last, it takes now several hours to see a color change even with treatment at high temperature. In the case of MeOH used as reducing agent, no Au NPs are formed after 24 hours but rather fractal-like NMs, see **Figure S21**. Trying to speed up the reaction in EtOH when EtOH is added last by performing the reaction at 70 °C did not lead to colloids. In addition, the approach using the ROH last was observed to not be as reproducible compared to a case where $HAuCl_4$ or the base was added last (e.g. for 6.5 mL in some cases NPs were obtained, see **Table S12**, in some cases not, see **Table S13**, when ROH was added last).

The relative order of time needed to observe a color change to blue/grey when different chemicals are added last is: $HAuCl_4$ < Base << ROH. It can be concluded that the kinetics of the reaction influence the resulting size. Importantly, the volume of chemical added was 1.9 mL of ROH, 0.222 mL of base (at 57 mM in water) and 0.159 mL of $HAuCl_4$ (at 20 mM in water) for the data set represented in **Table S12**. Therefore, the smaller size also corresponds to a smaller volume of $HAuCl_4$ solution added. To investigate a possible effect of the starting concentration of $HAuCl_4$ in the added volume before addition to an alkaline LiOH solution of EtOH, different EtOH and water mixtures were prepared and different volumes of aqueous $HAuCl_4$ solution at different concentrations were added last. The final concentration when all the chemicals were mixed was always 0.5 mM for $HAuCl_4$ and the final concentration of LiOH was 2 mM in 30 v.% EtOH in water.

The results in **Figure S23** and **Table S13** show that the concentration of $HAuCl_4$ added influences the results. The most promising Au NPs (characterized by a higher A_{spr} and lower λ_{spr} values) were obtained using a concentration of 20 mM (no higher concentrations were investigated). When most of the water is added with $HAuCl_4$ (0.7 mM of $HAuCl_4$) the reaction leads to the same products as a case where EtOH is added last. This makes sense since this is equivalent to adding the EtOH last to a solution containing most of the water and $HAuCl_4$. In that case, the product was a solid material deposited on the PP reactor wall. This illustrates further the poor reproducibility of adding the EtOH last. This result also stresses that adding EtOH last *does* have an effect that goes beyond a simple dilution, since using 1.7 mM $HAuCl_4$ (so a volume of 1.9 mL added last, which is the volume of EtOH used for these experiments) leads to more stable NPs than what is observed if EtOH (1.9 mL) is added last.

Interestingly some NPs obtained show different colors in transmission and absorption as it is detailed in **section SJ-D**.

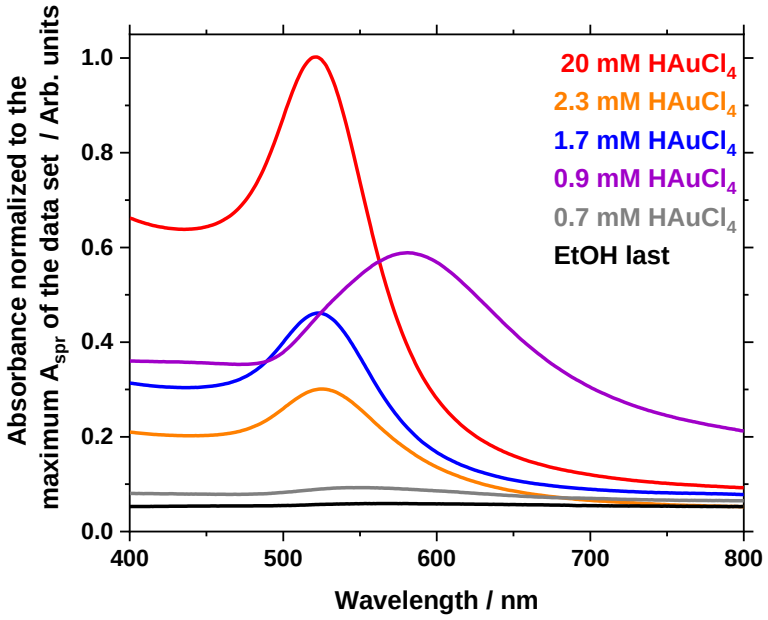

Figure S23. UV-vis spectra of different of the Au NP dispersions obtained at RT when $HAuCl_4$ was added last for different $HAuCl_4$ concentrations in the added solutions, after 24 hours at RT and light, for 30 v.% EtOH. The final concentrations were 0.5 mM $HAuCl_4$ and 2 mM LiOH (molar ratio LiOH/Au of 4), see **Table S13** for experimental details.

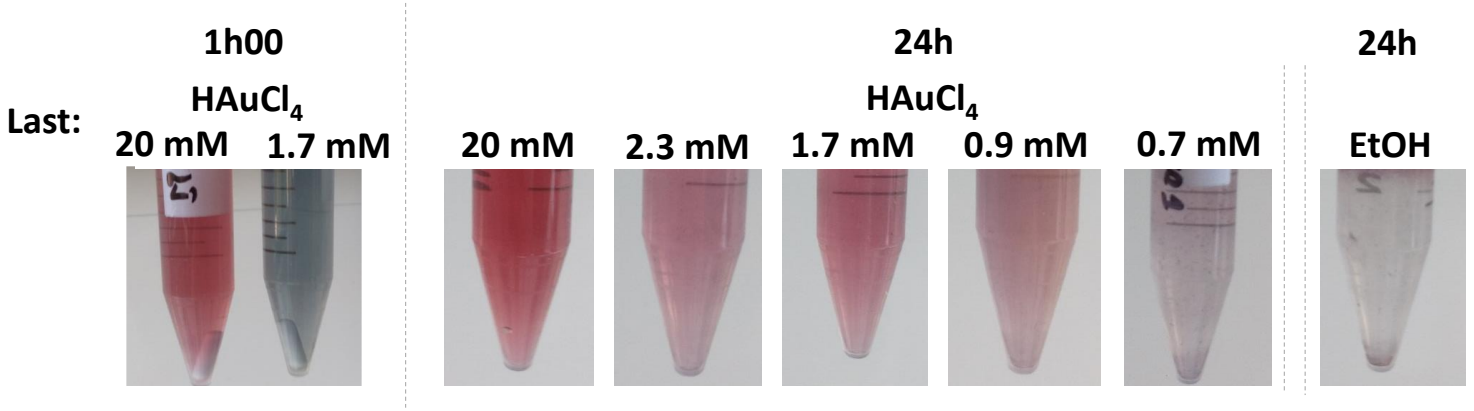

Figure S24. Pictures of Au NP dispersions obtained at RT when $HAuCl_4$ was added last for different $HAuCl_4$ concentrations or when EtOH was added last, for different times of the synthesis, as indicated. The final concentrations were 0.5 mM $HAuCl_4$ and 2 mM LiOH (molar ratio LiOH/Au of 4), see **Table S13** for experimental details.

Table S13. Influence of the $HAuCl_4$ concentration of the added fraction.

ROH	**H_2O** v.%*	**ROH** v.%*	**$HAuCl_4$** mM added last	**$HAuCl_4$** mM*	**Base**	**Base** mM*	**V** mL*	**T** °C	**Base/Au molar ratio**	**λ_{spr}** ($\Delta\lambda/\lambda_{spr}$) nm	**A_{spr}/A_{450}**	**Relative yield** **	**A_{650}/A_{spr}**	**A_{380}/A_{800}**
EtOH	70	30	20	0.5	LiOH	2	6.5	RT	4	521 (6.6%)	1.56	1.00	0.16	7.4
			2.3							526 (8.0%)	1.46	0.32	0.29	4.3
			1.7							523 (7.1%)	1.50	0.48	0.24	4.2
			0.9							**583 (11.7%)**	1.64	0.55	0.71	1.7
			0.7							550 (17.8%)	1.22	0.12	0.82	1.1
EtOH added last	70	30	20	0.5	LiOH	2	6.5	RT	4	[566 (x.x%)]	[1.17]	[0.08]	[1.00]	[1.0]

* before volume contraction; ** evaluated as the ratio of A_{400} for the sample and the maximum values of A_{400} for the dataset at a given v.% of ROH; values under brackets correspond to a case where the signal intensity is low and are purely indicative. The sample highlighted in bold show a different optical behavior in absorption and transmission.

SJ-B. Kinetics of the reaction for different order of addition of the chemicals

Since different colors and sizes are observed for different order of addition of the chemicals, UV-vis time resolved studies were performed using 0.5 mM $HAuCl_4$ and 2 mM of base. The results are gathered in **Table S14** and **Figure S25**.

Table S14. Kinetics of the synthesis of Au NPs followed by UV-vis.

Table S14A. Ambient light and $HAuCl_4$ added last using LiOH. The reaction mixture consisted of 0.5 mM $HAuCl_4$ and 2 mM LiOH in a PP container left to react at RT and light without stirring. $HAuCl_4$ was added last from a 20 mM solution. Aliquots of 2-3 mL were sampled over time for UV-vis measurements. The NP size after 24 hour is 7.8 ± 2.1 nm (PdI of 0.07). This is a repeat of the results from Figure 1 and the two datasets are consistent.

ROH	H_2O v.%*	ROH v.%*	$HAuCl_4$ mM* (added last)	Base	Base mM*	V mL*	T °C	t	Base/Au molar ratio	λ_{spr} ($\Delta\lambda/\lambda_{spr}$) nm	A_{spr}/A_{450}	Relative yield **	A_{650}/A_{spr}	A_{380}/A_{800}
EtOH	70	30	-	LiOH	2	3	RT	0h00	-	-	-	-	-	-
			0.5			39		0h05	4	-	-	0.49	-	13.5
								0h10		[520 (x.x%)]	0.94	0.63	0.92	2.7
								0h20		535 (x.x%)	1.02	0.76	0.84	1.7
								0h30		528 (12.2%)	1.24	0.92	0.51	2.9
								0h40		525 (8.8%)	1.43	0.94	0.23	9.0
								0h50		518 (9.5%)	1.38	0.97	0.09	> 50
								1h00		516 (6.8%)	1.50	0.96	0.07	> 50
								1h10		517 (6.6%)	1.51	0.99	0.07	> 50
								1h20		517 (6.8%)	1.49	0.99	0.08	> 50
								1h30		516 (6.9%)	1.52	0.98	0.07	> 50
								1h40		516 (6.9%)	1.51	0.99	0.08	> 50
								1h50		517 (6.6%)	1.48	0.97	0.06	> 50
								2h00		516 (6.8%)	1.52	0.97	0.06	> 50
								24h		517 (6.7%)	1.50	1.00	0.09	26.0

* before volume contraction; ** evaluated as the ratio of A_{400} for the sample and the maximum values of A_{400} for the dataset at a given v.% of ROH; values under brackets correspond to a case where the signal intensity is low and are purely indicative.

Table S14B. **Ambient light and LiOH added last**. The reaction mixture consisted of 0.5 mM $HAuCl_4$ and 2 mM LiOH left to react at RT and light without stirring. LiOH was added last from a 57 mM solution. Aliquots of 2-3 mL were sampled over time for UV-vis measurements. The NP size after 24 hour is 11.0 ± 3.3 nm (PdI of 0.09).

ROH	**H_2O** v.%*	**ROH** v.%*	**$HAuCl_4$** mM*	**Base**	**Base** mM* (added last)	**V** mL*	**T** °C	**t**	**Base/Au molar ratio**	**λ_{spr}** ($\Delta\lambda/\lambda_{spr}$) nm	**A_{spr}/A_{450}**	**Relative yield** **	**A_{650}/A_{spr}**	**A_{380}/A_{800}**
EtOH	70	30	0.5	-	-	3	RT	0h00	-	*310 (6.8%)*	-	0.20	-	-
				LiOH	2	39		0h05	4	535 (x.x%)	1.02	0.83	0.87	1.4
								0h10		531 (14.8%)	1.17	0.90	0.68	1.8
								0h20		529 (14.5%)	1.38	0.93	0.38	3.5
								0h30		528 (8.5%)	1.51	0.95	0.23	8.4
								0h40		527 (8.3%)	1.53	0.95	0.19	9.8
								0h50		527 (8.0%)	1.54	0.97	0.17	12.0
								1h00		527 (7.5%)	1.56	0.97	0.17	12.0
								1h10		527 (7.6%)	1.56	0.98	0.16	12.2
								1h20		526 (7.4%)	1.56	0.97	0.15	15.0
								1h30		525 (7.5%)	1.58	0.98	0.14	15.3
								1h40		522 (6.5%)	1.61	1.00	0.11	20.7
								1h50		521 (6.4%)	1.61	0.98	0.10	30.5
								2h00		521 (6.5%)	1.61	0.98	0.09	30.5
								24h		520 (6.3%)	1.60	0.95	0.10	19.7

* before volume contraction; ** evaluated as the ratio of A_{400} for the sample and the maximum values of A_{400} for the dataset at a given v.% of ROH.

Table S14C. **Ambient light and EtOH added last using LiOH**. The reaction mixture consisted of 0.5 mM $HAuCl_4$ and 2 mM LiOH in a PP container left to react at RT and light without stirring. EtOH was added last. Aliquots of 2-3 mL were sampled over time for UV-vis measurements. The NP size after 24 hour is > 50 nm.

ROH	**H_2O** v.%*	**ROH** v.%* (added last)	**$HAuCl_4$** mM*	**Base**	**Base** mM*	**V** mL*	**T** °C	**t**	**Base/Au molar ratio**	**λ_{spr}** ($\Delta\lambda/\lambda_{spr}$) nm	**A_{spr}/A_{450}**	**Relative yield** **	**A_{650}/A_{spr}**	**A_{380}/A_{800}**
-	100	-	0.5	LiOH	2	3	RT	0h00	4	-	-	-	-	-
EtOH	70	30				39		0h05		[555 (x.x%)]	-	0.00	-	-
								0h10		[563 (x.x%)]	-	0.00	-	-
								0h20		[562 (x.x%)]	-	0.00	-	-
								0h30		565 (x.x%)	-	0.00	-	-
								0h40		570 (19.5%)	1.51	0.08	0.85	2.4
								0h50		571 (19.4%)	1.27	0.11	0.86	1.8
								1h00		571 (22.9%)	1.21	0.13	0.94	1.7
								1h10		572 (24.0%)	1.25	0.16	0.90	1.6
								1h20		560 (19.8%)	1.04	0.24	0.96	1.7
								1h30		560 (20.7%)	1.36	0.21	0.77	1.6
								1h40		557 (23.5%)	1.19	0.24	0.87	1.6
								1h50		557 (18.9%)	1.27	0.24	0.85	1.6
								2h00		555 (19.1%)	1.25	0.26	0.86	1.6
								24h		537 (7.6%)	1.88	1.00	0.29	7.8

* before volume contraction; ** evaluated as the ratio of A_{400} for the sample and the maximum values of A_{400} for the dataset at a given v.% of ROH; values under brackets correspond to a case where the signal intensity is low and are purely indicative.

Table S14D. **Dark and $HAuCl_4$ added last using LiOH**. The reaction mixture consisted of 0.5 mM $HAuCl_4$ and 2 mM LiOH in a UV-vis cuvette left to react at RT in the UV-vis equipment without stirring. $HAuCl_4$ was added last from a 20 mM solution. The NP size after 24 hour is 8.8 ± 5.3 nm (PdI of 0.37) with larger NPs.

ROH	**H_2O** v.%*	**ROH** v.%*	**$HAuCl_4$** mM* (added last)	**Base**	**Base** mM*	**V** mL*	**T** °C	**t**	**Base/Au molar ratio**	**λ_{spr}** ($\Delta\lambda/\lambda_{spr}$) nm	**A_{spr}/A_{450}**	**Relative yield** **	**A_{650}/A_{spr}**	**A_{380}/A_{800}**
EtOH	70	30	-	LiOH	2	3	RT	0h00	-	-	-	-	-	-
			0.5					0h02	4	[285]	-	0.07	-	-
								0h05		542 (x.x%) + peak at 685	1.22	0.99	0.93	3.0
								0h10		539 (26.5%) shoulder 680	1.23	0.98	0.89	1.2
								0h20		536 (27.8%) shoulder 660	1.26	0.98	0.90	1.3
								0h30		536 (27.2%) shoulder 660	1.27	0.99	0.90	1.4
								0h40		536 (23.4%) shoulder 660	1.27	0.98	0.88	1.4
								0h50		536 (22.0%) shoulder 660	1.28	0.99	0.87	1.5
								1h00		536 (20.8%) shoulder 650	1.29	0.98	0.87	1.6
								1h10		536 (19.4%) shoulder 640	1.3	0.98	0.85	1.6
								1h20		536 (17.9%) shoulder 640	1.33	0.98	0.84	1.7
								1h30		535 (17.8%) shoulder 640	1.29	0.96	0.83	1.8
								24h		549 (21.3%)	1.43	1.00	0.85	1.8

* before volume contraction; ** evaluated as the ratio of A_{400} for the sample and the maximum values of A_{400} for the dataset at a given v.% of ROH; values under brackets correspond to a case where the signal intensity is low and are purely indicative.

Table S14E. **Dark and LiOH added last**. The reaction mixture consisted of 0.5 mM $HAuCl_4$ and 2 mM LiOH in a UV-vis cuvette left to react at RT in the UV-vis equipment without stirring. LiOH was added last from a 57 mM solution. After 24 hours, large chunks of materials are obtained together with smaller NPs.

ROH	**H_2O** v.%*	**ROH** v.%*	**$HAuCl_4$** mM*	**Base**	**Base** mM* (added last)	**V** mL*	**T** °C	**t**	**Base/Au molar ratio**	**λ_{spr}** ($\Delta\lambda/\lambda_{spr}$) nm	**A_{spr}/A_{450}**	**Relative yield** **	**A_{650}/A_{spr}**	**A_{380}/A_{800}**
EtOH	70	30	0.5	-	-	3	RT	0h00	-	*310 (6.8%)*	-	0.22	-	-
				LiOH	2			0h02	4	[542 (x.x%)]	1.00	0.45	0.67	9.0
								0h05		545 (17.1%)	1.33	0.96	0.69	2.0
								0h10		543 (14.6%)	1.37	1.00	0.62	2.6
								0h20		542 (14.1%)	1.38	0.95	0.59	2.8
								0h30		538 (13.3%)	1.42	0.93	0.54	3.3
								0h40		538 (12.6%)	1.43	0.89	0.52	3.5
								0h50		538 (12.4%)	1.43	0.87	0.51	3.6
								1h00		538 (12.9%)	1.41	0.87	0.51	3.9
								1h10		537 (12.2%)	1.43	0.87	0.50	3.9
								1h20		538 (12.7%)	1.43	0.89	0.48	3.9
								1h30		537 (12.0%)	1.46	0.89	0.48	3.9
								24h		538 (12.5%)	1.44	0.85	0.49	4.1

* before volume contraction; ** evaluated as the ratio of A_{400} for the sample and the maximum values of A_{400} for the dataset at a given v.% of ROH; values under brackets correspond to a case where the signal intensity is low and are purely indicative.

Table S14F. **Dark and EtOH added last using LiOH**. The reaction mixture consisted of 0.5 mM $HAuCl_4$ and 2 mM LiOH in a UV-vis cuvette left to react at RT in the UV-vis equipment without stirring. EtOH was added last. The material forms on the side of the UV-vis cuvette and no size could be estimated after 24 hour.

ROH	**H_2O** v.%*	**ROH** v.%* (added last)	**$HAuCl_4$** mM*	**Base**	**Base** mM*	**V** mL*	**T** °C	**t**	**Base/Au molar ratio**	**λ_{spr}** ($\Delta\lambda/\lambda_{spr}$) nm	**A_{spr}/A_{450}**	**Relative yield** **	**A_{650}/A_{spr}**	**A_{380}/A_{800}**
-	100	-						0h00		-	-	-	-	-
								0h02		583 (24.7%)	1.33	0.13	1.00	1.7
								0h05		588 (20.4%)	1.25	0.17	1.00	2.0
								0h10		588 (14.8%)	1.50	0.17	0.83	2.0
								0h20		589 (17.3%)	1.40	0.20	0.86	1.8
								0h30		592 (20.9%)	1.33	0.23	0.88	1.6
EtOH	70	30	0.5	LiOH	2	3	RT	0h40	4	594 (17.3%)	1.43	0.27	0.90	1.7
								0h50		595 (14.1%)	1.50	0.33	0.83	1.6
								1h00		592 (19.8%)	1.40	0.37	0.93	1.4
								1h10		595 (19.2%)	1.46	0.50	0.89	1.3
								1h20		595 (20.8%)	1.44	0.67	0.92	1.2
								1h30		601 (19.0%)	1.52	1.00	0.95	1.1
								24h		[580 (22.9%)]	[1.20]	[0.20]	[1.00]	[1.5]

* before volume contraction; ** evaluated as the ratio of A_{400} for the sample and the maximum values of A_{400} for the dataset at a given v.% of ROH; values under brackets correspond to a case where the signal intensity is low and are purely indicative.

Table S14G. Ambient light and $HAuCl_4$ added last using NaOH. The reaction mixture consisted of 0.5 mM $HAuCl_4$ and 2 mM NaOH in a PP container left to react at RT and light without stirring. $HAuCl_4$ was added last from a 20 mM solution. Aliquots of 2-3 mL were sampled over time for UV-vis measurements. The NP size after 24 hour is 11.2 ± 2.8 nm (PdI of 0.06).

ROH	**H_2O** v.%*	**ROH** v.%*	**$HAuCl_4$** mM* (added last)	**Base**	**Base** mM*	**V** mL*	**T** °C	**t**	**Base/Au molar ratio**	**λ_{spr}** ($\Delta\lambda/\lambda_{spr}$) nm	**A_{spr}/A_{450}**	**Relative yield** **	**A_{650}/A_{spr}**	**A_{380}/A_{800}**
			-			3		0h00	-	-	-	-	-	-
								0h05		[541 (x.x%)]	0.00	0.67	-	1.7
								0h10		537 (x.x%)	1.00	0.77	0.83	1.7
								0h20		533 (17.6%)	1.11	0.82	0.68	2.1
								0h30		530 (12.8%)	1.20	0.86	0.54	2.6
								0h40		530 (10.7%)	1.30	0.89	0.41	3.7
								0h50		530 (9.8%)	1.36	0.92	0.34	4.7
								1h00		530 (9.1%)	1.42	0.91	0.26	6.9
								1h10		529 (8.3%)	1.49	0.92	0.20	16.0
EtOH	70	30	0.5	NaOH	2	39	RT	1h20	4	529 (8.0%)	1.51	0.91	0.18	18.5
								1h30		529 (8.2%)	1.50	0.93	0.18	18.8
								1h40		528 (8.0%)	1.52	0.94	0.18	22.8
								1h50		528 (8.0%)	1.52	0.93	0.17	22.6
								2h00		528 (8.0%)	1.53	0.96	0.16	23.2
								2h10		528 (7.8%)	1.52	0.96	0.16	23.4
								2h20		528 (7.9%)	1.53	0.96	0.16	23.2
								2h30		528 (7.8%)	1.55	0.97	0.16	23.4
								24h		521 (6.4%)	1.58	1.00	0.10	30.3

* before volume contraction; ** evaluated as the ratio of A_{400} for the sample and the maximum values of A_{400} for the dataset at a given v.% of ROH; values under brackets correspond to a case where the signal intensity is low and are purely indicative.

Table S14H. **Ambient light and NaOH added last**. The reaction mixture consisted of 0.5 mM $HAuCl_4$ and 2 mM NaOH left to react at RT and light without stirring. LiOH was added last from a 57 mM solution. Aliquots of 2-3 mL were sampled over time for UV-vis measurements. The NP size after 24 hour is 15.2 ± 4.5 nm (PdI of 0.09).

ROH	**H_2O** v.%*	**ROH** v.%*	**$HAuCl_4$** mM*	**Base**	**Base** mM* (added last)	**V** mL*	**T** °C	**t**	**Base/Au molar ratio**	**λ_{spr}** ($\Delta\lambda/\lambda_{spr}$) nm	**A_{spr}/A_{450}**	**Relative yield** **	**A_{650}/A_{spr}**	**A_{380}/A_{800}**
				-	-	3		0h00	-	*310 (6.8%)*	-	0.20	-	-
								0h05		543 (x.x%)	0.00	0.55	#DIV/0!	1.8
								0h10		540 (x.x%)	1.05	0.62	0.81	1.8
								0h20		539 (16.3%)	1.14	0.67	0.68	2.2
								0h30		535 (13.0%)	1.21	0.73	0.57	2.6
								0h40		532 (10.9%)	1.29	0.76	0.47	3.1
								0h50		532 (9.8%)	1.37	0.77	0.38	4.1
								1h00		532 (9.2%)	1.42	0.79	0.30	5.3
								1h10		531 (8.9%)	1.47	0.81	0.24	7.3
EtOH	70	30	0.5	NaOH	2	39	RT	1h20	4	531 (8.3%)	1.51	0.82	0.22	10.3
								1h30		530 (8.2%)	1.53	0.82	0.20	14.7
								1h40		530 (8.1%)	1.55	0.82	0.21	17.3
								1h50		530 (8.2%)	1.55	0.84	0.19	15.1
								2h00		530 (8.0%)	1.56	0.84	0.19	17.7
								2h10		530 (8.0%)	1.55	0.84	0.18	17.7
								2h20		530 (8.1%)	1.54	0.87	0.20	13.8
								2h30		529 (7.8%)	1.58	0.87	0.18	18.3
								24h		524 (6.5%)	1.65	1.00	0.13	13.8

* before volume contraction; ** evaluated as the ratio of A_{400} for the sample and the maximum values of A_{400} for the dataset at a given v.% of ROH.

Table S14I. **Ambient light and EtOH added last using NaOH**. The reaction mixture consisted of 0.5 mM $HAuCl_4$ and 2 mM NaOH in a PP container left to react at RT and light without stirring. EtOH was added last. Aliquots of 2-3 mL were sampled over time for UV-vis measurements. The NP size after 24 hour is > 50 nm.

ROH	**H_2O** v.%*	**ROH** v.%* (added last)	**$HAuCl_4$** mM*	**Base**	**Base** mM*	**V** mL*	**T** °C	**t**	**Base/Au molar ratio**	**λ_{spr}** ($\Delta\lambda/\lambda_{spr}$) nm	**A_{spr}/A_{450}**	**Relative yield** **	**A_{650}/A_{spr}**	**A_{380}/A_{800}**
-	100	-	0.5	NaOH	2	3	RT	0h00	4	-	-	-	-	-
EtOH	70	30				39		0h05		-	-	0.03	-	-
								0h10		-	-	0.03	-	-
								0h20		[561 (x.x%)]	-	0.03	-	-
								0h30		[566 (x.x%)]	-	0.04	-	5.0
								0h40		571 (10.9%)	0.91	0.07	1.47	3.5
								0h50		580 (14.8%)	0.56	0.17	2.20	1.6
								1h00		599 (22.1%)	1.28	0.28	0.93	1.3
								1h20		592 (22.6%)	1.24	0.35	0.92	1.3
								1h40		590 (26.3%)	1.21	0.41	0.93	1.2
								1h50		588 (29.1%)	1.19	0.44	0.97	1.2
								2h00		586 (24.1%)	1.21	0.46	0.94	0.9
								24h		556 (19.4%)	1.37	1.00	0.86	1.1

* before volume contraction; ** evaluated as the ratio of A_{400} for the sample and the maximum values of A_{400} for the dataset at a given v.% of ROH; values under brackets correspond to a case where the signal intensity is low and are purely indicative.

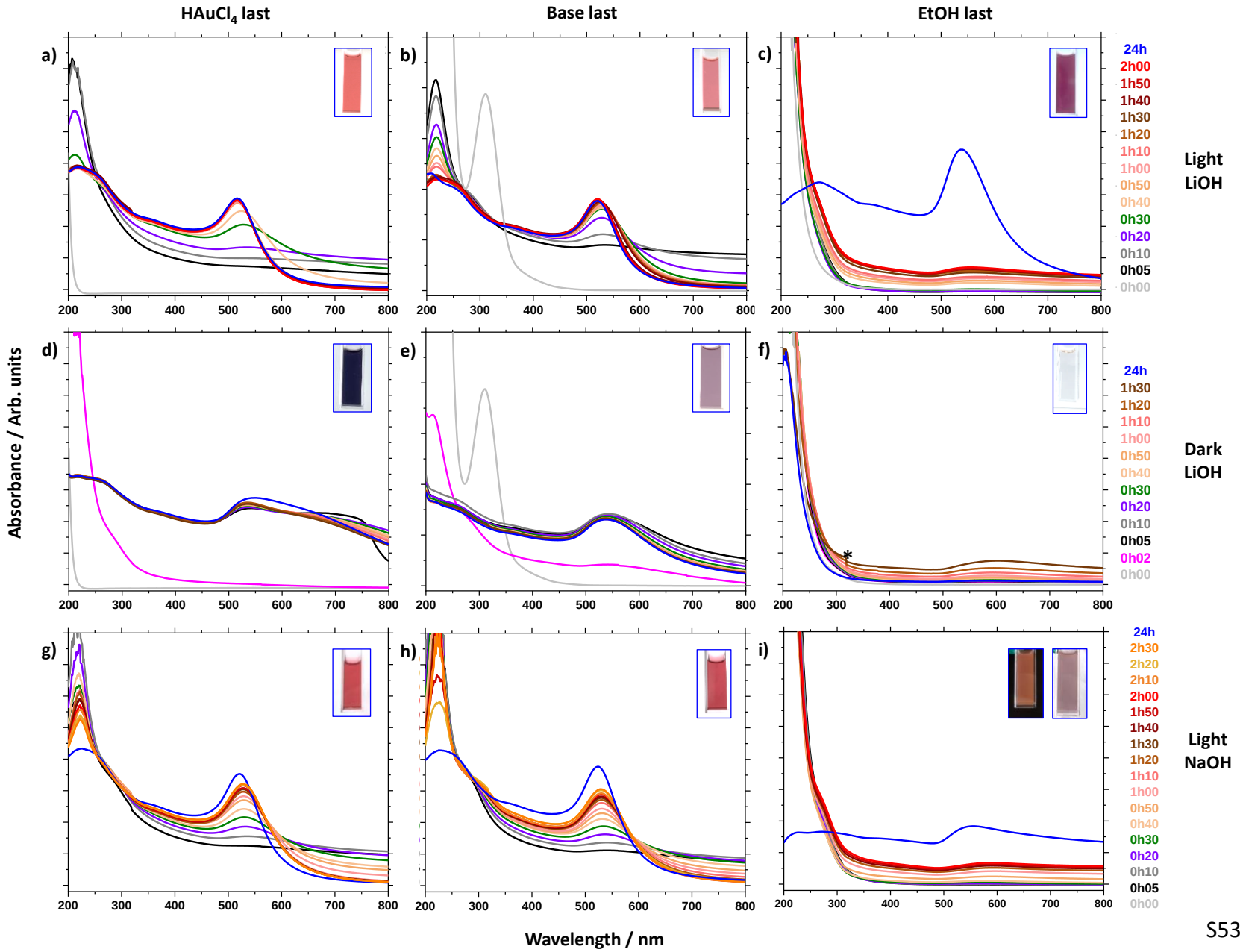
HAuCl4 last
Base last
EtOH last
a)
b)
c)
d)
e)
f)
g)
h)
i)
Absorbance / Arb. units
Wavelength / nm
200
300
400
500
600
700
800
24h
2h00
1h50
1h40
1h30
1h20
1h10
1h00
0h50
0h40
0h30
0h20
0h10
0h05
0h00
Light
LiOH
24h
1h30
1h20
1h10
1h00
0h50
0h40
0h30
0h20
0h10
0h05
0h02
0h00
Dark
LiOH
24h
2h30
2h20
2h10
2h00
1h50
1h40
1h30
1h20
1h10
1h00
0h50
0h40
0h30
0h20
0h10
0h05
0h00
Light
NaOH

Figure S25. UV-vis spectra recorded at different times of the synthesis for 0.5 mM $HAuCl_4$, 2 mM base and 30 v.% EtOH where the chemicals were added from a stock solution of 20 mM $HAuCl_4$ in water and 57 mM base in water in different orders. See experimental details in **Table S14**. The top row corresponds to experiments performed at RT and light using LiOH as base for which aliquots were taken over time. The middle row corresponds to experiments performed in the dark directly in the UV-vis cuvette using LiOH as base. The bottom row corresponds to experiments performed at RT and light using NaOH as base for which aliquots were taken over time. The left panel column corresponds to a case where $HAuCl_4$ was added last. The middle panel column corresponds to a case where the Base was added last. The right panel column corresponds to a case where EtOH was added last. The bump indicated by a * in (f) is an artefact from the instrument when a change of wavelength detection range occurs. For panel (h) the precursor spectrum before adding the base was not measured but would be identical to the related spectra presented in (b) or (e).

Results. The time resolved (light) and *in situ* (dark) experiments illustrate further the effect of the order of addition of the chemicals both at ambient light and in the dark. Using LiOH as base and at ambient light, the time needed to observe a well-defined plasmon resonance of Au NPs increases with the order of chemical added last LiOH < $HAuCl_4$ < EtOH. While the reaction is very slow if EtOH is added last, it ultimately leads to rather large NPs (> 50 nm) compared to a case where $HAuCl_4$ or LiOH is added last: 7.8 ± 2.1 nm and 11.0 ± 3.3 nm, respectively. However, we observed that adding EtOH last did not lead to NPs in too low volume of reaction. For instance, for 6.5 mL total volume no NPs are formed but instead a solid on the wall of the PP container, see **Figure S24**, and for 39 mL used here, some purple deposit was formed on the walls of the PP container while colloidal NPs were also formed. The intensity of the signal when $HAuCl_4$ was added last was actually about 1.6 (based on A_{spr}) to 1.7 (based on A_{400}) times more intense than in the case where LiOH was added last. This is observed with the higher color intensity of the picture in the inset of **Figure S25a** compared to **Figure S25b**. This suggests a lower yield of Au NPs formation when LiOH is added last. This was confirmed by electrochemical measurements (see **section SP. Electrochemical characterization**) where the mass activity for NPs prepared by adding $HAuCl_4$ or LiOH last are 72.5 ± 26.9 A g^{-1} and 44.2 ± 16.5 A g^{-1}, respectively, for the EOR (evaluated after 25 scans). The mass activity is 1481 ± 271 A g^{-1} and 1200 ± 140 A g^{-1}, respectively, for the EGOR (evaluated after 5 scans). This means that a mass activity in the ratio 1.6 (EOR) or 1.2 (EGOR) indicates that the decrease in intensity of ca. 1.6 in UV-vis data probably correlates with lower yields when LiOH is added last.

In dark conditions using LiOH, the same trend is observed. The time needed to identify a well-defined plasmon resonance of Au NPs increases in the order of chemical added last LiOH < $HAuCl_4$ < EtOH. In this case, when EtOH is added last, no NPs are formed but material forms on the wall of the UV-vis cuvette. Adding $HAuCl_4$ last leads to NPs ca. 8.8 ± 5.3 nm with also larger NPs in agreement with the UV-vis spectrum showing a large feature extending over 700 nm. Adding LiOH last also leads to a mixture of small and large NPs. Here again the plasmon intensity is ca. 2 times less intense if LiOH is added last *versus* if $HAuCl_4$ is added last.

The effect of light on the synthesis already addressed in **section SF. Kinetics of the reduction** is stressed again here. When adding $HAuCl_4$ or LiOH last, larger NPs with a broader size distribution are obtained in the dark than at ambient light. When EtOH is added last, no colloidal NPs are formed in the dark. When $HAuCl_4$ is added last, the reaction mechanism in the dark is different compared to a synthesis at ambient light. In both cases, a plasmon

resonance around 517 nm (light) or 535 nm (dark) is observed rapidly but in the dark large features at higher wavelength remain pronounced over time.

For experiments performed at ambient light but using NaOH, poorly defined NPs, see **Figure S26** were obtained and form slowly when EtOH was added last. The resulting material leads to different perceived color of the dispersion depending on different color background, **Figure S25**. Adding $HAuCl_4$ or NaOH last did not seem to change much the kinetics in this case nor the intensity of the signal, suggesting a similar yield as opposed to the case where LiOH was used. A noticeable difference with the case of using LiOH is that overtime the A_{spr} value and the general shape of the UV-vis spectra keeps changing. In particular this behavior is pronounced considering that the spectra recorded after 24 hours are significantly different from those after 2 hours. This difference is less pronounced when LiOH is used and so a steady state is reached faster using LiOH. The slightly slower kinetics using NaOH correlates with slightly larger NPs obtained compared to a case using LiOH (11.2 ± 2.8 nm *vs.* 7.8 ± 2.1 nm respectively, when $HAuCl_4$ is added last, and 15.2 ± 4.5 nm *vs.* 11.0 ± 3.3 nm, respectively when the Base is added last). Finally, the relative A_{spr} values normalized to the higher values are 1.00 > 0.97 > 0.84 > 0.47 obtained for NaOH-(NaOH last) > NaOH-($HAuCl_4$ last) > LiOH-($HAuCl_4$ last) > LiOH-(LiOH last) conditions, respectively. This suggests that the overall yield of the reaction is slightly higher with NaOH as base.

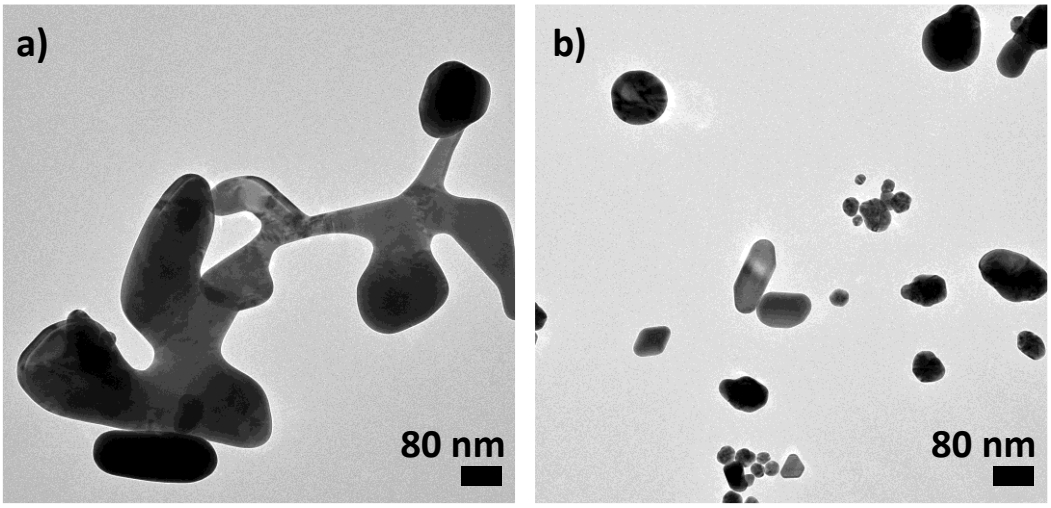

Figure S26. TEM micrographs of Au NMs obtained using 0.5 mM $HAuCl_4$ and 2 mM NaOH (NaOH/Au molar ratio of 4) in 30 v.% EtOH at ambient light with experimental conditions as reported in **Table S14I** and where EtOH was added last.

SJ-C. Effect of the order of addition on the colloidal Au NPs when one chemical is omitted

Some features are observed at low wavelengths in the above section. In particular at ambient light, when $HAuCl_4$ or the base is added last, using LiOH or NaOH, features at 212 nm, **Figure S25a,g**, or 218 nm, **Figure S25b,h**, tend to decrease over time. Spectra of different solutions when only one chemical was omitted (EtOH, $HAuCl_4$ or LiOH) were recorded and are presented in **Figure S27**. A first point to note is that $HAuCl_4$ spectrum is different in water only and water with 30 v.% EtOH. The characteristic peak of $[Au^{III}Cl_4]^-$ at 295 nm in water is shifted to 310 nm in presence of EtOH, in agreement with previous reports.[18] It is shifted to 304 nm if 30 v.% MeOH is used. This can be due to different hydrolysis of $AuCl_4^-$ to $[AuCl_x(OH)_y]^{n-}$ species with x+y=4 and/or ligand exchange of some chloride with EtOH/MeOH. $HAuCl_4$ solutions at high concentration (0.5 mM) in 100% water or in presence of 30 v.% ROH, lead to the saturation of the detector at low wavelengths. Upon dilution of $HAuCl_4$ to lower concentrations, the absorption peak around 295 nm (or 310 nm with 30 v.% EtOH) is still observed as a shoulder of another peak around 212 or 218 nm. The peak around 212-218 and 295-310 nm are attributed to ligand-to-metal charge transfer Cl $p_\pi \rightarrow 5d_{x^2-y^2}$ bands of the various chlorohydroxoaurate species.[18] These peaks can be interpreted as an indication of the presence of $AuCl_x(OH)_y$ complexes with low values of *y* (high *x* values since it is expected that x+y=4). Upon adding a base, no characteristic features can be identified anymore, as expected for $AuCl_x(OH)_y$ complexes with high values of *y* that can form in alkaline conditions.[19]

This feature at 212-218 nm overall decreases over time during the reduction of $HAuCl_4$ at ambient light, see **Figure S25a**. It is especially clear when LiOH is added last, see **Figure S25b**. The same occurs with NaOH as base, see **Figure S25g,i**. This suggests that when $HAuCl_4$ is added last, in a mixture of ROH and Base, some '$HAuCl_4$' remains present for ca. 30 minutes in solution using LiOH, this times goes up to ca. 2h30 with NaOH, and does not immediately convert to $[AuCl_x(OH)_y]^{n-}$ species with high *y* values. When LiOH is added last, the intensity of the peak at 218 nm decreases relatively slowly overtime compared to the case where $HAuCl_4$ is added last. This indicates the slower conversion of $[AuCl_x(OH)_y]^{n-}$ species with low *y* values to $[AuCl_x(OH)_y]^{n-}$ with high *y* values when LiOH is added last. The absorption at 400 nm does not significantly increase with time, suggesting that no or little extra Au^0 is formed or formed slowly over time. In addition, the features of the UV-vis spectra related to the Au NPs around 520 nm are not changed much after 30 minutes *despite* further changes in the precursor chemical state. In contrast, when $HAuCl_4$ is added last, features related to the Au NPs are still evolving with time after the features around 212 nm are not observed. Finally, if EtOH is added last, no features are observed suggesting that the precursor solution is in a high hydroxylated state (high y values) and large NPs form slowly. When NaOH is used, these features remain visible relatively longer than for LiOH, in agreement with the apparent slower reaction discussed above.

Interestingly, these features at low wavelengths are not observed in the dark conditions or disappear within 5 minutes after mixing all chemicals, **Figure S25d,e**. This strongly support further the role of light in the mechanism of $HAuCl_4$ complexation, stabilization and/or reduction in alkaline conditions in presence of ROH as it can be expected for a RT-synthesis.

The case of adding the base last is however challenging and was considered less reproducible. It was observed that $HAuCl_4$ solutions in presence of EtOH or glycerol change color over time from yellow to more pale brown. This is especially clear when the solutions are heated at 50 °C and this suggests that the ROH reduces the Au even in absence of base. It could also be

that in presence of ROH the Au complex undergoes different equilibria, which could explain the slower further reduction of the Au complex and/or slower formation of $[AuCl_x(OH)_y]^{n-}$ with high *y* values upon adding a base.

To illustrate this phenomenon, a solution comprising EtOH and water and $HAuCl_4$ but without base was left on purpose for 3 hours at RT and ambient light before adding NaOH so that the final concentration was 0.5 mM $HAuCl_4$ and 2 mM base. As illustrated in **Figure S27b**, this solution still shows a feature around 316 nm related to $HAuCl_4$ but its intensity has decreased compared to a freshly prepared solution. In addition, absorption from ca. 500 nm is pronounced whereas it was not the case for a fresher solution. A broad feature with a A_{spr} around 600 nm is also formed. Upon adding NaOH, the fresh solution turns to NPs with a well-defined plasmon resonance around 524 nm. Using the 'aged' solution, a plasmon resonance is also observed at 534 nm with a much lower intensity suggesting a lower conversion yield of the precursor. This lower yield can also be inferred from the fact that a feature around 227 nm is still observed suggesting the presence of '$HAuCl_4$' precursor. Interestingly, using the aged solution of $HAuCl_4$ in water and EtOH leads to a very fast reaction within seconds upon addition of the Base, as illustrated in **Figure S27c**. The resulting NPs show a very wide size distribution 35.6. ± 11.5 nm. The faster reaction with lower yield compared to a case where $HAuCl_4$ is added last is in agreement with the results obtained using LiOH in **Figure S25b,e**.

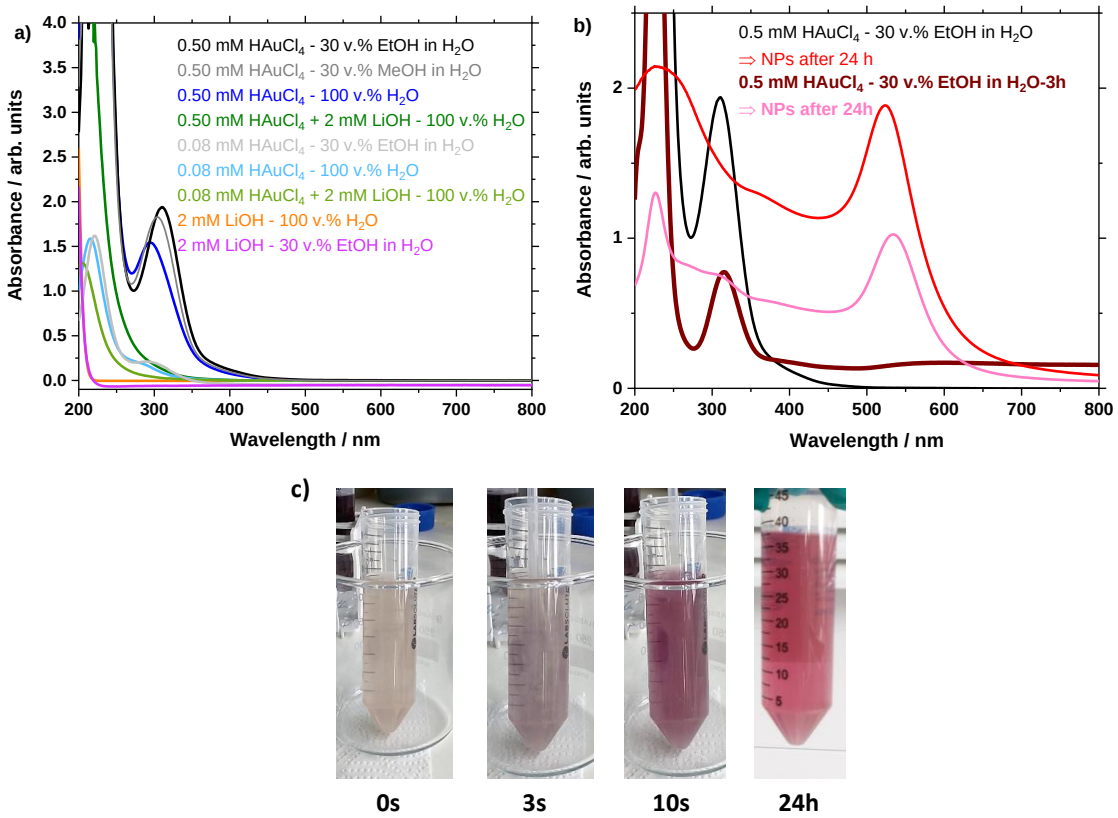

Figure S27. UV-vis spectra of (a) different solutions that do not lead to Au NPs: dispersion without $HAuCl_4$, or with $HAuCl_4$ but without base, in different solvents as indicated. (b) Solution of 30 v.% EtOH in water with ca. 0.5 mM $HAuCl_4$ freshly prepared and after 3 hours and the corresponding Au NPs UV-vis spectra after adding NaOH so that the final base concentration is 2 mM for 0.5 mM $HAuCl_4$ (molar ratio NaOH/Au of 4). The synthesis was conducted at ambient light and RT without stirring for a total volume of 39 mL. (c) Pictures of the fast reaction observed when the 3 hour-aged solution of 30 v.% EtOH in water with $HAuCl_4$ was used. The times correspond to the time after adding NaOH.

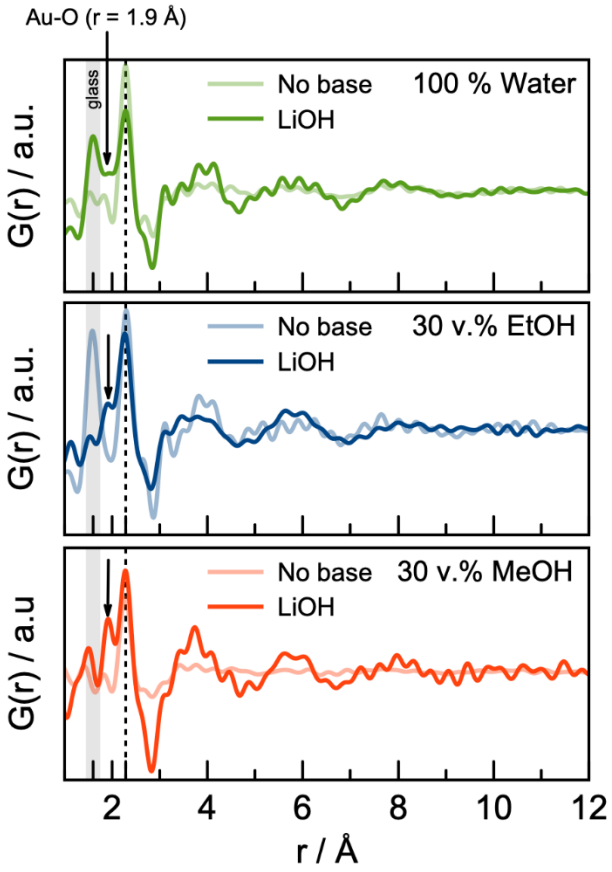

Figure S28. PDF analysis of 50 mM $HAuCl_4$ in 100% water, 30v.% EtOH or 30 v.% MeOH in water, with or without 150 mM LiOH, as indicated. The measurements were performed within ca. 10 min after mixing the reagents and the ROH added last.

While the effect of different solvents is not as clear as in UV-vis spectra, **Figure S27a**, the PDF results suggest that upon adding a base, a distance attributed to Au-O at 1.9 Å is more pronounced in the PDFs shown in **Figure S28**. However, it is important to interpret these results considering that O is a poor scattering element compared to Au and the related bond distance is close to a region where a poor background subtraction will strongly influence the resulting PDF.

Conclusions

Adding the base last does not seem a suitable option to form Au NPs in a controlled way. The synthesis will only be controlled if the time of mixture of $HAuCl_4$ with EtOH and water before adding the base is controlled. It is concluded that adding $HAuCl_4$ last at ambient light from a concentrated aqueous stock solution (here 20 mM) leads to a more reproducible synthetic approach. Adding the Base last does not lead to reproducible results and often lower relative yields. Adding the ROH last typically does not lead to stable colloids. This simple experimental consideration might explain the limited interest to date for the synthesis approach presented here, see **Table S1**, despite its multiple benefits. These results overall suggest that the complex equilibria between the different species and the influence of light will play a key role in the formation of the Au NPs and can account for the different kinetics observed.

SJ-D. Optical properties of the Au NPs

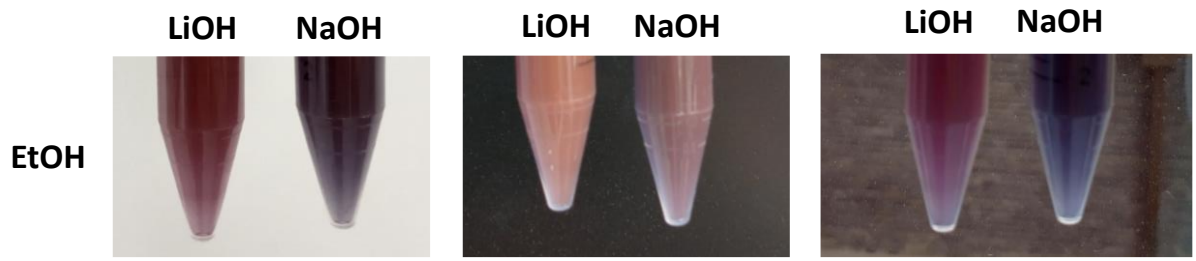

Figure S29. Pictures of colloidal Au NP dispersions obtained for different experimental conditions as indicated from 0.5 mM $HAuCl_4$ and 2 mM of base (molar ratio Base/Au of 4) in 30 v.% EtOH with a treatment at 50 °C for 1 hour. The dispersions were obtained adding EtOH last in the reaction mixture. The left panel corresponds to the same dispersions imaged with a white background, the middle panel was obtained with a dark background whereas the right panel was obtained by placing the samples in front of a window facing the outdoors of the room and the grey background is a building wall.

A behavior of *turbid* dispersions with different optical properties in absorption and reflection is obtained when ROH is added last, see **Figure S29**, **Figure S20** and **Figure S19**. This is typically associated with a UV-vis spectra showing large features at relatively high wavelengths, ca. 540 nm with a pronounced tail at higher wavelengths. This illustrates the strong effect of the order of addition of the chemicals. While *see-through* yet colored dispersions are obtained when $HAuCl_4$ is added last, **Figure S19**, the colloidal NPs appear *turbid* when ROH is added last. It is unclear if this corresponds to the *turbidity* mentioned in some reports.[13] This turbidity can be attributed to the formation of NMs that are not perfect spheres.[20] The results presented in **Figure S19** illustrate further that the order of addition of the chemicals is crucial even at RT and severely influences the kinetics of the reaction. A same effect was observed using NaOH as base and is further achieved for other experimental conditions, as detailed below.

SK. Discussion of Au NP formation

In the next page are given the possible reactions accounting for the reduction of the Au precursor. Other possible species involved in the Au NP formation are acetaldehyde (T_{bp}=20 °C) and formaldehyde (T_{bp}=-19 °C) which are challenging to characterize due to their low boiling point. Formic acid is known to be a strong reducing agent but in the present case, it does not seem to form from MeOH in large quantities and/or not fast enough to enable a rapid nucleation (which would lead to fast kinetics and small NPs). In any case, the oxidation products of EtOH and MeOH themselves are potential reducing agents, such as ultimately CO_2.[21] By combining the most likely redox reactions, the OH^-/Au molar ratio to convert EtOH to acetaldehyde (2 electrons oxidation) is theoretically 4, **equation A**, and to convert EtOH to acetate (4 electrons oxidation) it is 4.75, **equation C**.[22] In a similar way, this ratio is only 4 to convert MeOH to formaldehyde, **equation D** and 4.75 to convert MeOH to formate, **equation F**. According to **equations A-F**, the OH^- concentration will drop as the reduction proceeds, shifting the equilibria towards $HAuCl_4$ that is then available for further reduction. However, we do not observe a mix of large and small NPs in EtOH, which suggests that while the pH may decrease, if any precursor remains in solution after a *nucleation* event, it will tend to be reduced on existing NPs. This stresses the importance of controlling the initial steps (nucleation) of the synthesis to control NP size.

Table S15. Properties of various possible intermediates.

Solvent	EtOH	Acetaldehyde	Acetic acid	MeOH	Formaldehyde	Formic acid
Formula	H_3CCH_2OH	H_3CCOH	H_3CCOOH	H_3COH	H_2CO	HCOOH
Molar Mass / g mol^{-1}	46	44	60	32	30	46
T_{bp} / °C	78	20	118	65	-19	100

In grey are the less likely redox reactions involving more than 2 electrons:

Redox reactions:

$HAuCl_4 + 3\ e^- \rightarrow Au^0 + 4\ Cl^- + H^+$ -1.00 V [23-25]

This reduction is likely to proceed first *via* an intermediate 2 electrons process leading to Au^I that is even more easily reduced than Au^{III}.[23,24]

	Acidic conditions				*Alkaline conditions*		
(1)	H_3CCH_2OH	→	$H_3CCOH + 2\ H^+ + 2\ e^-$	0.20 V [26]	$H_3CCH_2OH + 2\ OH^-$	→	$H_3CCOH + 2\ H_2O + 2\ e^-$
(2)	$H_3CCOH + H_2O$	→	$H_3CCOOH + 2\ H^+ + 2\ e^-$	-0.39 V [26]	$H_3CCOH + 3\ OH^-$	→	$H_3CCOO^- + 2\ H_2O + 2\ e^-$
(1+2)	$H_3CCH_2OH + H_2O$	→	$H_3CCOOH + 4\ H^+ + 4\ e^-$		$H_3CCH_2OH + 5\ OH^-$	→	$H_3CCOO^- + 4\ H_2O + 4\ e^-$
(3)	$H_3CCOOH + 2\ H_2O$	→	$2\ CO_2 + 8\ H^+ + 8\ e^-$		$H_3CCOO^- + 7\ OH^-$	→	$2\ CO_2 + 5\ H_2O + 8\ e^-$
(4)	H_3COH	→	$H_2CO + 2\ H^+ + 2\ e^-$	0.18 V [26]	$H_3COH + 2\ OH^-$	→	$H_2CO + 2\ H_2O + 2\ e^-$
(5)	$H_2CO + H_2O$	→	$HCOOH + 2\ H^+ + 2\ e^-$	-0.18 V [21]	$H_2CO + 3\ OH^-$	→	$HCOO^- + 2\ H_2O + 2\ e^-$
(4+5)	$H_3COH + H_2O$	→	$HCOOH + 4\ H^+ + 4\ e^-$		$H_3COH + 5\ OH^-$	→	$HCOO^- + 4\ H_2O + 4\ e^-$
(6)	$HCOOH$	→	$CO_2 + 2\ H^+ + 2\ e^-$	0.20 V [26]	$HCOO^- + OH^-$	→	$CO_2 + 2H_2O + 2\ e^-$

Overall reactions:

(A)	$2\ HAuCl_4 + 3\ H_3CCH_2OH + 8\ OH^-$	→	$3\ H_3CCOH + 8\ H_2O + 2\ Au^0 + 8\ Cl^-$	OH^-/Au molar ratio : 4
(B)	$2\ HAuCl_4 + 3\ H_3CCOH + 11\ OH^-$	→	$3\ H_3CCOO^- + 8\ H_2O + 2\ Au^0 + 8\ Cl^-$	OH^-/Au molar ratio : 5.5
(C)	$4\ HAuCl_4 + 3\ H_3CCH_2OH + 19\ OH^-$	→	$3\ H_3CCOO^- + 16\ H_2O + 4\ Au^0 + 16\ Cl^-$	OH^-/Au molar ratio : 4.75
(D)	$2\ HAuCl_4 + 3\ H_3COH + 8\ OH^-$	→	$3\ H_2CO + 8\ H_2O + 2\ Au^0 + 8\ Cl^-$	OH^-/Au molar ratio : 4
(E)	$2\ HAuCl_4 + 3\ H_2CO + 11\ OH^-$	→	$3\ HCOO^- + 8\ H_2O + 2\ Au^0 + 8\ Cl^-$	OH^-/Au molar ratio : 5.5
(F)	$4\ HAuCl_4 + 3\ H_3COH + 19\ OH^-$	→	$3\ HCOO^- + 16\ H_2O + 4\ Au^0 + 16\ Cl^-$	OH^-/Au molar ratio : 4.75

The less likely reactions involving several electrons are given in grey.

SL. Reproducibility

Table S16. Examples of the reproducibility of the results using 30 v.% ROH, 0.5 mM $HAuCl_4$ and 2 mM of base.

Table S16A. Using EtOH as reducing agent.

ROH	H_2O v.%*	ROH v.%*	Base	V mL*	T °C	t h	Base/Au molar ratio	λ_{spr} ($\Delta\lambda/\lambda_{spr}$) nm	A_{spr}/A_{450}	A_{650}/A_{spr}	A_{380}/A_{800}	d_N nm	d_S nm	d_V nm	PdI
EtOH	70	30	LiOH	13	RT	24	4	515 (6.6%)	1.53	0.10	26.3	8.6 ± 2.0	9.5	10.0	0.05
								516 (6.2%)	1.55	0.10	28.8	9.2 ± 2.4	10.4	11.1	0.07
								521 (6.4%)	1.61	0.09	31.5	11.8 ± 3.3	13.7	14.9	0.08
								523 (7.5%)	1.64	0.17	12.6	15.8 ± 3.9	17.7	18.7	0.06
								519 (6.4%)	1.62	0.10	21.5	11.5 ± 2.9	13.1	14.0	0.06
								523 (6.9%)	1.53	0.19	5.95	12.3 ± 3.0	13.8	14.6	0.06
				6.5				521 (6.5%)	1.62	0.09	23.2	12.3 ± 2.7	13.5	14.0	0.05
								521 (6.4%)	1.60	0.13	11.3	11.6 ± 2.5	12.6	13.2	0.05
			NaOH	13				517 (6.4%)	1.63	0.12	20.0	9.9 ± 2.3	11.0	11.5	0.05
								518 (6.9%)	1.52	0.10	34.0	8.9 ± 2.2	10.0	10.5	0.06
				6.5				524 (6.8%)	1.60	0.21	6.2	15.3 ± 4.4	18.3	20.5	0.08
								521 (6.6%)	1.60	0.10	33.0	10.9 ± 2.7	12.2	12.9	0.06
EtOH	70	30	LiOH	13	50	1-23	4	523 (6.5 %)	1.63	0.17	29.4	9.3 ± 2.8	11.02	11.9	0.09
								517 (6.6%)	1.55	0.17	12.0	9.2 ± 2.6	10.7	11.5	0.08
								518 (6.2%)	1.62	0.09	24.2	9.9 ± 3.1	12.5	14.4	0.10
								522 (6.7 %)	1.65	0.17	16.6	8.5 ± 2.1	9.5	9.9	0.06
				6.5		0.5-23.5		523 (6.4%)	1.69	0.10	32.3	10.0 ± 3.9	13.2	14.7	0.16
				13	60	1-23		524 (8.8%)	1.47	0.55	2.9	9.3 ± 2.4	10.6	11.3	0.07
								524 (9.0%)	1.45	0.49	3.7	10.3 ± 2.3	11.3	11.8	0.05
			NaOH	13	50	1-23		519 (6.6%)	1.57	0.16	18.5	9.5 ± 2.9	11.2	12.0	0.09
				6.5		0.5-23.5		524 (6.0%)	1.75	0.09	25.8	16.3 ± 3.9	18.1	19.0	0.06
EtOH	70 (deionised)	30	LiOH	13	RT	24	4	521 (6.6%)	1.71	0.10	19.5	11.2 ± 2.6	12.4	13.1	0.05
	70 (tap)							X	X	X	X	X	X	X	X
EtOH (snaps)	68	32						533 (12.6%) + large shoulder	1.41	0.78	1.49	Worm (> 20)	X	X	X

* before volume contraction.

Table S16B. Using MeOH as reducing agent.

ROH	H_2O v.%*	ROH v.%*	Base	V mL*	T °C	t h	Base/Au molar ratio	λ_{spr} ($\Delta\lambda/\lambda_{spr}$) nm	A_{spr}/A_{450}	A_{650}/A_{spr}	A_{380}/A_{800}	d_N nm	d_S nm	d_V nm	PdI
MeOH	70	30	LiOH	13	RT	24	4	529 (5.8%)	1.89	0.11	32.3	21.8 ± 7.4	26.6	28.7	0.12
								524 (5.9%)	1.90	0.08	32.5	15.3 ± 8.3	23.9	27.0	0.29
								527 (5.9%)	1.53	0.14	17.2	14.5 ± 5.1	17.9	19.4	0.12
								535 (7.1%)	1.87	0.25	9.4	20.1 ± 7.9	27.2	32.1	0.15
								534 (6.9%)	0.85	0.24	8.62	-	-	-	-
								534 (7.4%)	1.82	0.23	10.6	27.9 ± 17.3	53.2	69.2	0.38
				6.5				534 (6.6%)	1.82	0.14	21.2	22.4 ± 6.6	26.3	28.2	0.09
MeOH	70	30	LiOH	13	50	1-23	4	533 (6.6%)	1.92	0.13	20.3	21.4 ± 9.5	29.6	33.5	0.20
								534 (6.6%)	1.92	0.15	19.8	-	-	-	-
				6.5		0.5-23.5		533 (7.2%)	1.82	0.17	23.7	15.2 ± 10.7	32.2	40.9	0.50
			NaOH	13		1-23		532 (6.5%)	1.92	0.13	20.2	28.6 ± 6.8	31.9	33.4	0.06
				6.5		0.5-23.5		540 (8.1%)	1.79	0.26	10.2	21.7 ± 7.6	26.7	28.9	0.12

* before volume contraction.

Reproducibility of NP synthesis can be a challenge since several factors can influence the outcome.[1,2,27-30] For instance the Turkevich-Frens method is sensitive to pH that can be challenging to control.[29] While we believe that the present study provides a solid starting point, we also made sure to repeat experiments with the same parameters several times on different days and from different batches of chemicals especially using EtOH that leads to the smallest NPs. As illustrated in **Table S16**, the results are relatively reproducible using EtOH (from 8.6 to 12.3 nm with an outlier at 15.8 nm for the RT-synthesis and around 10 nm with a heat treatment) and less reproducible in MeOH (where the average diameter can vary from 15 to 30 nm for the RT-synthesis). This can be related to the different kinetics of the reactions using these two reducing agents. As a comparison, repeats of the Turkevich-Frens synthesis, considered to be a relatively reproducible method, could lead to variation in the range 6.5 to 10 nm average diameter. It is worth stressing that the Turkevich methods uses surfactants which are expected to favor size control[31] and is a method that has been studied and refined since the mid-1950s. The main results presented here were successfully reproduced in three different laboratories.

The purity of the chemicals used is known to be a source of potential reproducibility issues in NP synthesis.[2,28,32] For example water purity can be a source of irreproducibility.[28] We made sure than the general recipe works with deionized water and observed that it does not proceed with Danish (Copenhagen) tap water, **Table S16A**. Commercial spirits previously were shown to be suitable for surfactant-free Pt NPs synthesis.[33] A commercial spirit with high EtOH contents like snaps is suitable to obtain Au NPs, tough the later lead to relatively large NPs, as it can be expected due to the different chemical composition of commercial spirits compared to laboratory grade EtOH.

SM. Scalability

Background. The scalability of a NM synthesis is a common bottleneck for its industrial application, since often scaling up leads to slightly different products.[29,34,35] For a range of applications, e.g. in catalysis, supported Au NPs with a loading around 1 wt.% are required.[36] As a first step toward upscaling the synthesis of Au NPs, experiments in 1 L of solution (1018 mL), with 0.5 mM $HAuCl_4$ leading to an expected 100 mg of Au NPs were performed. This amount would lead to 10 g of 1 wt.% supported catalysts and is reasonable step towards further upscaling. For these experiments the RT-synthesis using LiOH and $HAuCl_4$ in 30 v.% EtOH was first considered adding $HAuCl_4$ or LiOH last. The same experiments performed with a 1 hour step at the relatively low temperature of 50 °C were also performed. Last, due to the relatively higher price of LiOH, experiments at RT where also performed using NaOH. The detailed experimental conditions are reported in **Table S17**. Pictures of the resulting dispersions are reported in **Figure S30** and **Figure S31** and close up pictures of the samples in UV-vis cuvettes are reported in **Figure S33**.

Table S17. Experimental parameters for scaling up experiments performed in 1 L glass bottles. $HAuCl_4$ was added as 2.6 mL of an aqueous solution at 200 mM, LiOH as 36 mL of an aqueous solution at 57 mM, under stirring.

ROH	**H_2O** v.%*	**ROH** v.%*	**$HAuCl_4$** mM*	**Base**	**Base** mM*	**V** mL*	**T** °C	**t** h	**Base/Au** molar ratio	**Added last**	**λ_{spr} ($\Delta\lambda/\lambda_{spr}$)** nm	**A_{spr}/A_{450}**	**Relative yield** **	**A_{650}/A_{spr}**	**A_{380}/A_{800}**	**d_N** nm	**d_S** nm	**d_V** nm	**PdI**
EtOH	70	30	0.5	LiOH	2	1018	RT	24	4	$HAuCl_4$	536 (6.2%)	1.89	1.00	0.14	20.8	30.3 ± 17.8	52.8	58.8	0.35
										LiOH	517 (6.4%)	1.47	0.45	0.18	5.6	8.7 ± 2.7	10.1	10.9	0.10
							50-RT	1-23		$HAuCl_4$	523 (6.7%)	1.52	0.84	0.32	4.2	8.0 ± 2.3	9.3	9.9	0.08
										LiOH	**543 (10.5%)**	1.74	0.87	0.50	3.8	17.8 ± 14.9	51	67	0.70
				NaOH			RT	24		$HAuCl_4$	521 (6.3%)	1.62	0.98	0.10	30.8	10.2 ± 2.8	11.9	12.7	0.08
										NaOH	522 (6.1%)	1.65	0.97	0.09	41.0	11.6 ± 3.7	13.7	14.7	0.10

* before volume contraction; ** evaluated as the ratio of A_{400} for the sample and the maximum values of A_{400} for the dataset at a given v.% of ROH. The sample highlighted in bold show a different optical behavior in absorption and transmission.

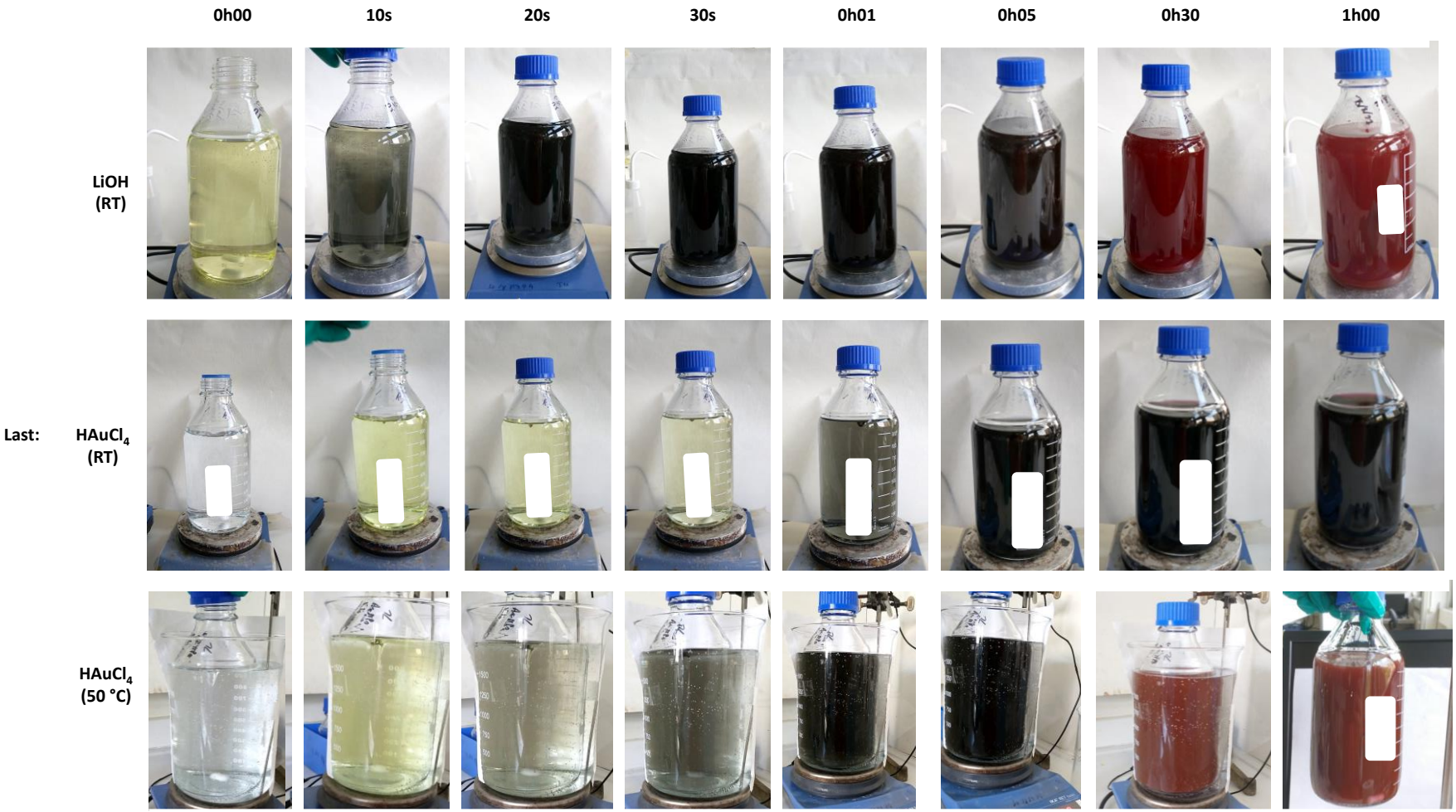

Figure S30. Pictures of different Au NP dispersions obtained for scaling up experiments to 1 L for different times after mixture of all the chemicals and for different chemicals added last, as indicated. See experimental details in **Table S17**.

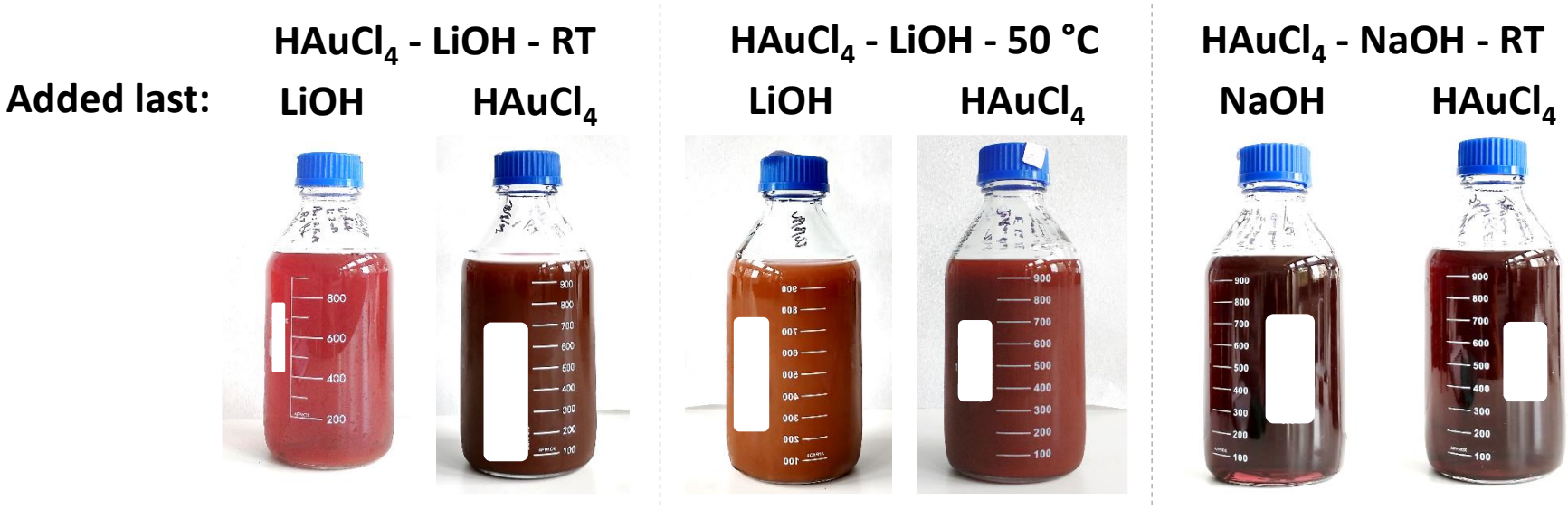

Figure S31. Pictures of different of the Au NP dispersions obtained for scaling up experiments after 24 hours of mixing all the chemicals and for different chemicals added last, as indicated. See experimental details in **Table S17**.

Results. It is clear that the kinetics of the reaction differ for the different conditions. Just like in the case of LiOH added last discussed in **section SJ. Influence of the order of addition of the chemicals**, adding LiOH last at RT lead to an initially faster formation of NPs compared to the case where $HAuCl_4$ is added last. Furthermore UV-vis suggests a lower yield when LiOH is added last, see **Figure S32a**, just like in the case using only 6.5 mL. The case of NaOH showed that if NaOH is added last the time needed to see a pronounced dark color was longer than for LiOH last but shorter than for $HAuCl_4$ added last (with NaOH). It only took ca. 3 minutes for the dark color to form if NaOH was used and $HAuCl_4$ added last, which is faster than the case where LiOH was used and $HAuCl_4$ added last. The fastest reaction happened using LiOH last at 50 °C. In this later case the NPs show a different optical behavior in transmission and absorption. This behavior was not observed for similar conditions with 6.5 mL, which highlights the complex interplay of scaling up.

We believe that the differences observed behavior different behavior might come from the fact that the synthesis undergoes a phase where the solution turns dark, which in large volume can reproduce the dark conditions and their related effects detailed in **section SJ**. . **Influence of the order of addition of the chemicals**. The 'light' conditions might then be changed *as* the reaction proceeds explaining for instance the larger NPs obtained when $HAuCl_4$ is added last in 1 L synthesis (30.3 ± 17.8 nm) compared to 6.5 mL (12.3 ± 2.7 nm). It is anticipated that careful reactor design could address this issue. Identifying reaction conditions where this 'dark' phase is maintained for a minimal amount of time might also improve the size control.

Most importantly for practical considerations, due to the cheaper price of NaOH, the NPs obtained at RT using NaOH lead to small size NPs ca. 10 nm of regardless of the chemicals order of addition (however a fast injection of the NaOH was preferred just after mixing water, $HAuCl_4$ and EtOH). The size obtained for the 1 L synthesis is comparable to a synthesis performed in 6.5 mL (10.2 ± 2.8 nm *vs.* 10.9 ± 2.7 nm, respectively if $HAuCl_4$ is added last, and 11.6 ± 3.7 nm *vs.* 13.3 ± 3.4 nm, respectively if NaOH is added last) and in similar yields estimated from UV-vis spectra for 6.5 mL or 1 L synthesis, see absorption intensity around 400 nm in **Figure S32a**. As a comparison , the Turkevich method prepared in 1 L for $HAuCl_4$ at 0.16 mM lead to ca. 12 nm NPs.[29]

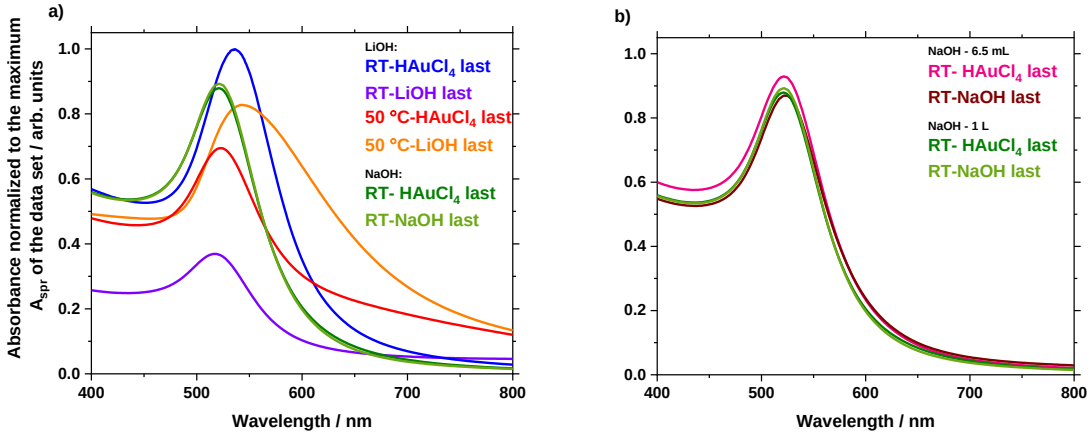

Figure S32. UV-vis spectra of different Au NP dispersions obtained for scaling up experiments to 1 L, as indicated. See experimental details in **Table S17**.

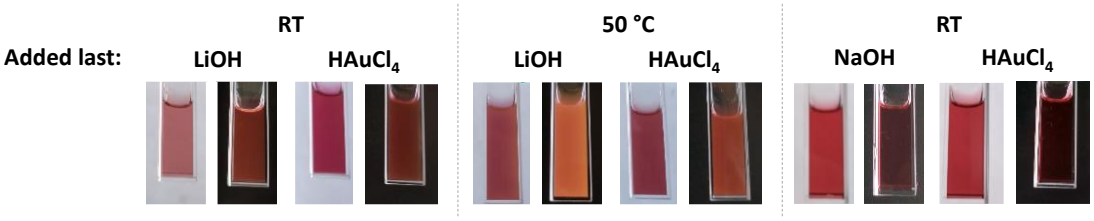

Figure S33. Pictures of the resulting solutions after 24 hours in UV-vis cuvettes (1 cm path length) for 1 L syntheses with 0.5 mM $HAuCl_4$ and 2 mM LiOH adding the base last or $HAuCl_4$ last for, (left) RT-synthesis using LiOH, (middle) 1 hour treatment at 50 °C using LiOH, (right) RT-synthesis using NaOH. In all cases a white and a black background were used to picture the same dispersions. See experimental details in **Table S17**.

Conclusion. The SurFree NPs can be obtained are relatively large scale (1 L) and the use of different chemicals and/or order of addition leads to different NP sizes and shapes with different optical properties. These results make the synthesis promising for further scale up. In particular, the chemicals used here are safe, environmentally friendly and the concentration of base is relatively low. These features make the synthesis readily compatible with flow systems expected to lead to even finer size control.[37]

SN. Mixture of mono-alcohols

Background. In the previous **sections** the challenges to achieve size control are highlighted. Temperature, Base type and concentration, light conditions or order of chemicals addition are all not-straightforward variables to achieve size control. In particular, achieving size control without changing the ionic strength of the solution by adding species like chlorides[38] or a base[39] is a general challenge. Indeed, adding these species might shift the many equilibria at play and detailed in **section SK. Discussion of Au NP formation** , leading to different reaction pathways. Furthermore, changing the ionic strength might impair the colloidal stability.

Results. We here report a simple approach to achieve a relatively fine control over the NP size by simply mixing MeOH and EtOH in different ratios while keeping the total ROH content at 30 v.%. Note that it was key to keep the total amount to 30 v.%, see for instance results in **section SC. Effect of mono-alcohol, mono-alcohol content and cation**, with 10 v.% EtOH or MeOH that does not lead to a significant size control (compared to 30 v.% of the same ROH). Interestingly, it is not two different population sizes that are observed, as it would be the case if MeOH and EtOH played their role independently, see **Table S18** and **Figure S4**. By mathematically adding the populations expected from a mixture of NPs obtained using 30 v.% EtOH or 30 v.% MOH so that the final EtOH:MeOH ratio matches the ratio explored experimentally, it appears that narrower size distributions are obtained if EtOH and MeOH are directly used in the synthesis, **Figure S34** and **Figure S35**. This last observation supports a complex ROH-Au-Base interplay. Interestingly, the RT approach leads to samples with lower PdI.

Table S18. Physical characteristics of the Au NPs obtained for different MeOH and EtOH v.% for a total ROH amount of 30 v.%.

H_2O v.%*	EtOH v.%*	MeOH v.%*	$HAuCl_4$ mM*	Base	Base mM*	V mL*	T °C	t h	Base/Au molar ratio	λ_{spr} ($\Delta\lambda/\lambda_{spr}$) nm	A_{spr}/A_{450}	Relative yield **	A_{650}/A_{spr}	A_{380}/A_{800}	d_N nm	d_S nm	d_V nm	PdI
70	30	-	0.5	LiOH	2	13	RT	24	4	519 (6.4%)	1.62	0.98	0.10	21.5	11.5 ± 2.9	13.1	14.0	0.06
	22.5	7.5								520 (6.3%)	1.66	1.00	0.11	20.3	13.6 ± 3.7	15.6	16.7	0.07
	15	15								523 (6.1%)	1.77	0.97	0.12	17.1	17.2 ± 5.3	21.1	24.6	0.09
	7.5	22.5								527 (6.2%)	1.84	0.99	0.14	20.2	19.3 ± 6.0	23.7	27.4	0.10
	-	30								535 (7.1%)	1.87	0.93	0.25	9.4	20.1 ± 7.9	27.2	32.1	0.15
70	30	-	0.5	LiOH	2	13	50-RT	1-23	4	518 (6.2%)	1.62	0.91	0.09	24.2	9.9 ± 3.1	12.5	14.4	0.10
	22.5	7.5								520 (6.3%)	1.66	0.94	0.13	20.8	12.1 ± 5.7	21.7	36.2	0.22
	15	15								523 (6.1 %)	1.76	0.98	0.15	16.3	14.1 ± 5.2	18.4	21.0	0.14
	7.5	22.5								530 (6.6%)	1.83	1.00	0.12	26.6	17.1 ± 6.1	20.6	22.4	0.13
	-	30								533 (6.6%)	1.92	0.94	0.13	20.3	21.4 ± 9.5	29.6	33.5	0.20

* before volume contraction; ** evaluated as the ratio of A_{400} for the sample and the maximum values of A_{400} for the dataset at a given v.% of ROH.

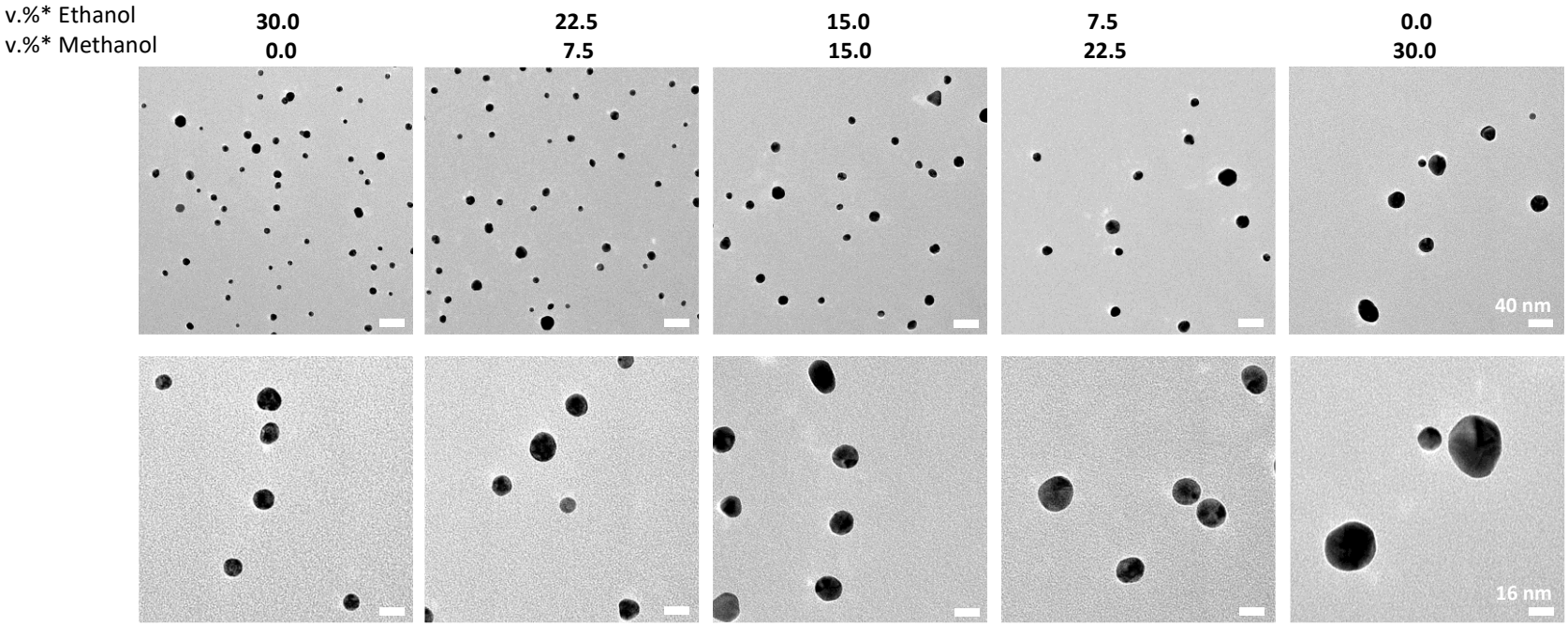

Figure S34. TEM micrographs of Au NPs obtained with different mixture of EtOH and MeOH with water as indicated from 0.5 mM $HAuCl_4$, 2 mM LiOH (LiOH/Au molar ratio of 4) for a RT-synthesis. All scale bars on the top rows are 40 nm, all scale bars on the bottom row are 16 nm.

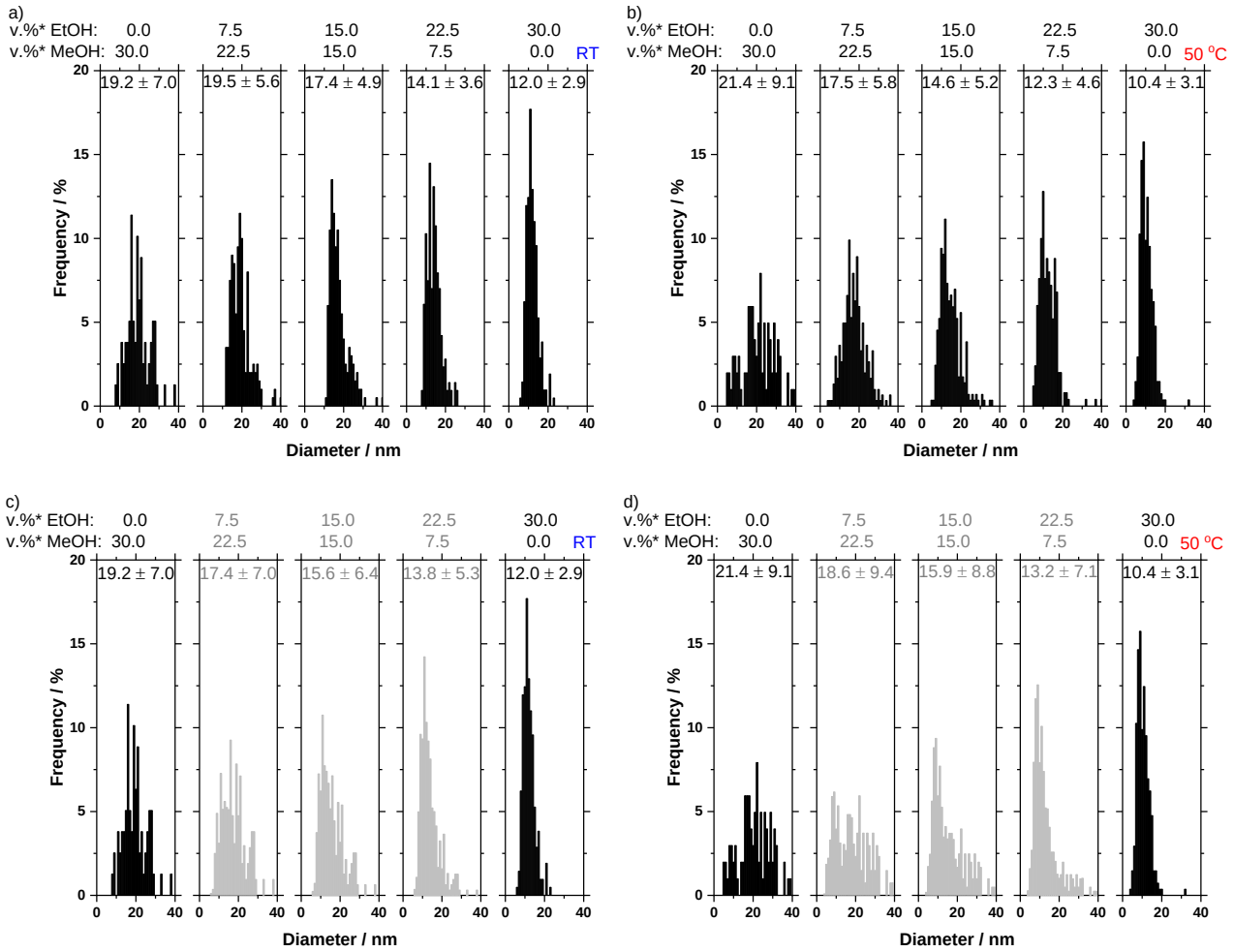

Figure S35. Size distributions retrieved from TEM analysis for Au NPs obtained (a) at RT and (b) at 50 °C as detailed in **Table S18**. The average value and deviation in nm are reported at the top of each data set. (c) and (d) display the size distribution estimated (grey) by mathematically adding the size distribution evaluated for NPs obtained with 30 v.% MeOH and 30 v.% EtOH weighted by the relevant final desired ratio of MeOH and EtOH (* v.% before volume contraction). The size estimation was done from the same dataset as in **Table S18** but the size estimated from the histograms provided include a binning of the data resulting in a slightly different size.

Conclusion. This approach of mixing different ROH to achieve size control does not require extra chemicals (e.g. adding surfactants to achieve smaller size[30] or extra base[39]) or changing the ionic strength of the solution. Given the number of mono-alcohols and polyols available, this opens a new range of parameter space to explore in order to control the synthesis of Au NPs. Interestingly, with the ease to perform the synthesis at a relatively high throughput and the important information retrieved from UV-vis spectra, the use of machine learning[40-42] is anticipated to bring important knowledge on the synthesis of Au NPs.

SO. Cation and surfactant effect

Background. An important aspect of surfactant-free synthesis is to be sensitive to parameters otherwise likely screened in presence of additives. In particular here, the effect of the cations can be investigated. While surfactant-free syntheses are desirable,[43] the synthesis presented here accommodates the use of surfactants. We therefore illustrate the effect of introducing different cations and surfactants in the synthesis.

While a stronger focus has been given in the past to the effect of anions on gold surfaces,[44] the influence of cations on Au surfaces is well established in electrocatalysis[45,46] or corrosion.[47] A general model to explain the effect of cation via non covalent interaction with metal surfaces has been proposed: ''non-covalent interactions between hydrated alkali metal cations $M^+(H_2O)_x$ and adsorbed OH (OH_{ad}) species increase in the same order as the hydration energies of the corresponding cations ($Li^+ >> Na^+ > K^+ > Cs^+$) and also correspond to an increase in the concentration of OH_{ad}–$M^+(H_2O)_x$ clusters at the interface.''[48] In other words, Li^+ leads to stronger non-covalent interactions with the metal surfaces, explaining the lower catalytic activity observed since Li^+-containing electrolytes prevent access to the catalytic surface. Based on this knowledge, using Li^+ is likely to be the key to achieve a better stabilization of metal NPs as we demonstrated with Pt using MeOH as solvent, where the relative stability of the colloids decrease with $Li^+ > Na^+ > K^+ \approx Cs^+$.[17] This effect was less pronounced using EG for Pt NPs. It is however important to keep in mind that the process of forming the metal surface involves different complexes that have different interactions with different cations.[49] For the specific case of Au, there is to the best of our knowledge almost no work on the effect of the cation.

Results. The results presented in **section SC. Effect of mono-alcohol, mono-alcohol content and cation**, as well as **section SJ. Influence of the order of addition of the chemicals** and **section SM. Scalability**, suggest an effect of the cation in the present synthesis of Au NPs. It must be kept in mind that impurities in different bases (e.g. LiOH and NaOH) might also influence the outcome of the synthesis.[2,32] To confirm further the effect of the cation, several experiments were performed using additives like Li_3Ct, Na_3Ct and PVP. Note that these species are also reducing agents so will contribute to the reduction.[26] Conveniently, citrate species can be obtained with Li^+ or Na^+ counter ions. However Na_3Ct is largely preferred with only few reports using Li_3Ct.[50,51] For this study we chose here to use the optimal synthesis parameters established above: 0.5 mM $HAuCl_4$, 2 mM base (Base/Au molar ratio of 4), RT-synthesis. The amount of additives was chosen as 2.5 mM (since it is gives an optimal molar ratio of 5 between Na_3Ct/Au to obtain small size NPs,[31] but of course usually in studies without ROH and without base).

Discussion. As illustrated in **Table S19**, regardless of the cation present, the Turkevich-Frens method adapted to the experimental protocol used in this study leads to the same size NPs around 12 nm, which is only slightly larger than for the synthesis developed here, while we do not use surfactants. In previous reported work, similar size were reported but it was shown that using Li_3Ct different kinetics of reduction were obtained.[51] Different combos LiOH/Li_3Ct, LiOH/Na_3Ct, NaOH/Na_3Ct, NaOH/Li_3Ct were used with 30 v.% EtOH or MeOH. It must be kept in mind that for the ratio mixed, 3.75 cations will come from the citrate species for 1 cation from the base. However the cations coming from the citrate are not expected to be as free in

solution as the cation from the base. As reported in **Figure S36**, a clear effect on the morphology of the NPs is obtained in the different combinations. Using EtOH, the smallest NPs are obtained using LiOH as base. If NaOH is used as base, larger NPs are obtained. The extreme cases were obtained with LiOH/Li_3Ct leading to the smallest and NaOH/Na_3Ct to the largest structures. This underlines the effect of the cation in the synthesis. Using MeOH, a different interplay is observed. The smallest NPs are obtained using Li_3Ct. However, using NaOH seems to give smaller NPs using both Li_3Ct and Na_3Ct. It is then observed that using Li^+-containing species in EtOH, smaller NPs tend to form compared to using Na^+-containing species. This effect is less pronounced with methanol.

To confirm further these results, NaCl and LiCl were also used as additives and while the synthesis using EtOH did not proceed with NaCl, it leads to Au NPs with LiCl. In MeOH, NaCl favored smaller structures. This points towards a more robust synthesis using MeOH as already pointed out, see **section SD. Effect of experimental parameters: HAuCl4 concentration, volume of solution, type of container used, light**, and a different *cation-ROH* interaction.

To confirm further the effect of the cation, similar experiments were performed with PVP, see **Figure S37**. It must be kept in mind that PVP is a reducing agent and will contribute just like citrate to the reduction.[26] In this case, the synthesis using LiOH leads to smaller NPs that in the cases using NaOH. The NPs were also smaller than in a case not using PVP, as it can be expected by using a protective agent. Using NaOH, no NPs are obtained. This challenges the widespread belief that surfactants are *needed* in colloidal syntheses.[52] These results show the detrimental effects of surfactants on the synthesis itself. In previous work using NaOH, PVP and EtOH, NPs were obtained. Although the experiments were performed with 0.4 mM $AuCl_3$, 10 mM NaOH (NaOH/Au molar ratio of 25) and 3 v.% EtOH with 10 g L^{-1} PVP (PVP/Au molar ratio of 225) leading to ca. 6 nm NPs.[15] Interestingly, in that study no NPs were obtained using MeOH whereas NPs are obtained here, in particular when LiOH is used.

Conclusion. These results provide experimental evidence of the complex and probably overlooked interplay between cation-ROH-additives in the process of Au NP formation and stabilization. These results highlight the importance of cations to develop surfactant-free colloidal synthesis of Au NPs and their potential to achieve shape/morphology control, which remains a challenge in surfactant-free syntheses.[43]

Table S19. Influence of the cations Li^+ and Na^+ in the Turkevich-Frens and mono-alcohols synthesis with surfactants using 0.5 mM $HAuCl_4$, 2 mM of base and a volume of 13 mL.

ROH	H_2O v.%*	ROH v.%*	Base	T °C	t h	Base/Au molar ratio	Additive	Additive mM*	Additive/ Au molar ratio	λ_{spr} ($\Delta\lambda/\lambda_{spr}$) nm	A_{spr}/A_{450}	Relative yield **	A_{650}/A_{spr}	A_{380}/A_{800}	d_N nm	d_S nm	d_V nm	PdI
-	100	-	-	85	1	-	Li_3C	2.5	5	517 (6.4%)	1.59	0.97	0.08	28.3	12.4 ± 1.3	12.7	12.8	0.01
			-			-	Na_3C	2.5	5	517 (6.4%)	1.58	0.97	0.07	37.7	12.3 ± 1.2	12.5	12.6	0.01
			LiOH			4	Li_3C	2.5	5	517 (6.4%)	1.57	1.00	0.06	38.7	-	-	-	-
			LiOH			4	Na_3C	2.5	5	517 (6.5%)	1.58	0.99	0.07	38.0	-	-	-	-
			-			-	LiCl+Li_3C	2.0+2.5	4+5	517 (6.4%)	1.58	0.97	0.07	37.3	-	-	-	-
			-			-	LiCl+Na_3C	2.0+2.5	4+5	517 (6.4%)	1.58	0.97	0.07	37.7	-	-	-	-
EtOH	70	30	LiOH	RT	24	4	Li_3C	2.5	5	524 (9.0%)	1.48	0.96	0.27	7.00	9.8 ± 3.6	12.3	13.8	0.13
			LiOH				Na_3C			540 (18.8%)	1.32	0.83	0.81	1.83	12.3 ± 4.0 Elongated	15.1	17.0	0.11
			NaOH				Na_3C			583 (24.0%)	1.49	0.63	0.93	1.32	23.9 ± 9.3 + Chunks	X	X	0.15
			NaOH				Li_3C			593 (21.2%)	1.18	0.74	0.93	1.43	10.6 ± 6.3 + > 20 chunks	18.9	23.4	0.35
			LiOH				LiCl	2	1	524 (6.2%)	1.74	0.89	0.12	19.5	-	-	-	-
							NaCl			X	X	X	X	X	X	X	X	X
			LiOH				PVP	2.5	5	518 (7.3%)	1.45	1.00	0.10	29.0	7.1 ± 1.5	7.7	7.9	0.04
			NaOH							625 (x.x%)	1.20	0.54	1.00	0.97	Network (20)	X	X	X
			LiOH				CTAB			X	X	X	X	X	X	X	X	X
MeOH	70	30	LiOH	RT	24	4	Li_3C	2.5	5	526 (17.0%)	1.56	0.99	0.24	8.3	12.6 ± 5.4	16.8	18.3	0.18
			LiOH	RT	24	4	Na_3C	2.5	5	529 (11.5%)	1.46	0.97	0.49	2.5	17.4 ± 5.2 Elongated	X	X	0.09
			NaOH	RT	24	4	Li_3C	2.5	5	521 (7.0%)	1.61	0.95	0.11	21.2	13.0 ± 3.0	14.5	15.5	0.05
			NaOH	RT	24	4	Na_3C	2.5	5	524 (6.0%)	1.63	0.99	0.37	4.3	15 Network > 50	X	X	X
			LiOH	RT	24	4	LiCl	2	1	534 (7.1%)	1.87	0.77	0.23	8.6	-	-	-	-
				RT	24	4	NaCl	2		528 (6.0%)	1.93	X	0.12	17.6	18.3 ± 7.4	23.4	25.3	0.16
			LiOH	RT	24	4	PVP	2.5	5	532 (8.3%)	1.57	1.00	0.18	15.8	10.1 ± 4.0 > 50	X	X	0.16
			NaOH							681 (x.x%)	1.23	0.49	1.00	0.93	Network (20)	X	X	X
			LiOH	RT	24	4	CTAB	2.5	5	X	X	X	X	X	X	X	X	X

* before volume contraction; ** evaluated as the ratio of A_{400} for the sample and the maximum values of A_{400} for the dataset at a given v.% of ROH. Using CTAB the solutions turned orange and were not investigated further.

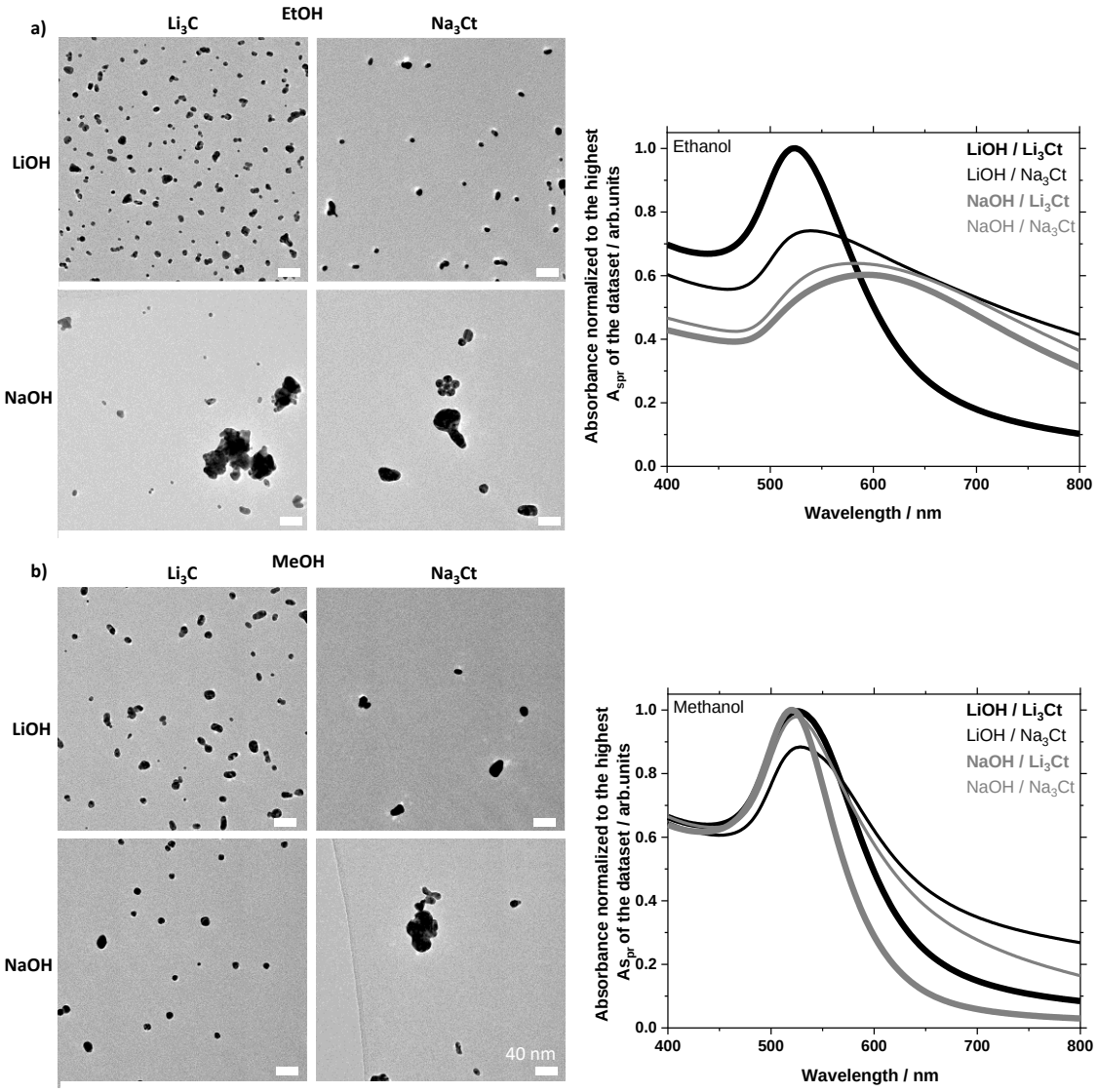

Figure S36. TEM and UV-vis characterization of Au NPs obtained with different base (2 mM) and Li_3Ct or Na_3Ct (2.5 mM) combination as indicated. The synthesis was performed at RT with 0.5 mM $HAuCl_4$.

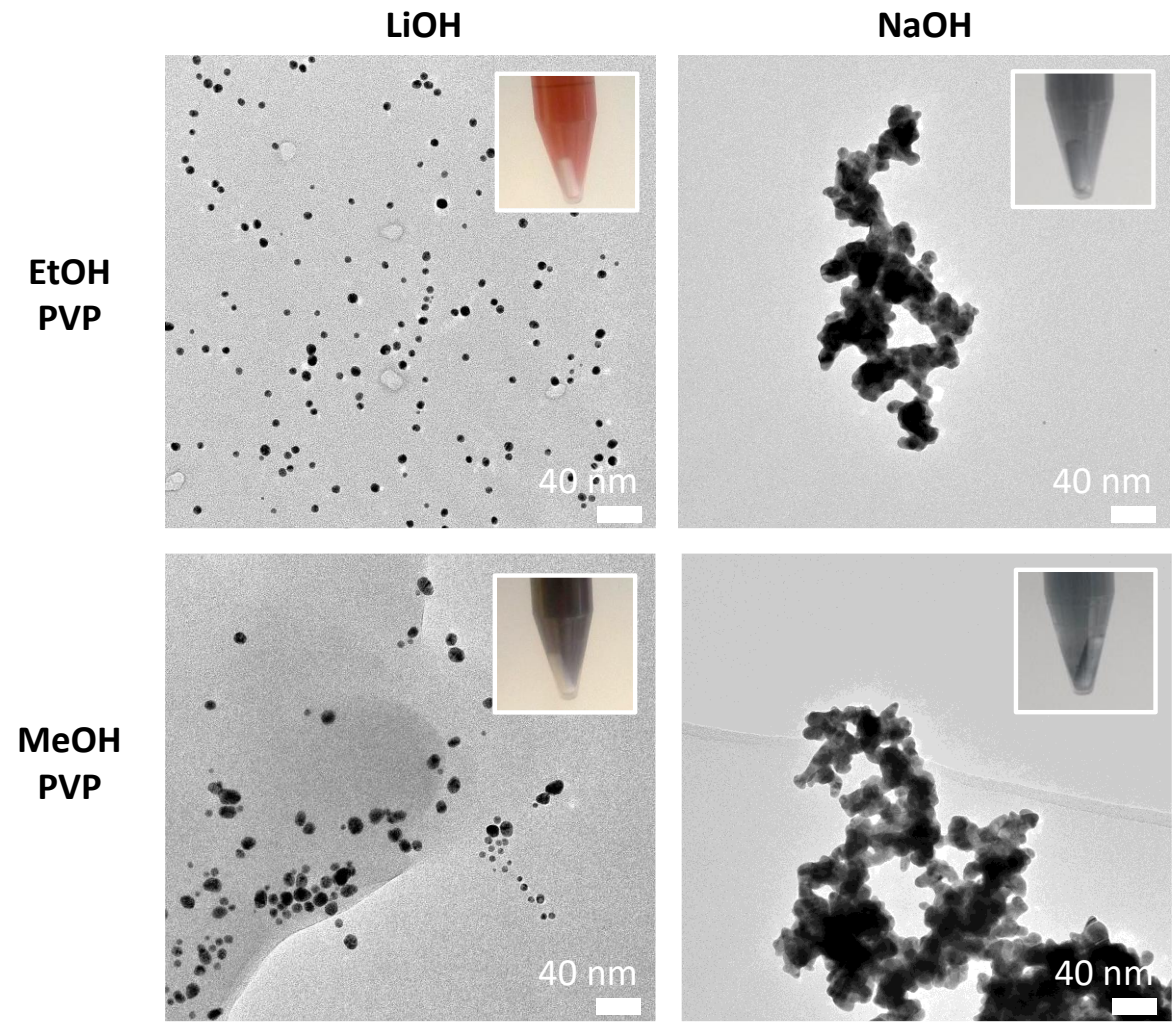

Figure S37. TEM and UV-vis characterization of Au NPs obtained with different base (2 mM) and PVP (2.5 mM) combination as indicated. The synthesis was performed at RT with 0.5 mM $HAuCl_4$.

SP. Electrochemical characterization of Au NPs

Background. Up to date, there are only few methods to obtain SurFree NPs readily active for catalysis. Surfactant-protected NPs are preferred, which requires cleaning/washing steps to remove the surfactants.[53-55] The Turkevich-Frens method in particular is popular, but it is challenging to establish how relevant a synthesis it is, without a comparison with SurFree NPs. Indeed, the use of Na_3Ct may block some active sites and impair a full use of the Au surface atoms for catalysis. Whether citrate does or does not impair electrochemical activity is a relatively open question.

Although Au NPs are not necessarily the most active catalysts for the EOR, they are still active in alkaline media leading mainly to acetic acid / acetate as products.[56] The EOR is a suitable reaction to develop alcohols fuel cells for energy conversion moving away from fossil fuels based technologies.[57] We use this reaction as model reaction here since it will be also used in section **SR. Pd and bimetallic NPs**.

Results. The properties of SurFree NPs prepared by the method introduced in this work with or without PVP or the Turkevich method are compared, see experimental conditions for the syntheses in **Table S2** and **Table S19**. It is common in electrochemistry to develop PM NPs on conductive carbon support.[58] A careful control of the supporting steps and later on *ink* formulation (i.e. dispersion of the supported NPs in the right solvents to facilitate further processing) can require a careful optimization and strongly influences the comparison in electrochemical testing.[58] In the present study, it was observed that for a same metal loading, the preparation of 30 wt.% Au or Pd on carbon redispersed at the same catalyst concentration in 30 v.% EtOH in water, lead to stable inks for Pd but not for Au. This is probably due to the difference in size of the NPs, see section **SR. Pd and bimetallic NPs**, that therefore cover the carbon support surface differently for the same loading, which leads to different ink stability. In addition, the presence of surfactants will ultimately complicate the supporting of the surfactant-protected NPs that will be stabilized in solutions and so less prone to be supported. As an extra challenge, upon drying, the NPs obtained with surfactant may aggregate due to stabilizer-stabilizer interaction, see for instance **Figure S39**. To alleviate these extra challenges in comparative studies, we here compare the NPs directly deposited on the glassy carbon electrode.

The NPs prepared using PVP, LiOH and EtOH were smaller than without PVP, ca. 7 nm and 8-10 nm respectively, see **Table S19** and **Table S16**. However no electrochemical activity could be measured when PVP was used. The PVP blocks the electrochemically active sites of the Au NPs, in agreement with previous work.[59,60] The gain of a smaller and more monodisperse size using PVP, that in theory should lead to NPs with higher electrochemically active surface area (ECSA) and higher mass activity (MA), appears irrelevant due to the absence of electrochemical activity. In contrast, the SurFree NPs are only slightly larger and do show electrochemical activity. This illustrates once more the benefits of a surfactant-free approach.

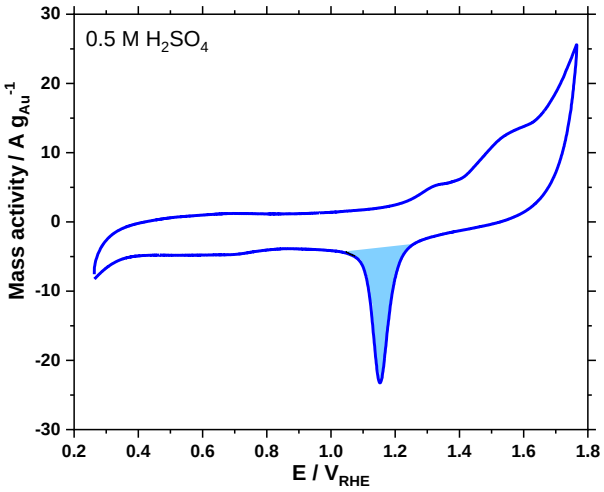

Figure S38. Example of cyclic voltammogram of SurFree Au NPs obtained using EtOH and LiOH, recorded in 0.5 M H_2SO_4 at 50 mV s^{-1} showing that the Au NPs are readily electroactive. The area highlighted in blue corresponding to the reduction of gold oxide was used to establish the ECSA of the Au NPs as detailed in **the experimental section of the manuscript**.

Figure S displays TEM of Au NPs prepared by the Turkevich-Frens method and SurFree NPs. The Au NPs obtained by the Turkevich method are slightly larger than SurFree NPs, ca. 12 and 10 nm respectively see **Table S19** and **Table S16**, and upon drying on the TEM grids significantly agglomerate, yet without connecting with another. This *gathering* is commonly observed on TEM micrograph of NPs obtained by the Turkevich-Frens method[30] and is attributed to attractive citrate-citrate interaction in the outer-functionalized shells of the NPs. In contrast, the SurFree NPs are well dispersed on the TEM grid.

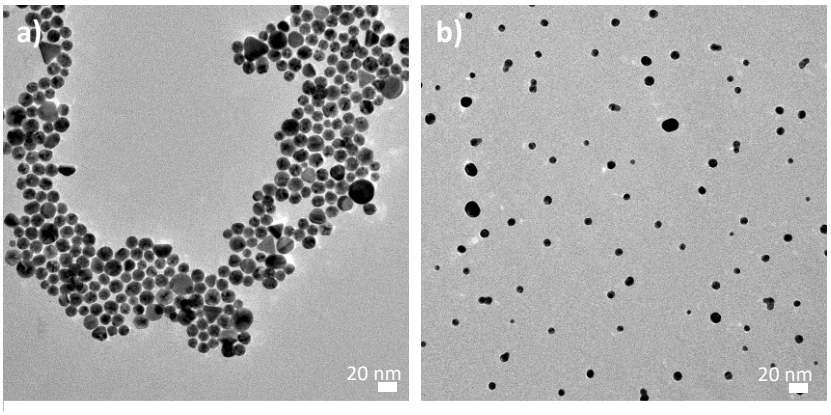

Figure S39. TEM micrographs of Au NPs obtained by (a) the Turkevich method and (b) the surfactant-free synthesis detailed here.

As a further comparison, the electrochemical properties of SurFree Au NPs prepared using different ROH with 30 v.% ROH, 0.5 mM $HAuCl_4$, 2 mM LiOH and RT-synthesis, see **Table S4**, were evaluated. The highest activities were obtained when mono-alcohols were used. While

the size of the NPs obtained in EtOH and glycerol for instance are about the same around 10 nm, the activity obtained is the highest for EtOH and the lowest for glycerol. This is explained by the challenge to actually drop the NPs and evaporate the solvent when the high boiling point polyols are used. This results in NPs that likely do not get supported on the glassy carbon. Interestingly, despite having a size nearly twice larger around 20 nm, the NPs prepared using MeOH show the second highest activity, see **Figure S40**.

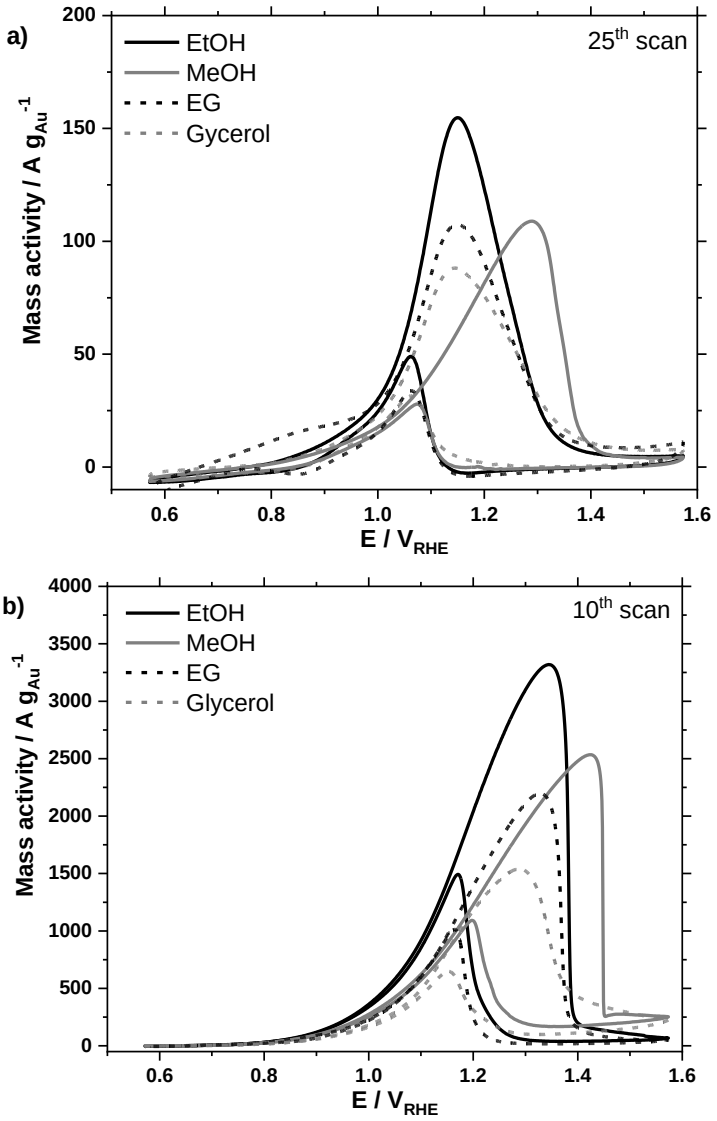

Figure S40. Cyclic voltammograms au Au NPs prepared using 30 v.% ROH and 0.5 mM $HAuCl_4$ and 2 mM LiOH at RT where ROH is EtOH, MeOH, EG or glycerol, as indicated, for (a) the EOR in 1 M KOH and 1 M EtOH at a scan rate of 50 mV s^{-1} and (b) the EGOR in 1 M KOH and 1 M EG at a scan rate of 20 mV s^{-1}.

Conclusion. By using the introduced surfactant-free synthesis of Au NPs, it is here demonstrated that the Turkevich-Frens method is not only a convenient synthesis but also the citrate does not prevent the development of relatively active electrocatalysts. It appears that upon electrochemical treatment, the citrate gets removed and relatively active catalytic NPs compared to SurFree NPs are obtained. However, for practical reasons, the use of citrate

will prevent a simple supporting of the NPs, see section **section SQ. Supported NPs**. The SurFree NPs are relatively more active especially when EtOH is used as reducing agent. These results finally illustrate the benefits of using mono-alcohols *versus* polyols and surfactant-based syntheses of NPs.

SQ. Supported NPs

Background. As pointed out in **section SP. Electrochemical characterization**, NPs used as catalysts are typically supported on another material to avoid NP agglomeration under catalytic conditions and/or confer different catalytic properties, or conductivity in the case of electrochemistry. Typical support materials are oxides like Al_2O_3, MnO_2, TiO_2, CeO_2, etc. and carbon materials.

Results. To develop supported materials, the surfactant-free synthesis developed here can be performed directly in presence of a support. **Figure S41** provides representative TEM micrographs of the Au NPs obtained from a solution of 0.5 mM $HAuCl_4$ using 30 v.% EtOH and 2 mM LiOH in presence of TiO_2 so that the nominal loading of Au is 2 wt.%. The synthesis was performed at RT and light in PP container (ca. 50 mL) left under stirring for 24 hours. After synthesis, the dispersion was centrifuged and washed with water.

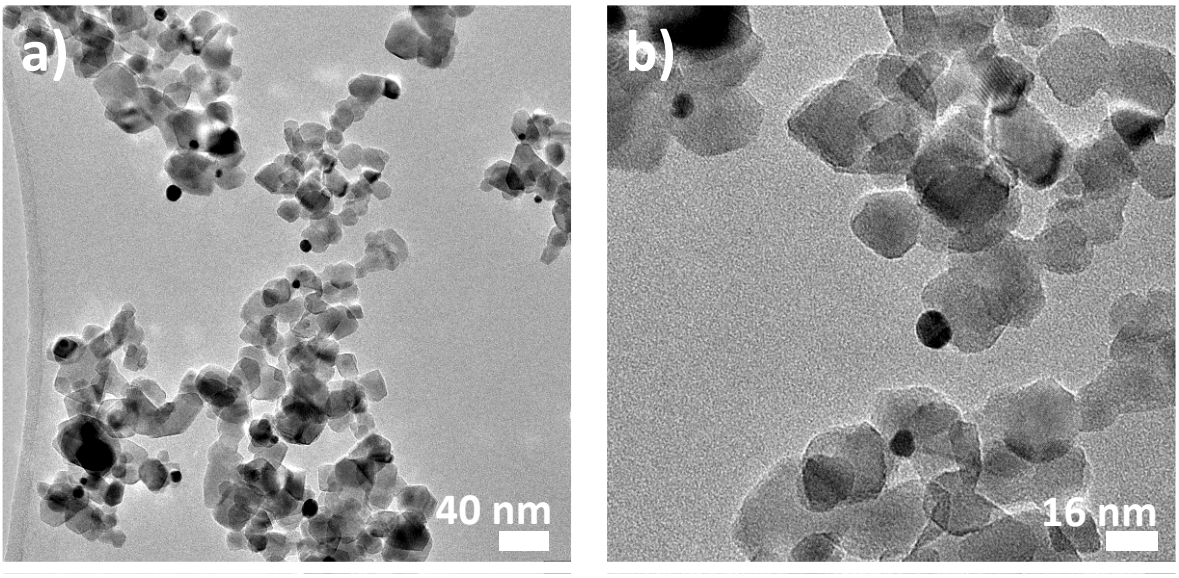

Figure S41. TEM micrographs of Au NPs directly obtained on TiO_2. The grey features are the TiO_2 whereas the darker circular features are the Au NPs.

Discussion. While this one-pot synthesis works well, there are two drawbacks in this approach. First, the benefits of separating colloidal syntheses from supporting steps are lost.[53] Second, if dark supports are used like MnO_2 or carbon, we observed that the NPs tend to be larger than what is obtained in absence of support for otherwise similar conditions. This is in line with the different mechanisms observed with or without light, see **section SJ. Influence of the order of addition of the chemicals**. Conveniently, supported Au NPs are also obtained by simple evaporation of the low boiling point solvents from pre-formed colloidal dispersions. **Figure S42** is a representative TEM micrograph of the Au NPs obtained from a solution of 0.5 mM $HAuCl_4$ using 30 v.% EtOH and 2 mM LiOH that was left to react 24 hours before being mixed with a required amount of MnO_2 to obtain a 2 wt.% loading of Au. The synthesis solvent (mixture of EtOH and water) was left to evaporate at RT overnight under stirring in a glass petri dish. The solid powder obtained was then centrifuged and washed with water. A similar approach used carbon as support to co-immobilize Au, Pd or Au *and* Pd NPs in a molar ratio

of 2:3 (see **sections SR and ST**) with a nominal metal loading of 30 wt.%. The TEM characterization confirms the supporting of small size Au and/or Pd NPs. This approach is challenging to perform with EG or glycerol due to the high viscosities and high boiling points of these solvents (see **section SP**).

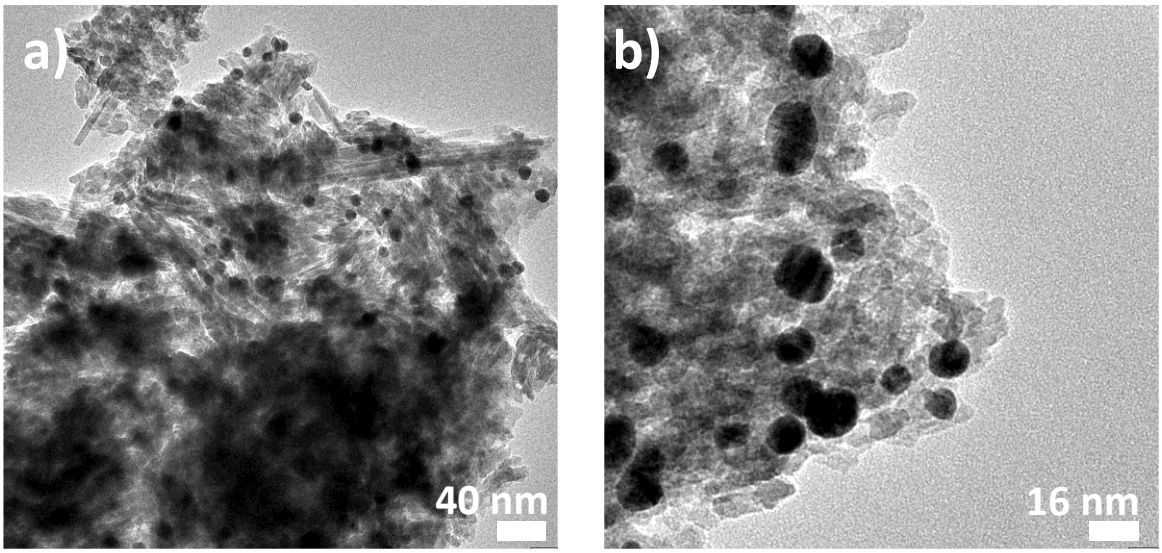

Figure S42. (a,b) TEM micrographs of Au NPs obtained from a SurFree colloidal dispersion after solvent removal (30 v.% EtOH in water) in presence of MnO_2. The grey features are the MnO_2 whereas the darker features are the Au NPs.

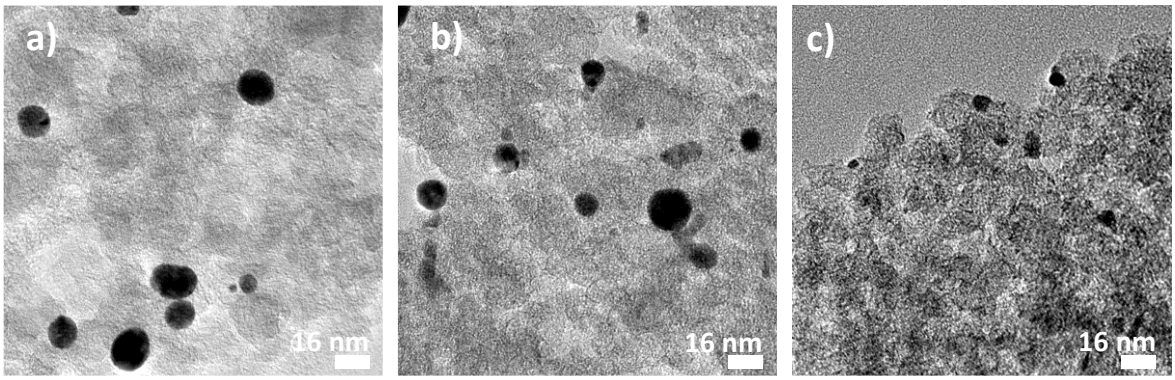

Figure S431. TEM micrographs of (a) Au NPs, (b) Au and Pd NPs in a molar ratio of 2:3 and (c) Pd NPs from colloidal dispersions using 30 v.% EtOH after solvent removal in presence of carbon for a metal loading of 30 wt.%. The darker features are the NPs. In (b) the larger and darker NPs correspond to Au and the smaller and lighter NPs correspond to Pd, based on the NP size observed in (a) and (c).

SR. Pd and bimetallic NPs

Background. Developing bi-metallic NPs is a promising strategy to tune the properties of catalysts.[61] So-called bi-metallic NPs and alloys bring new features to NPs.[62] In this study we investigated the relevance of the surfactant-free synthesis method using 30 v.% EtOH and LiOH as starting point, to develop Au_xPd_y NPs. Conveniently the synthesis also leads to SurFree Pd NPs at RT and different colloidal Au_xPd_y NPs were obtained. It must be stressed that just like Au NPs, the present synthesis present multiple benefits over alternative synthetic methods of Pd NPs,[63-65] in light of the need for green syntheses and the multiple applications of Pd in medicine,[66] sensing and catalysis.[67] Au_xPd_y NPs are relevant catalysts for various reactions like, hydrogen evolution reaction, CO_2 reduction reaction, CO oxidation, hydrogenation or small molecules oxidation.[62] An example of use of these Au_xPd_y NPs is for the EOR. Au NPs are relatively poor catalysts for this reaction compared to Pd NPs. However, Au NPs are more stable. The rationale to develop Au_xPd_y NPs is therefore to improve the catalytic performances, relative to Au or Pd NPs.[68,69] With the approach proposed here, small size NPs around 3-4 nm are obtained, see **Table S20**, which is a relatively small NP size compared for instance to a RT-synthesis using plant extracts leading to ca. 7 nm NPs[70] or synthesis using L-ascorbic acid and PVP in water and ethylene glycol leading to ca. 10-20 nm NPs.[71] The electrocatalytic properties of the bimetallic NPs are further characterized in **section ST. Electrochemical characterization of AuxPdy NPs and [x Au + y Pd] nanocomposites.**

Structural characterization.

Table S20. Physical characteristics of Au_xPd_y NPs retrieved from TEM-EDS.

ROH	**H_2O** v.%*	**ROH** v.%*	**$HAuCl_4$** mM*	**$PdCl_2$** mM*	**Base**	**Base** mM*	**V** mL*	**T** °C	**t** h	**Base/Au** molar ratio	Resulting **composition****	**d_N** nm	**d_S** nm	**d_V** nm	**PdI**
EtOH	70	30	0.50	-	LiOH	2	13	RT	24	4	Au	9.0 ± 2.2	10.0	10.6	0.06
			0.38	0.12							$Au_{83}Pd_{17}$	4.4 ± 1.3	5.2	5.7	0.09
			0.25	0.25							$Au_{65}Pd_{35}$	3.4 ± 0.7	3.7	3.9	0.04
			0.13	0.37							$Au_{33}Pd_{67}$	3.0 ± 0.6	3.3	3.4	0.04
			0.07	0.44							$Au_{20}Pd_{80}$	3.5 ± 0.8	3.9	4.2	0.05
			-	0.5							Pd	4.3 ± 1.1	4.9	5.5	0.07
	70	30	0.5	-	LiOH	2	13	50	1-23	4	Au	7.9 ± 2.1	9.0	9.6	0.07
			0.38	0.12							$Au_{87}Pd_{13}$	5.4 ± 1.3	6.2	6.8	0.06
			0.25	0.25							$Au_{66}Pd_{34}$	3.7 ± 0.9	4.1	4.4	0.06
			0.13	0.37							$Au_{53}Pd_{57}$	3.2 ± 0.7	3.6	3.8	0.05
			0.07	0.44							$Au_{42}Pd_{58}$	3.5 ± 1.2	4.4	4.9	0.12
			-	0.5							Pd	3.5 ± 1.1	4.3	4.9	0.10

* before volume contraction; ** evaluated by EDS.

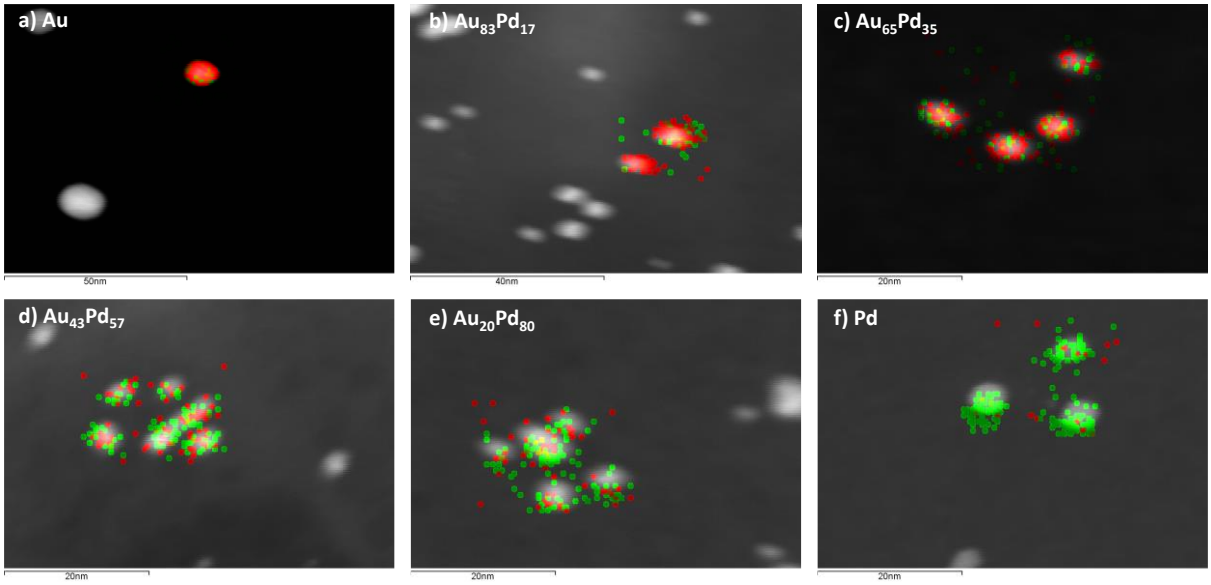

Figure S44. STEM-EDS map of individual Au_xPd_y NPs obtained at RT as detailed in **Table S20** and as indicated with signal from Au in red (M peak) and Pd in green (L peak). Red dots in (f) are artefacts from the background.

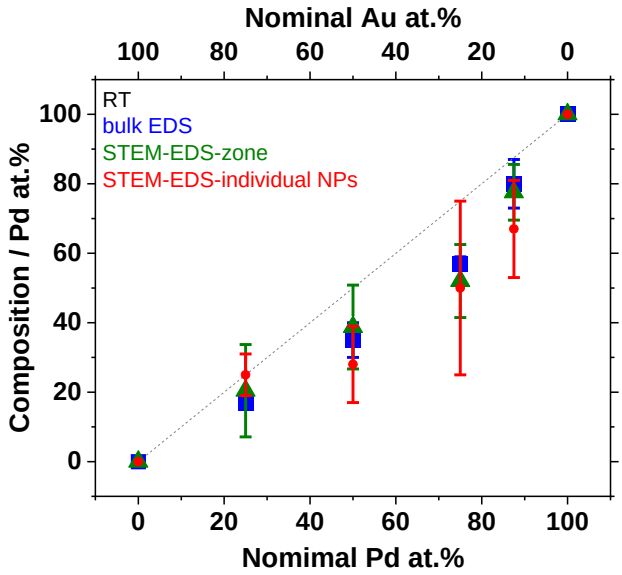

Figure S45. Comparison of Au or Pt content in Au_xPd_y NPs prepared at RT as indicated in **Table S20**, as a function of nominal Au or Pd content retrieved from bulk EDS measurement, STEM-EDS measurements on selected zone comprising several (e.g. 3-4) NPs and individual NPs, as indicated.

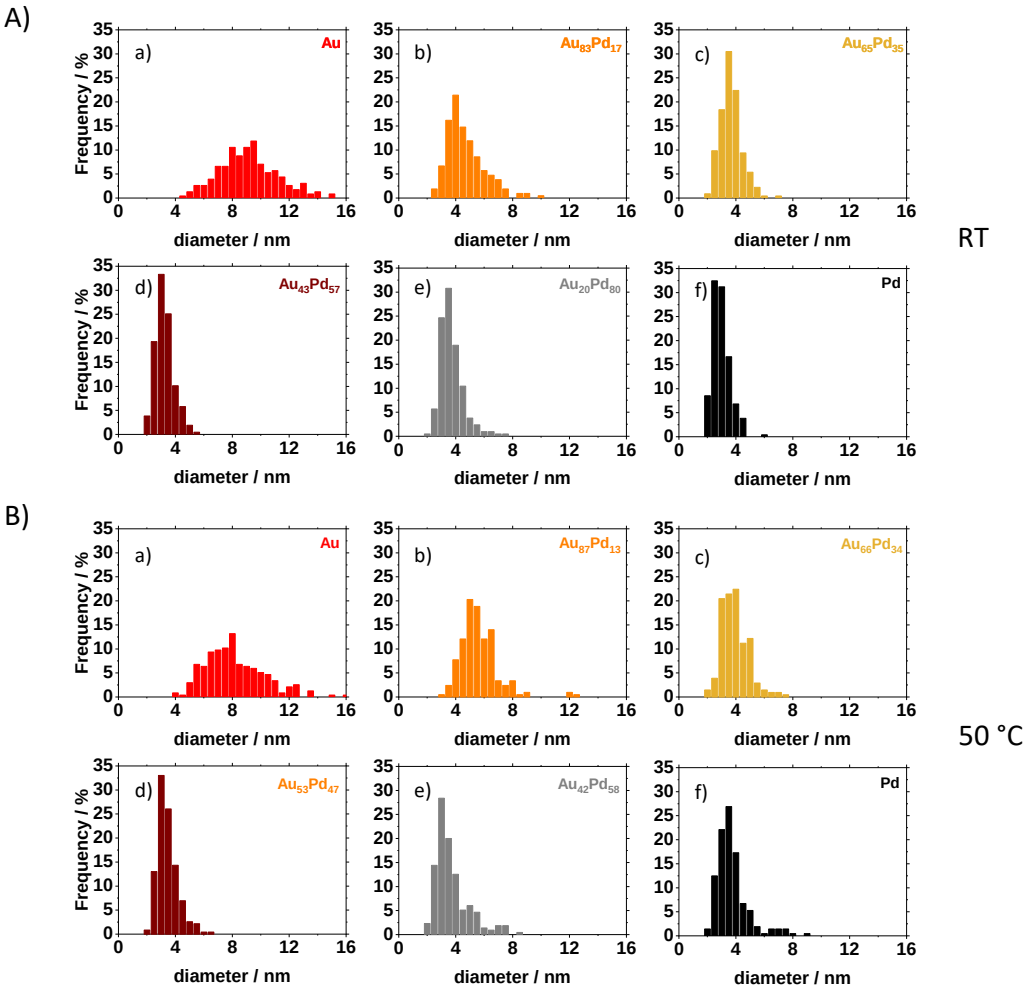

Figure S46. Size distribution retrieved from TEM micrographs for Au_xPd_y NPs prepared (a) at RT and (b) using a synthesis step at 50 °C for 1 hour, see **Table S20**.

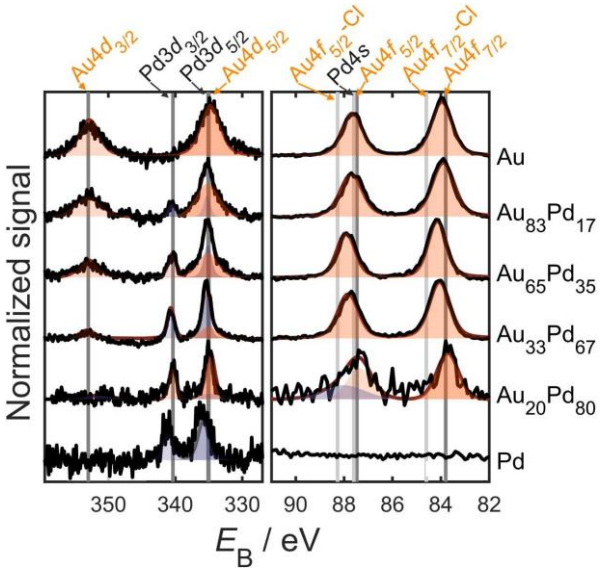

Figure S47. Background subtracted (*Shirley* type) and normalized XPS spectra of (left) the Au4*d* and Pd3*d* region and the (*right*) Au4*f* region. The relevant peaks from NIST database have been included for Au_xPd_y NPs obtained at RT.

Table S21. XPS parameters used to quantifying Au and Pd ratios for Au_xPd_y NPs prepared at RT, see **Table S20**.

Peak name	Selection rule	Peak position (eV)	Max FWHM (eV)	Sensitivity factors	Peak shape
Au4$f_{7/2}$	-	83.9*	2.0	9.58	GL(30)
Au4$f_{5/2}$	$\frac{3}{4}S_{\mathrm{Au}4f_{7/2}}$	87.5	2.0	7.54	GL(30)
Au4$d_{5/2}$	-	335.1	4.6	11.74	GL(30)
Au4$d_{3/2}$	$\frac{2}{3}S_{\mathrm{Au}4d_{5/2}}$	-	4.6	8.06	GL(30)
Pd3$d_{5/2}$	-	335.0	2	9.48	GL(30)
Pd3$d_{3/2}$	$\frac{2}{3}S_{\mathrm{Pd}3d_{5/2}}$	-	2	6.56	GL(30)
Pd4*s*	-	87.6	2.0	0.598	GL(30)

* Au coordinated to Cl (*e.g.* in a salt) will reach Au4$f_{7/2}$ peak positions around 84.6 eV rather than the normally reported 83.9 eV.

The *CasaXPS* peak shape GL(30) gives satisfactory results mainly due to the low S/N, i.e. for more idealised and planar Au-Pd catalyst the Doniach-Šunjić modified Gaussian-Lorentzian shapes DS(0.1, 150) or similar is recommended. The Pd4*s* peak is not expected to be visible due to its low scattering-cross section and consequent sensitivity factor. However, due to the low Au content in the $Au_{13}Pd_{87}$ sample it is considered reasonable to account for its contribution in the spectrum as *ca.* 2/3 of the signal arising around the Au4$d_{3/2}$ peak would arise due to Pd4*s* and not Au.

XPS results confirm the presence of Au^0 and Pd^0 in the sample.[69] In **Figure S47**, it is observed that increasing the amount of Pd in the NP tends to shift the Pd3*d* peaks position to higher energies, see **Table S21**, suggesting either significant oxidation, or coordination to Cl, or alternatively very slight charging. Spectra of the Au4*f* region suggest that increasing the amount of Pd in the sample shifts the binding energies of the Au4*f* to higher values ($Au_{13}Pd_{87}$ does not follow this trend). This trend can be a result of oxidation and/or is due to the formation of increasingly under-coordinated Au sites. By using the peaks of **Figure S47**we are able to establish the elemental ratios, presented in **Table S22**. The ratio estimated agrees well with the ratio evaluated by EDS.
While Au4$f_{7/2}$ peak maintain a quite fixed value around 83.9 eV, as expected,[72] the Pd3$d_{5/2}$ peaks are often 0.5 eV above the excepted 335 eV, see **Table S21**. This can be explained by the ability to form Au rich overlayer [73] in a Au_xPd_y structure and the tendency for Pd to bind stronger with advantageous species; either originating form synthesis or the ambient environment it was exposed to prior to XPS.

Table S22. Elemental ratio estimated from XPS for Au_xPd_y NPs prepared at RT, see **Table S20**.

Sample[a]	Au:Pd[b]	Sample[b]	$E_{\mathrm{Au}4d5/2}$ / eV	$E_{\mathrm{Pd}3d5/2}$ / eV	$E_{\mathrm{Au}4f7/2}$ / eV
Au	100:0 (±0%)	Au	334.9	-	84.0
$Au_{87}Pd_{17}$	89.8:10.2 (±8.1%)	$Au_{90}Pd_{10}$	335.1	335.2	83.9
$Au_{65}Pd_{35}$	59.6:40.4 (±7.0%)	$Au_{60}Pd_{40}$	335.5	335.6	84.1
$Au_{33}Pd_{67}$	31.3:68.7 (±16.3%)	$Au_{31}Pd_{69}$	335.3	335.7	84.1
$Au_{20}Pd_{80}$	21.1:78.9 (±5.2%)*	$Au_{21}Pd_{79}$	335.2	335.5	83.7
Pd	0:100 (±0%)	Pd	-	335.8	-

a) Composition evaluated by EDS. b) Ratios have been derived from the Au4*d* and Pd3*d* peaks, except * where Pd4*s* and Au4*f* also have been used. The uncertainties have been estimated from the Au4*f* and Au4*d* peaks. Note: $E_{\mathrm{Au}4f5/2} - E_{\mathrm{Au}4f7/2} = 3.67$ eV, $E_{\mathrm{Au}4d5/2} - E_{\mathrm{Au}4d3/2} = 18$ eV and $E_{\mathrm{Pd}3d5/2} - E_{\mathrm{Pd}3d3/2} = 5$ eV.

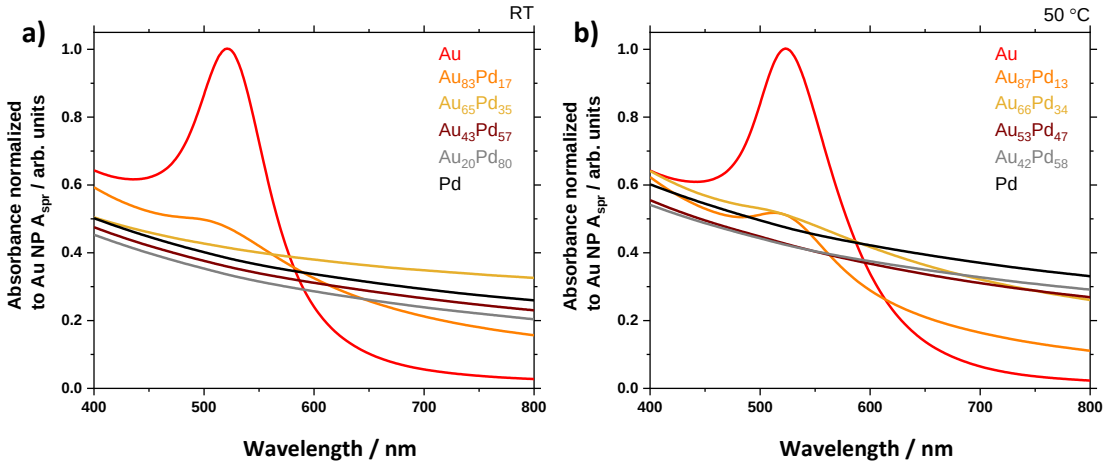

Figure S48. UV-vis characterization of Au_xPd_y NPs obtained (a) at RT and (b) using a synthesis step at 50 °C for 1 hour, see **Table S20**.

Table S23. Refinement parameters from PDF analysis of X-ray TS data acquired on an Empyrean lab source instrument (Au) and at the DanMAX beamline for Au_xPd_y NPs obtained at RT as detailed in **Table S20**.

	Empyrean	**DanMAX**					
	Au	**Au**	**$Au_{83}Pd_{17}$**	**$Au_{65}Pd_{35}$**	**$Au_{33}Pd_{67}$**	**$Au_{20}Pd_{60}$**	**Pd**
Scale Factor	0.38	0.70	0.54	0.52	0.35	0.30	0.23
Fit range	2 Å – 100 Å	2 Å – 50 Å	2 Å – 40 Å	2 Å – 30 Å	2 Å – 30 Å	2 Å – 30 Å	2 Å – 30 Å
Number of refined parameters	5	5	5	5	5	5	5
R_w	0.33	0.27	0.19	0.17	0.28	0.38	0.22
Q_{damp} (Å^{-1})	0.011	0.022	0.022	0.022	0.022	0.022	0.022
Q_{broad} (Å^{-1})	0.004	0.00013	0.00013	0.00013	0.00013	0.00013	0.00013
Q_{max} (Å^{-1})	18.0	19.9	19.9	19.9	19.9	19.9	19.9
U_{iso} (Å^2)	0.0421	0.0110	0.0125	0.0131	0.0139	0.0113	0.0187
Lattice par., *a* (Å)	4.10	4.10	4.06	4.01	4.02	3.98	3.96
δ_2 (Å^2)	3.59	1.08	2.37	3.11	3.18	2.29	3.69
Sp-diameter (Å)	172	40.7	30.9	25.9	22.0	23.4	27.4

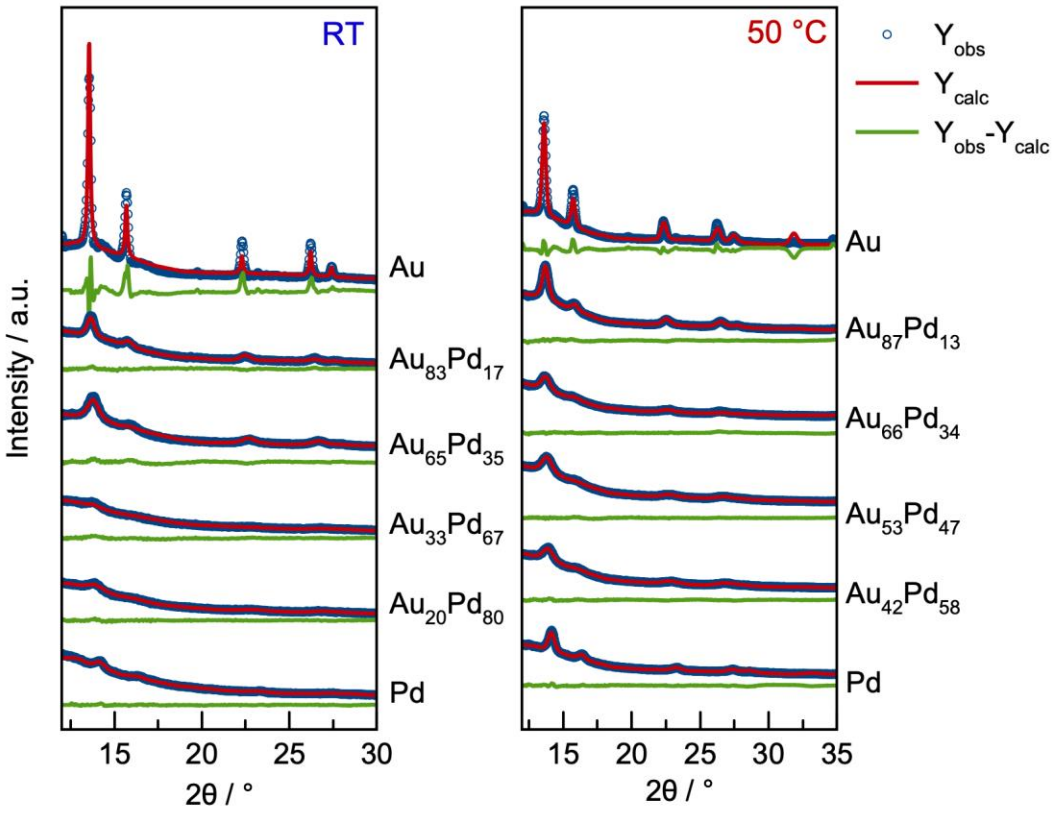

Figure S49. XRD characterization and LeBail fit results for Au_xPd_y NPs obtained at RT or using a synthesis step at 50 °C for 1 hour, as indicated, see **Table S20**.

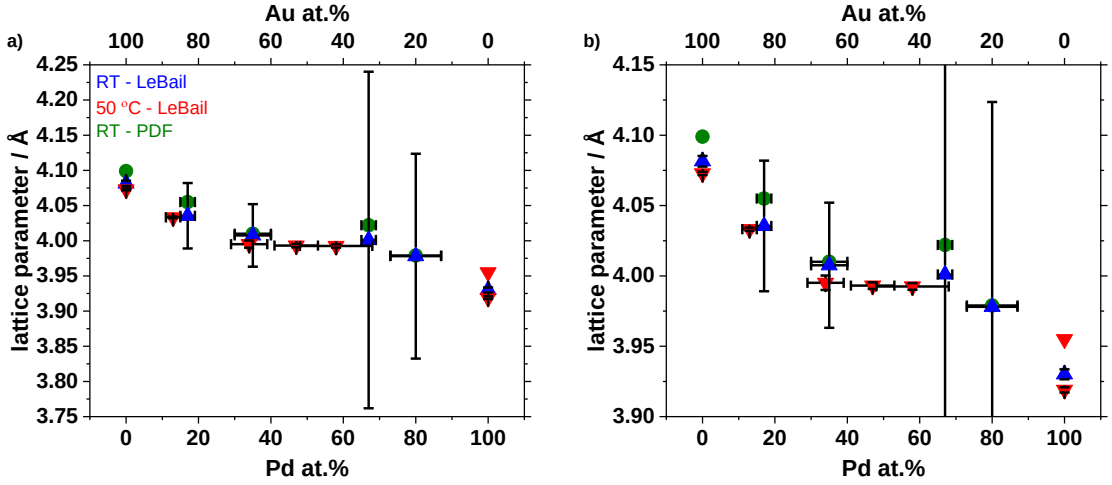

Figure S50. (a,b) Lattice parameters retrieved from X-ray TS experiments for different samples and different methods, as indicated. The Au_xPd_y NPs were prepared at RT (blue triangles) or using a synthesis step at 50 °C (red triangles) for 1 hour as detailed in **Table S20**. The green dots correspond to syntheses performed at RT but for a lattice parameter retrieved from PDF analysis. (b) is a zoomed-in version of (a) to better picture the trend.

Table S20 summarizes the properties of the Au_xPd_y NPs. While the nominal Au:Pd ratio does not match exactly the ratio observed in the resulting materials, the trend 'more Au precursor leads to more Au in the final sample' is confirmed, see also **Figure S45**. In agreement with previous report, it is observed that Au_xPd_y NPs tend to be more Au rich than expected. This can be explained because Au is a more noble metal than Pd, so the Au^{3+} ions reduce more rapidly than Pd.[71] The Au:Pd ratio in the sample is further confirmed by XPS, **Table S22**, and the composition estimated by EDS and XPS agree well. In order to confirm the formation of Au_xPd_y NPs and not a mixture of Au and Pd NPs, a statistical particle size analysis was performed from TEM micrographs, see **Figure S46**. Since a single size was observed and not a mixture of small (ca. 4 nm, Pd) and large (ca. 10 nm, Au) NPs, this suggests the formation of bimetallic NPs. The smallest mean size obtained correspond to ca. 40-60 at.% Au. The formation of bimetallic is further confirmed by UV-vis, **Figure S48**, where a pronounced plasmon resonance observed with Au NPs disappears as the Pd content increases.

Furthermore, crystallographic characterization was performed. For structural insight, XRD and X-ray TS experiments were conducted on the Au_xPd_y NPs. It is observed that Au NPs are characterized by sharp Bragg peaks in agreement with the larger size of the Au NPs, **Figure S49**. Increasing the amount of Pd in the Au_xPd_y NPs results in a broadening of the peaks, in agreement with the size decrease observed by TEM. Simultaneously, a peak shift to higher Q-values is observed as a consequence of the Pd doping. This is expected due to the smaller unit cell parameters for Pd *fcc* compared to the Au *fcc*.[12,69] The symmetric nature of the Bragg peaks of the Au_xPd_y NPs indicates single phase *fcc*. Therefore, the XRD characterization together with XPS, EDS and TEM, points towards the formation of a bimetallic NPs of decreasing size as the Pd content increases.[12] The lattice parameters of structures of the samples were determined through real space Rietveld refinement of the PDFs using the PDFgui software.[74] The XRD patterns were analyzed using the Le Bail analysis in the FULLPROF suite program.[75] In agreement with an alloyed structure, the lattice parameters follow an increasing linear trend with increasing Au content, see **Figure S50**.

Conclusion. Bimetallic NPs are formed using the synthesis presented.

SS. Nanocomposites

Background. Recently, the development of nanocomposites made of a mixtures of different NPs rather than alloyed NPs has (re)gained interest.[76-78] A first (**I**) goal in this approach is to develop dual versatile catalysts that can operate for different reactions, while not necessarily being the optimal catalyst for all the reactions. A second argument is that (**II**) proximity effects at the nanoscale can confer positive features like higher stability or activity for a given reaction.[79,80] A third driving force for this approach is more conceptual. (**III**) It is preferred in R&D to know *as well as possible* the structure, size, composition of NPs *before* any catalysis is performed. This allows relating the assessed catalytic performances to the *initial* physico-chemical properties of the NPs. This knowledge is used to understand how these properties change to ultimately propose improvement in the design of the *well-defined starting* catalyst material. In an ideal scenario, the catalyst can be characterized after reaction. This *post-mortem* characterization brings new insights in degradation mechanism(s) but does not give information on what is happening *under* catalytic reaction. *Post-mortem* characterization might also be performed after cooling down the catalyst, or after washings, and often on very limited amount of recovered material, which can render post-catalysis analysis challenging. These approaches provide a relatively limited insight since under catalytic conditions (including temperature, pressure, chemical concentration like strong acid etc.) and under the catalytic reaction itself, where chemicals interact with the NP surface atoms and a lot is happening. In this respect, *in situ* studies have brought precious knowledge.[81] Understanding the transformation occurring on monometallic NPs under catalytic conditions however remains a challenge. Understanding the transformation occurring on bi-metallic NPs is even more challenging since extra phenomena like phase segregation, leaching etc. might take place.

Benefits of nanocomposites. While a detailed understanding is certainly a must to rationally improve nanocatalysts, the remaining challenges in the characterization of NMs make the option to develop nanocomposites attractive, and ultimately more practical, especially at large scale production to make sure to obtain the same material composition *before* catalysis. Indeed, preparing bimetallic NPs is relatively more challenging than mono-metallic NPs, and the later easier to characterize, see above **sections**. While in this nanocomposite approach there is still little known on what is happening to the catalysts, it is in the first place not so different to many studies performed where only the initial state of the catalysts is thoroughly established. For a detailed comparison and studies of these nanocomposites, all NPs should ideally be produced by the same synthesis methods, which is often challenging when Au NPs are involved,[77] but now possible here.

Results. Following this nanocomposite strategy, a batch of Au and Pd NPs were prepared separately and mixed in different ratios of Au and Pd, their electrochemical properties were assessed following the same protocols as for Au_xPd_y NPs, see **section ST. Electrochemical characterization of AuxPdy NPs and [x Au + y Pd] nanocomposites**.

We first confirm that a mixture of Au and Pd NPs does not lead to Au_xPd_y which could be observed due to remaining unreacted precursor complexes in the colloids. Upon mixing the colloidal dispersions of Au and Pd NPs, there is no evidence of reaction between the large ca. 10 nm Au and smaller ca. 4 nm Pd NPs, as confirmed by the bimodal experimental NP size distribution retrieved from TEM, **Figure S51**-**Figure S53**. The size retrieved shows two

populations for which the histogram size distribution matches the theoretical distribution expected from mathematically adding the size distribution of Au NPs and Pd NPs weighted by the ratio of the mixture used. If alloys were formed, according to results presented in **section SR. Pd and bimetallic NPs**, a mono-modal size distribution would be obtained.

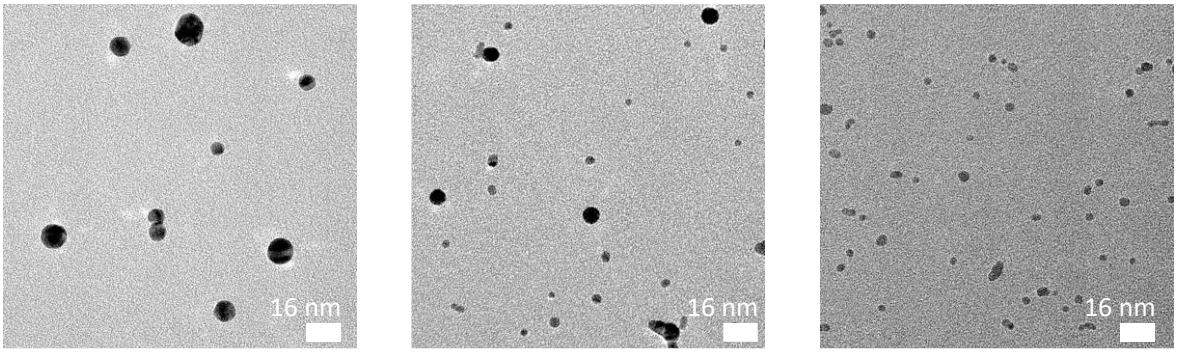

Figure S51. TEM micrographs of (a) Au, (b) [50 Au + 50 Pd] and (c) Pd NP samples prepared at RT.

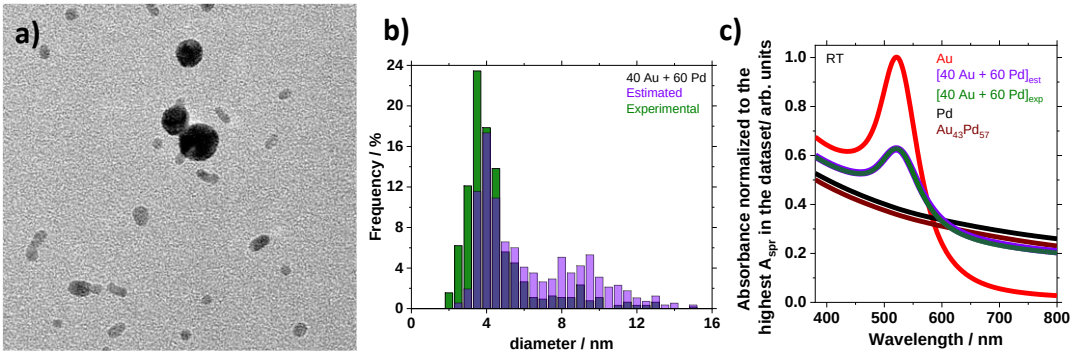

Figure S52. (a) TEM micrograph of [40 Au + 60 Pd] nanocomposite. (b) Size distribution evaluated from TEM for [40 Au + 60 Pd]. The experimental size distribution as well as the expected size distribution estimated by mathematically adding the size distribution of Au NPs and Pd NPs in a ratio 40:60 are reported, as indicated. (c) Experimental UV-vis spectra of (red) Au NPs, (green) [40 Au + 60 Pd] nanocomposite, (brown) $Au_{43}Pd_{57}$ and (black) Pd NPs obtained at RT. The expected UV-vis spectrum estimated by adding the UV-vis spectra of Au NPs and Pd NPs mathematically weighted by a ratio 40:60 is also reported in purple but almost perfectly overlap with the experimental UV-vis spectrum of [40 Au + 60 Pd] nanocomposite.

UV-vis analysis confirms that nanocomposites are obtained, **Figure S52**, where bimetallic NPs do not show a well-defined plasmon resonance, but where the spectrum of a mixture of Au and Pd NPs in different ratios matches the UV-vis spectra obtained by mathematically adding the spectrum characteristic of Au and Pd weighted by the relative coefficients for a given Au:Pd ratio.

A)

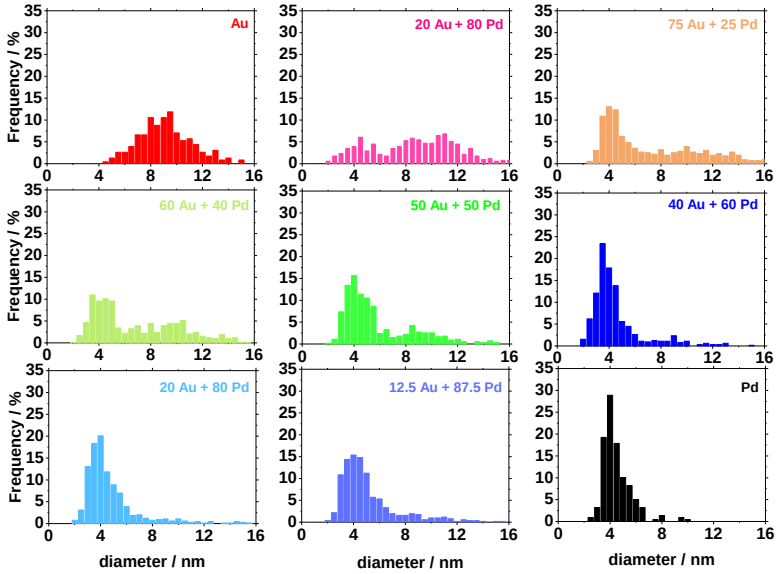

B)

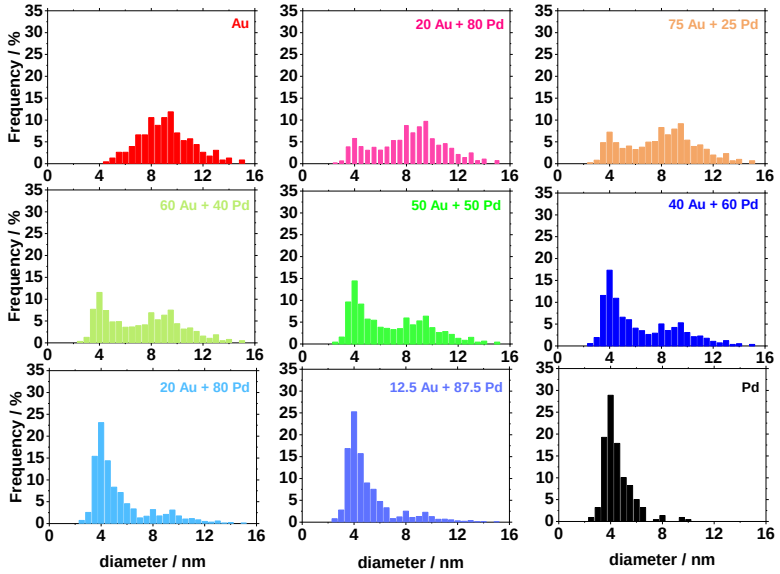

Figure S53. (A) Size distribution retrieved from TEM micrographs for various [x Au + y Pd] NPs as indicated. (B) Theoretical size distribution expected by mathematically adding the size distribution of Au and Pd NPs weighted by the desired ratio of x and y.

ST. Electrochemical characterization of Au_xPd_y NPs and [x Au + y Pd] nanocomposites

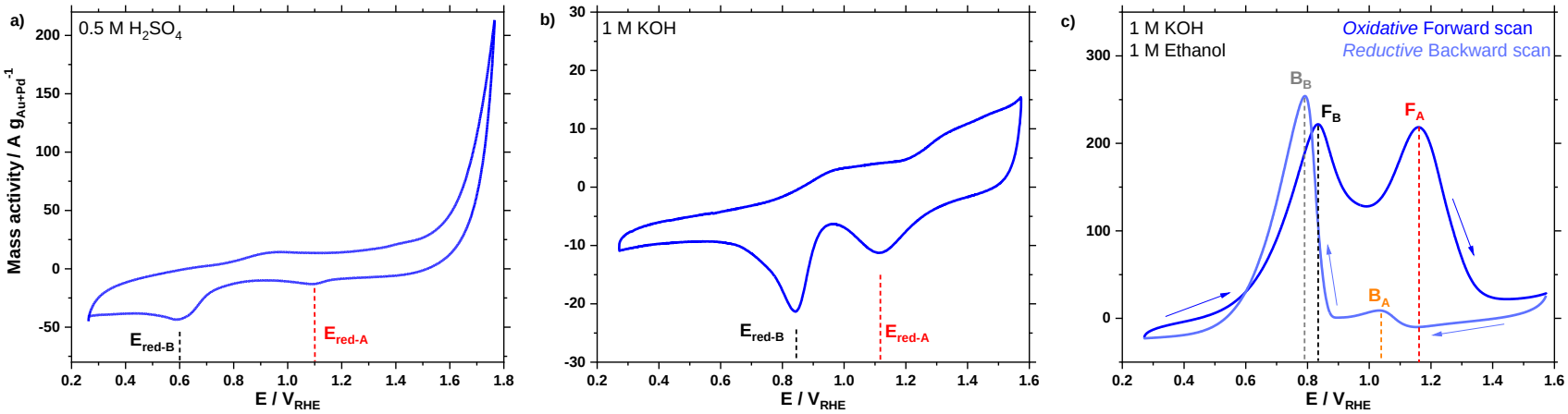

Figure S54. Illustrative CVs of Au_xPd_y NP electrochemical characterization following *Protocol A* detailed in **the experimental section of the manuscript** in (a) 0.5 M H_2SO_4, (b) 1 M KOH and (c) 1 M KOH and 1 M EtOH. All scans were recorded at 50 mV s^{-1} with (a) $Au_{20}Pd_{80}$, (b) $Au_{65}Pd_{35}$ and (c) $Au_{83}Pd_{17}$ NP samples. Different features discussed later are annotated for clarity.

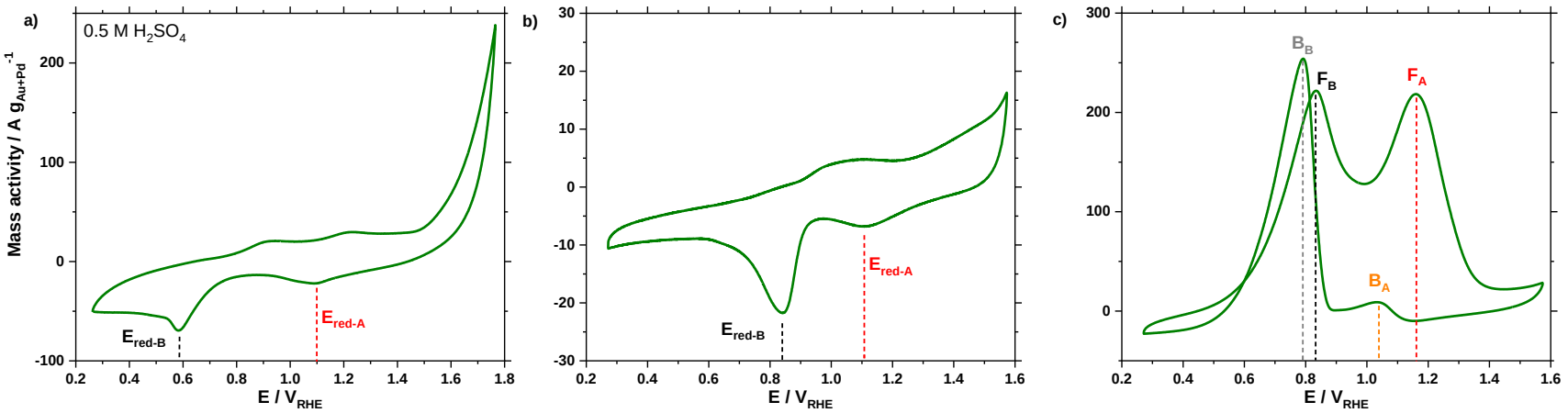

Figure S55. Illustrative CVs of [x Au + y Pd] nanocomposite samples, electrochemical characterization following the *Protocol A* detailed in **the experimental section of the manuscript** in (a) 0.5 M H_2SO_4, (b) 1 M KOH and (c) 1 M KOH and 1 M EtOH. All scans were recorded at 50 mV s^{-1} with (a) [20 Au + 80 Pd], (b) [60 Au + 40 Pd] and (c) [80 Au + 20 Pd]. Different features discussed later are annotated for clarity.

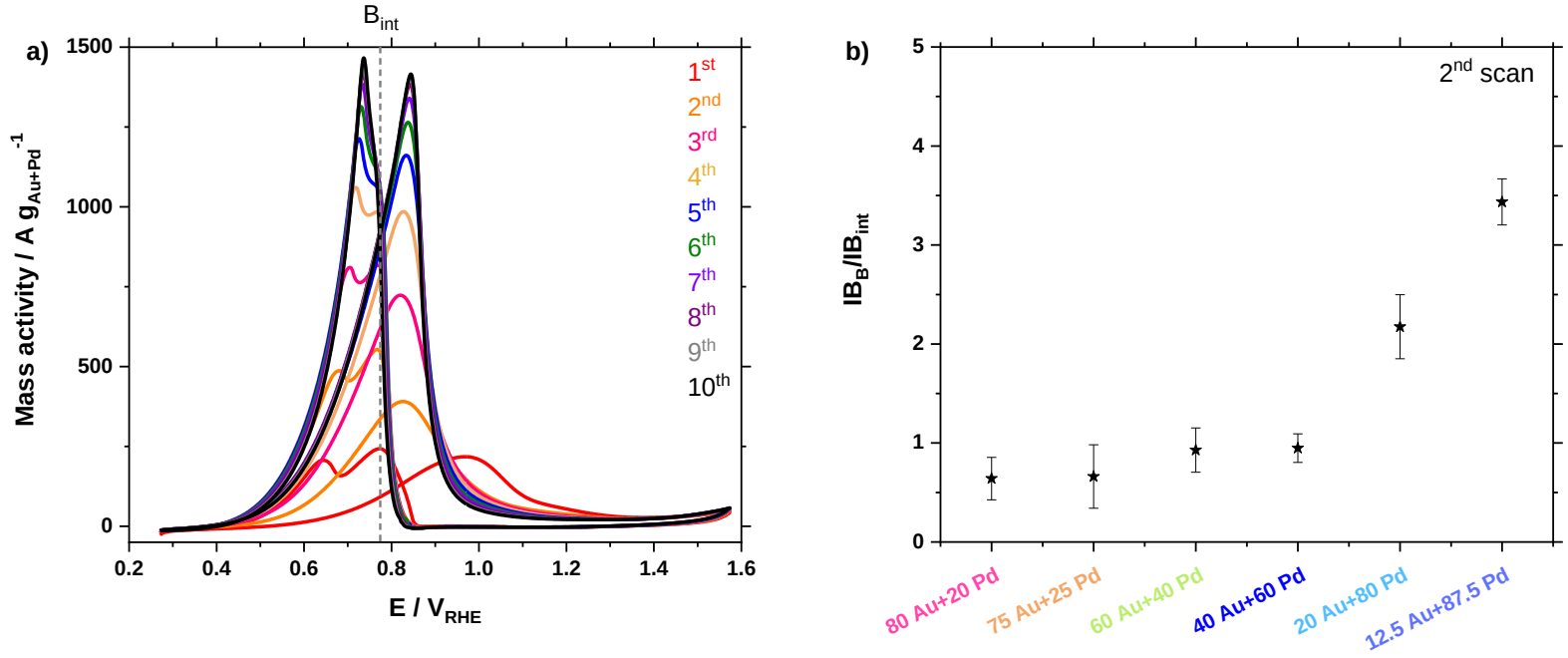

Figure S56. (a) Examples of the first 10 CVs for [40 Au + 60 Pd] NPs obtained at RT recorded following the *Protocol B* detailed in **the experimental section of the manuscript** and example of the intermediate peak B_{int} in between B_A and B_B as defined in **Figure S55a-b**. (b) Ratio of the intensity of B_B and B_{int} peaks for different [x Au + y Pd] NP samples.

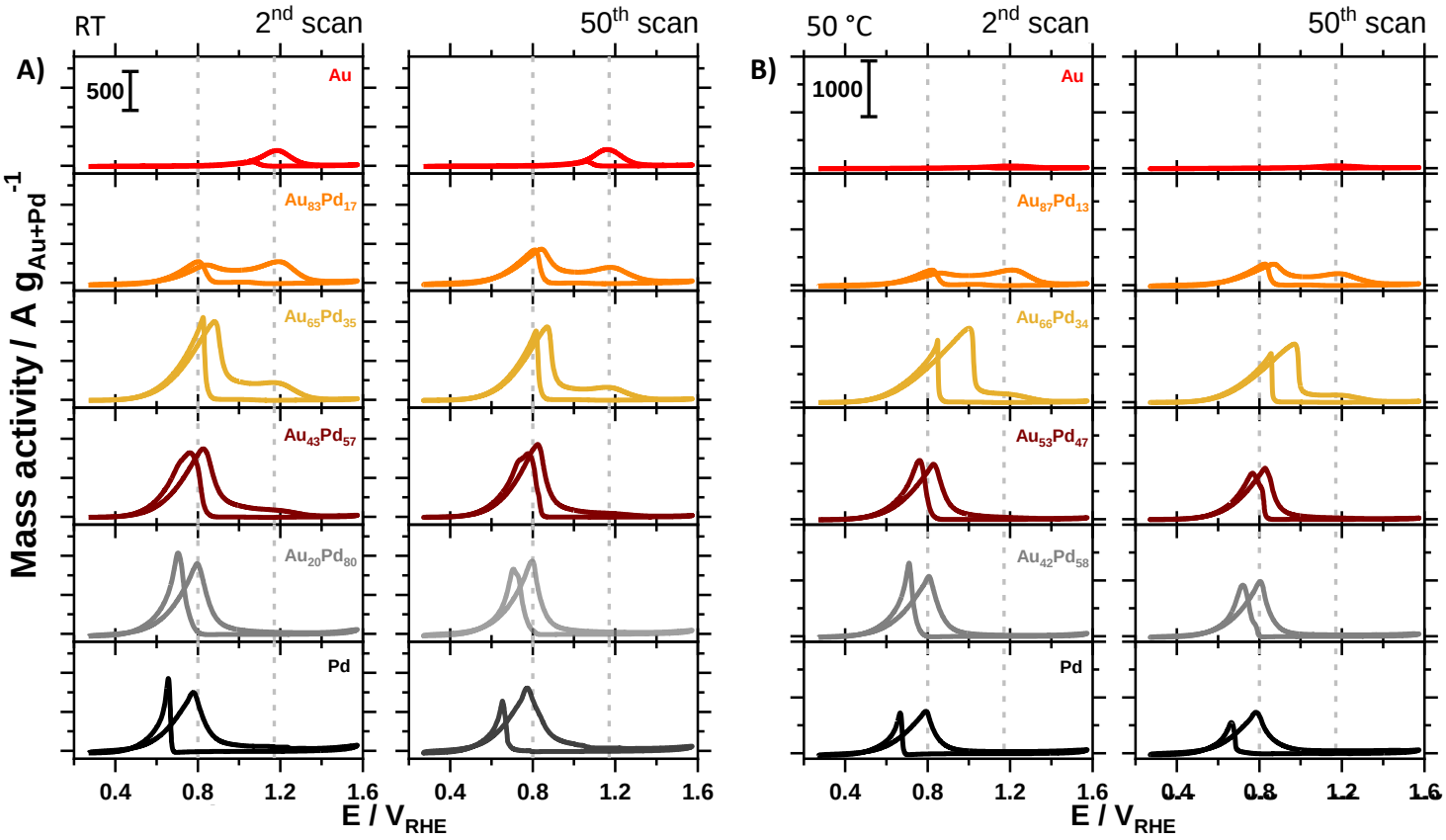

Figure S57. Examples of CVs for Au_xPd_y NPs obtained (A) at RT or (B) using a synthesis step at 50 °C for 1 hour, as indicated, after 2 scans and 50 scans, as indicated, at 50 mV s^{-1} in 1 M EtOH and 1 M KOH, following the *Protocol A* detailed in **the experimental section of the manuscript**.

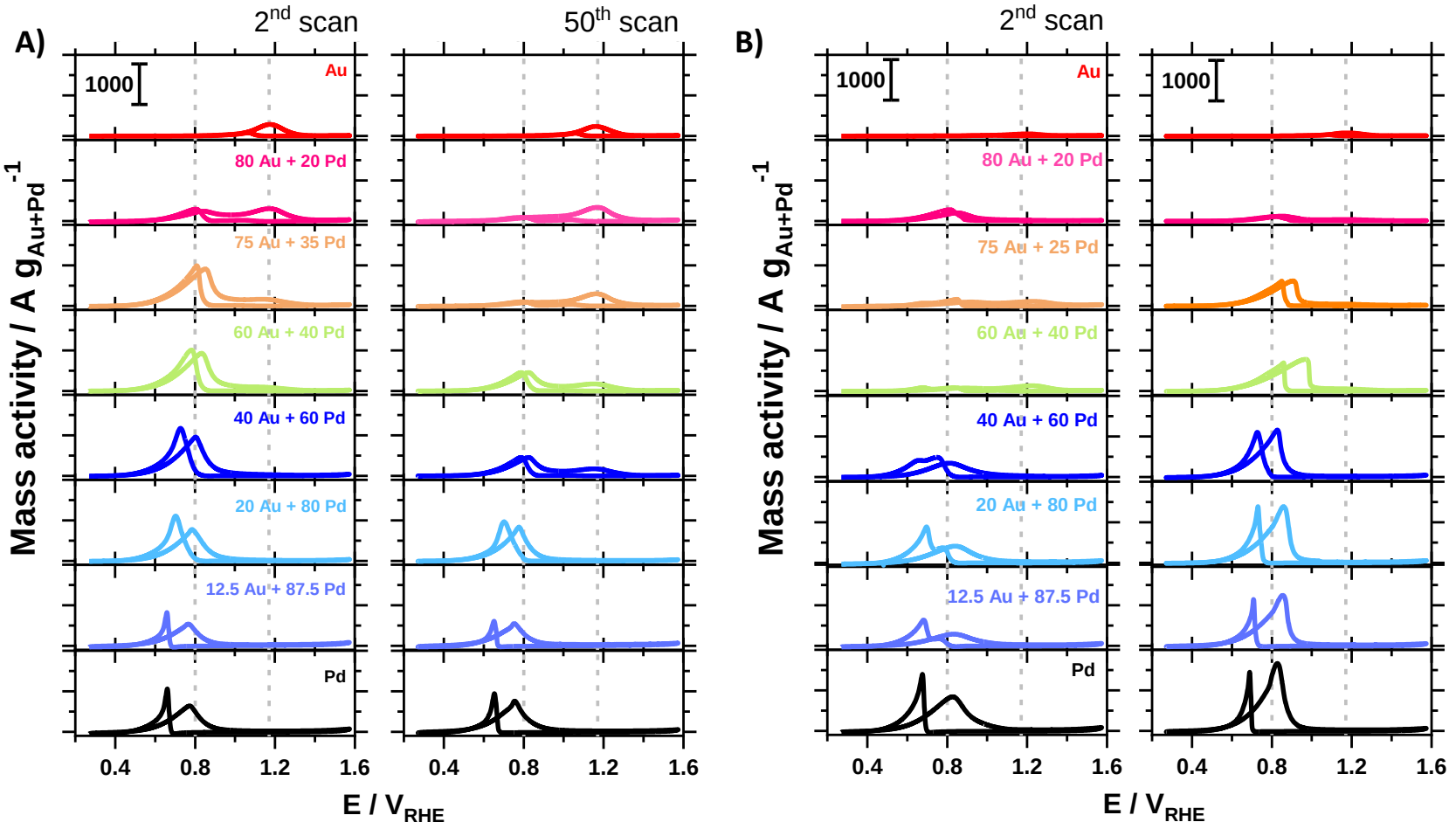

Figure S58. Examples of CVs for [x Au + y Pd] NPs obtained at RT after 2 scans and 50 scans, as indicated, at 50 mV s^{-1} in 1 M EtOH and 1 M KOH following (A) the *Protocol A* and (B) the *Protocol B* detailed in **the experimental section of the manuscript**.

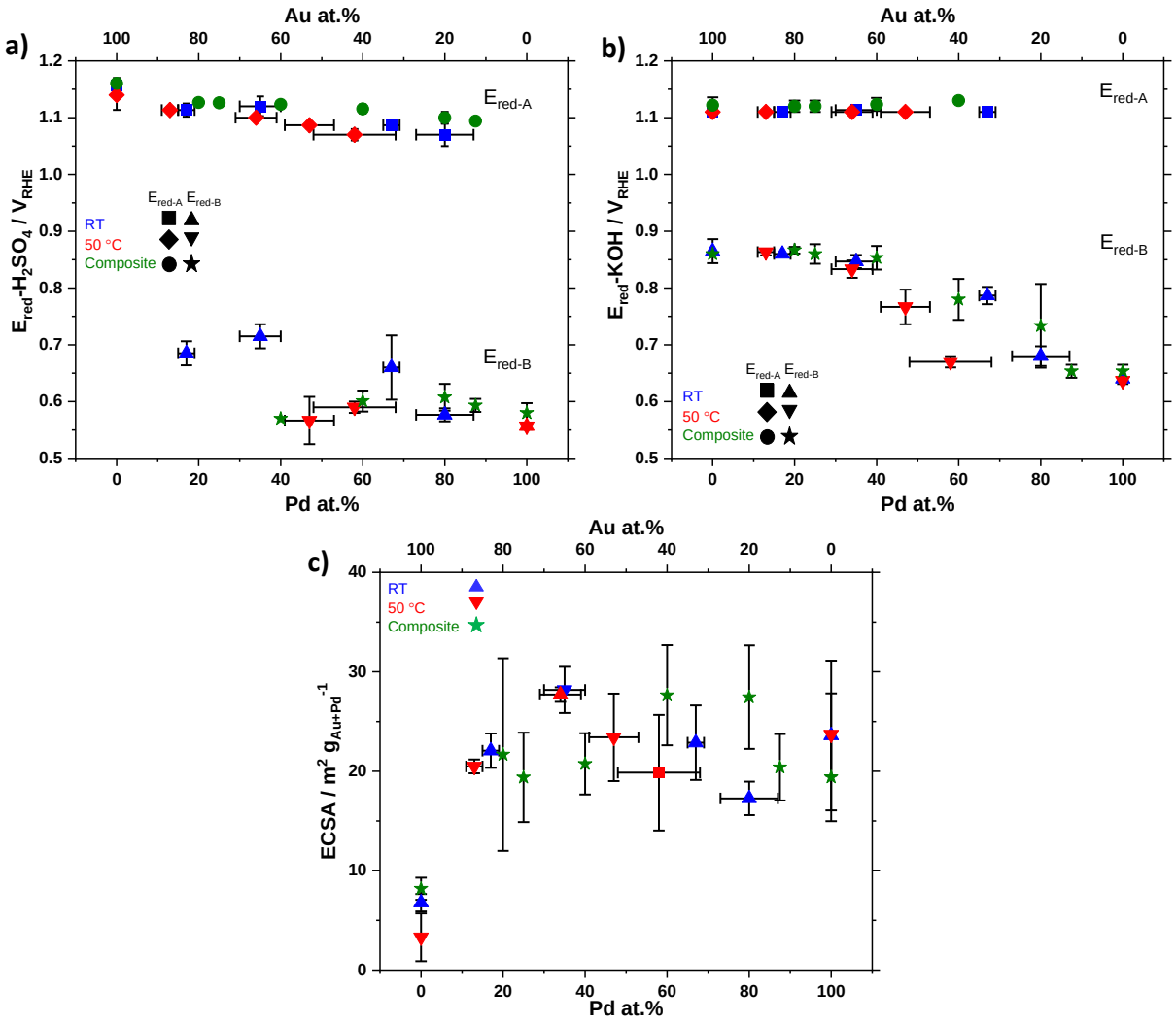

Figure S59. Characteristics of Au_xPd_y obtained (blue) at RT or (red) using a synthesis step at 50 °C for 1 hour and (green) [x Au + y Pd] nanocomposite samples obtained by mixing Au and Pd NP dispersions synthesized at RT. Main reduction peak positions as defined in **Figure S54a-b** and **Figure S55a-b** (a) in acid, (b) in alkaline conditions and (c) the evaluated ECSA retrieved. The samples were subjected to the *Protocol A* detailed in **the experimental section of the manuscript**.

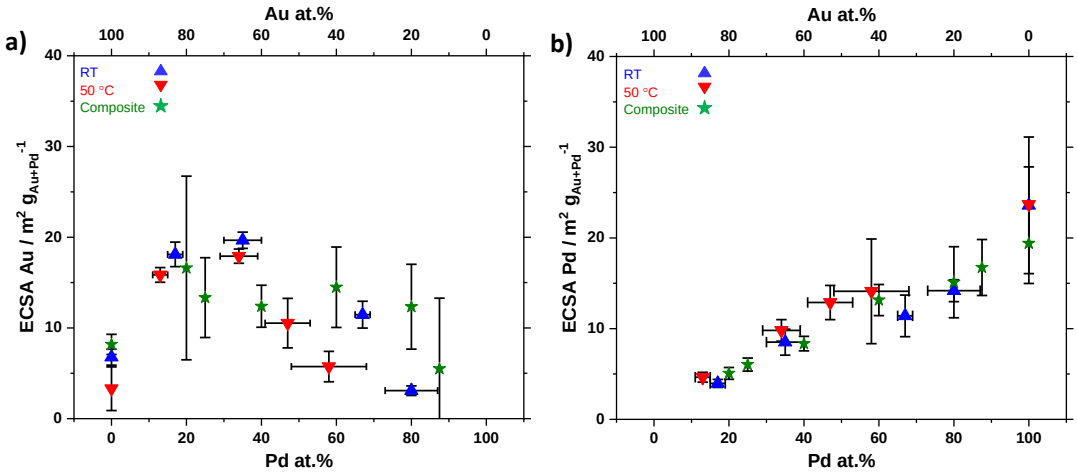

Figure S60. Characteristics of Au_xPd_y obtained (blue) at RT or (red) using a synthesis step at 50 °C for 1 hour and (green) [x Au + y Pd] nanocomposite samples obtained by mixing Au and Pd NP dispersions synthesized at RT. (a) ECSA related to Au evaluated in acid solution and (b) ECSA related to Pd evaluated in alkaline conditions. The samples were subjected to the *Protocol A* detailed in **the experimental section of the manuscript**.

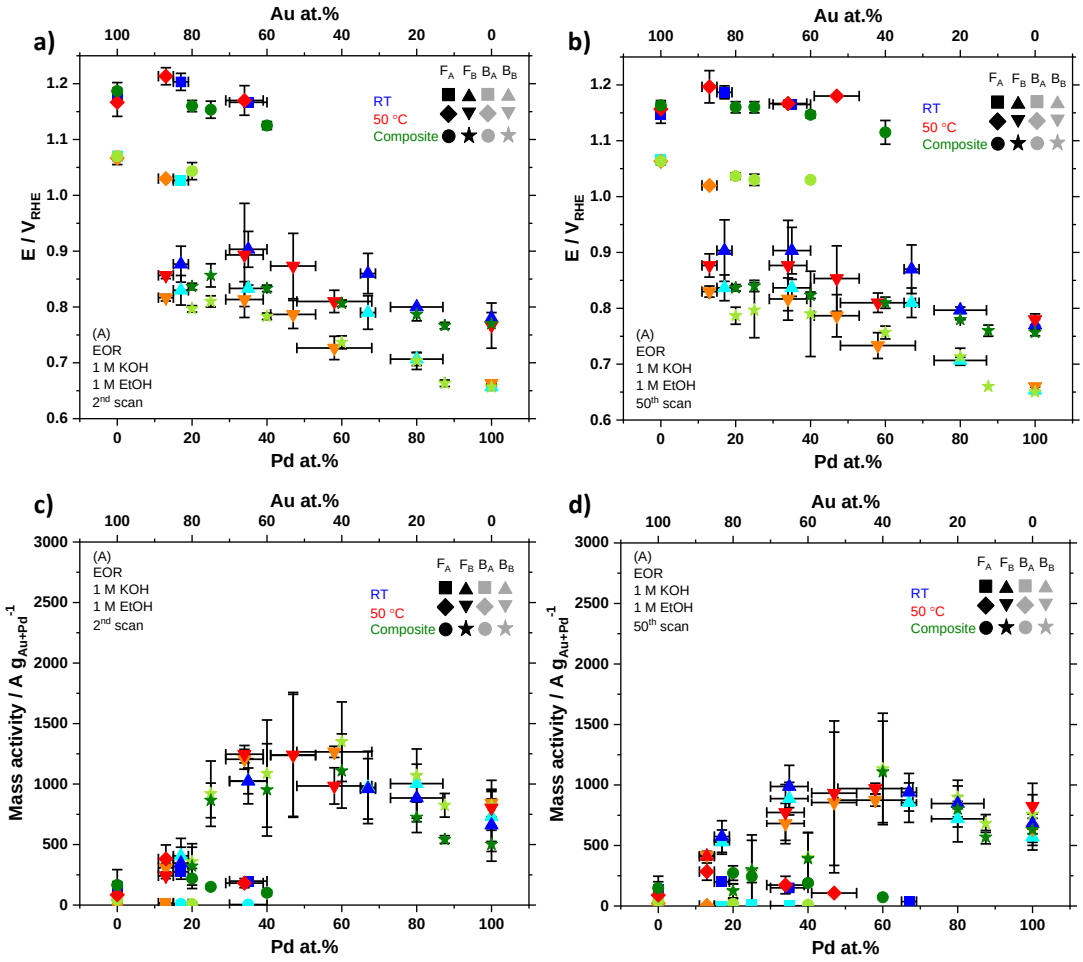

Figure S61. Characteristics of Au_xPd_y obtained (blue) at RT or (red) using a synthesis step at 50 °C for 1 hour and (green) [x Au + y Pd] nanocomposite samples obtained by mixing Au and Pd NP dispersions obtained at RT. (a,b) Peak positions as defined in **Figure S54c** and **Figure S55c** in 1 M EtOH and 1 M KOH (a) after 2 scans and (b) after 50 scans at 50 mV s^{-1}. (c,d) Mass activity for the EOR after (c) 2 scans and (d) 50 scans at 50 mV s^{-1}. The samples were subjected to the *Protocol A* detailed in **the experimental section of the manuscript**.

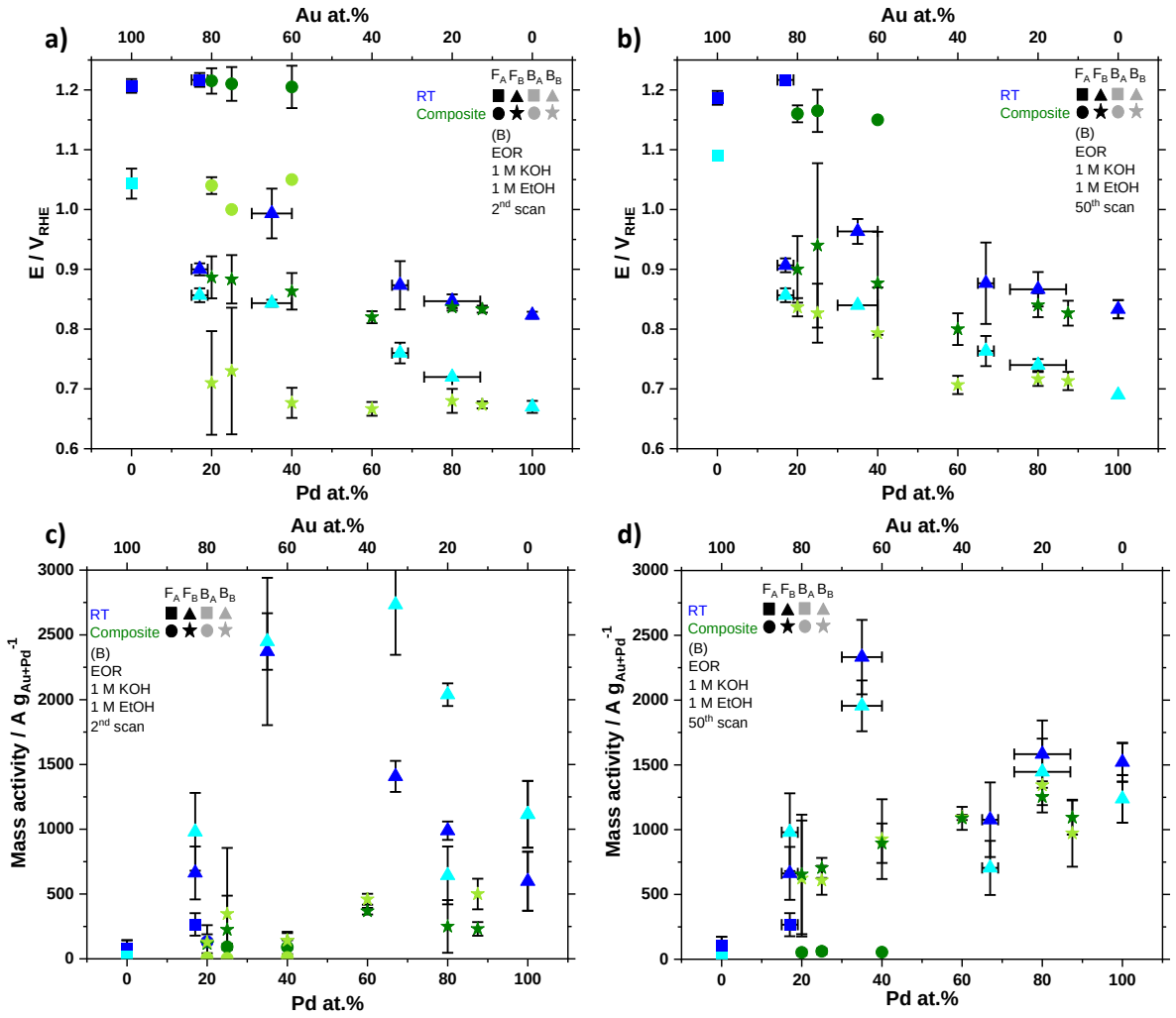

Figure S62. Characteristics of Au_xPd_y obtained (blue) at RT and (green) [x Au + y Pd] nanocomposite samples obtained by mixing Au and Pd NP dispersions obtained at RT. (a,b) Peak positions as defined in **Figure S54c** and **Figure S55c** in 1 M EtOH and 1 M KOH (a) after 2 scans and (b) after 50 scans at 50 mV s^{-1}. (c,d) Mass activity for the EOR after (c) 2 scans and (d) 50 scans at 50 mV s^{-1}. The samples were subjected to the *Protocol B* detailed in **the experimental section of the manuscript**.

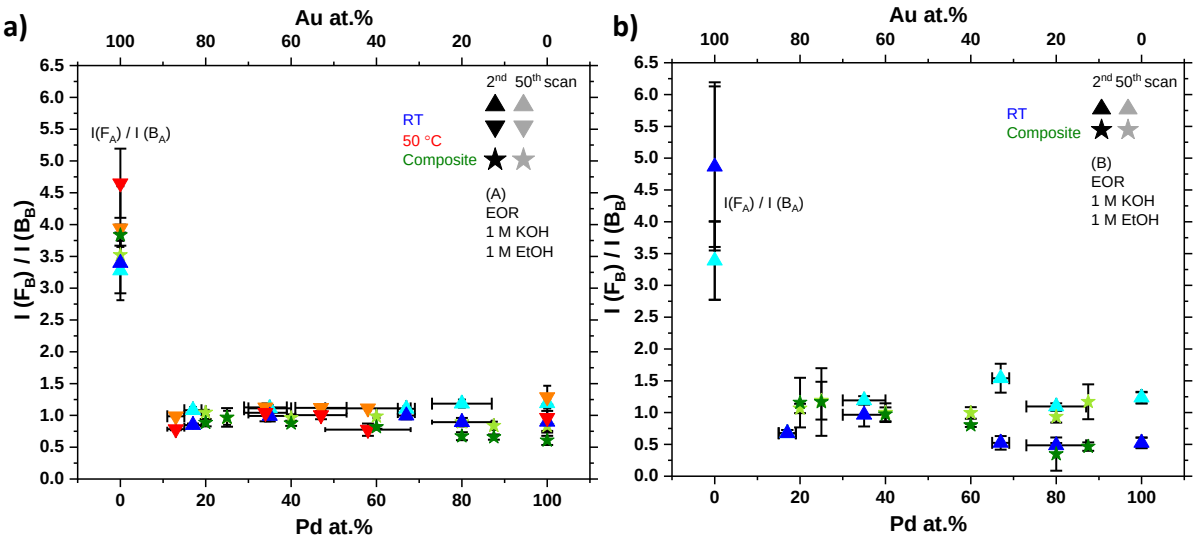

Figure S63. Ratio of the intensity of the oxidation peaks observed in the forward (F) and backward (B) scans for the 2nd or 50th scans at 50 mV s^{-1} in 1 M EtOH and 1 M KOH, for different Au_xPd_y NPs obtained (blue) at RT or (red) using a synthesis step at 50 °C for 1 hour and (green) [x Au + y Pd] nanocomposite samples obtained by mixing Au and Pd NP dispersions synthesized at RT. The peak positions are defined in **Figure S54c** and **Figure S55c** for the EOR. The samples were subjected to (a) the *Protocol A* or (b) the *Protocol B* detailed in **the experimental section of the manuscript**.

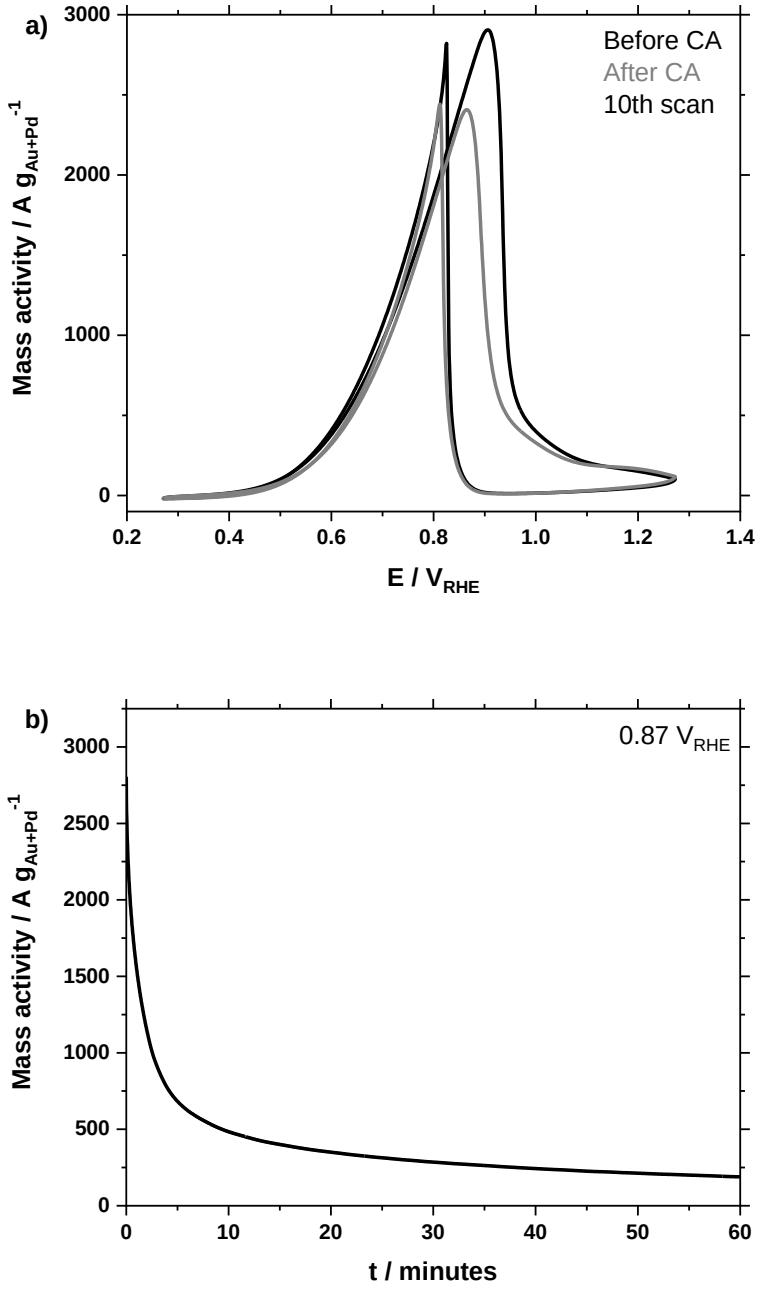

Figure S64. (a) 10th CV for $Au_{65}Pd_{35}$ NPs obtained at RT and recorded in 1 M EtOH and 1 M KOH at a scan rate of 50 mV s^{-1} before and after CA at 0.87 V_{RHE} following the *Protocol C* detailed in **the experimental section of the manuscript**. (b) CA at 0.87 V_{RHE}.

Au_xPd_y NPs

The Au_xPd_y NPs were characterized using two different protocols detailed in **the experimental section of the manuscript**. *Protocol A* includes the evaluation of the ECSA. Since more treatment is performed to higher voltages to best evaluate the ECSA of Au NPs,[12] this protocol also indirectly evaluates the stability of the Au_xPd_y NPs due to the relatively poor stability of Pd at high voltages. As the amount of Pd increases, the reduction peaks in acidic and alkaline media shift towards lower potentials, see **Figure S59**. The ECSA tends to increase as the amount of Pd increases, which can be related to the decrease in NPs size. The contribution of Au to the ECSA decreases as the Pd amount increases, **Figure S60**. For the EOR, the MA evaluated at the maximum current density recorded in the CVs, is maximal for a composition in Au around 40-60 at.%. As the amount of Pd increases, the related peak position shifts towards lower potentials, see **Figure S57** and **Figure S61**. The ratio between the maximum intensity of the forward and backward scans during the EOR has been used as a metric to evaluate how resistant to poisoning a catalysts is.[82] Despite their lower MAs, the Au NPs stand out as much more tolerant to poisoning, see **Figure S63**. This stresses the rationale to develop Au_xPd_y NPs.

To assess the properties of the Au_xPd_y NPs without extensive treatments at high potentials, that can lead to Pd dissolution before the actual performance towards the EOR is evaluated,[12] a *Protocol B* detailed in **the experimental section of the manuscript** was used. The focus was here on NPs obtained at RT due to the simplicity of this synthetic approach. While the trends observed with *Protocol A* are the same, a noticeable difference is the higher activity of the sample $Au_{65}Pd_{35}$ reaching ca. 2500 A g_{Au+Pd}^{-1}. The comparison between *Protocol A* and *Protocol B* suggests that a significant improvement in activity can be achieved by developing Au_xPd_y NPs and this activity remains relatively high despite the relatively harsh conditions (high upper potential) used here. For instance, a relatively high activity is maintained after CA, see **Figure S64**. The highest mass activity observed on the CV is ca. 2900 A g_{Au+Pd}^{-1}. Based on the CV the MA after CA is 2406 A g_{Au+Pd}^{-1} which is still much higher than the average MA evaluated for the other Au_xPd_y and [x Au + y Pd] samples detailed below and correspond to a decrease in activity of only 17% after 1 hour at 0.87 V_{RHE}.

$Au_{65}Pd_{35}$ is identified as the bimetallic NPs with maximum activity for the EOR. This optimal composition was found using a very simple approach to synthesize the materials and screen different composition.

[x Au + y Pd] nanocomposites

The mixtures [x Au + y Pd] and Au_xPd_y present the same electrochemical features in terms of peak position and ECSA, **Figure S59**, i.e. shift of the reduction peak at lower potential as the Pd amount increase and increase of Pd contribution to the ECSA as the Pd amount increase, **Figure S60**. However, a difference is that features related to gold are more present even at high Pd amount, see **Figure S58**. As the Au content decreases, a higher MA is achieved and the related peak potentials shifts towards lower values, **Figure S61**. When *Protocol A* detailed in **the experimental section of the manuscript** was used, the sample [40 Au + 60 Pd] leads to the highest MA around 1200 A g_{Au+Pd}^{-1}. In contrast when *Protocol B* was used, the MA increased with the amount of Pd. This suggests that bimetallic NPs might form *in situ.*

This suggestion is further backed up by the trend observed using the electrochemical *Protocol B*, where in the initial stage of the cyclic voltammetry unusual features for the EOR are observed with not 2 different oxidative waves on the backward scan but three of them and where two of them ultimately merge, see **Figure S56**. The intermediate peak observed seem to relate to the presence of Au-only sites and disappears as several scans are performed. This intermediate peak was not observed when the *Protocol A* was used.

While developing [40 Au + 60 Pd] samples does not significantly improve the poisoning tolerance of the catalyst, see **Figure S63**, it remains nevertheless a convenient strategies to develop catalyst more active than Au alone or Pd alone, especially when the sample is subjected to relatively harsh conditions (*Protocol A*).

Since the MA retrieved for nanocomposites or bimetallic NPs are in the same range, **Figure S61c,d**, these results illustrate a very practical way to prepare well-defined catalyst and use them to develop nanocomposite with improved properties. The catalysts are here conveniently obtained by the same RT surfactant-free synthesis in low boiling point alcohols-water mixture with moderate amount of base. The catalyst [40 Au + 60 Pd] was identified as the most active nanocomposite for the EOR.

SU. Outlook into multi-metallic nanomaterials

Background. As our understanding of complex materials increases, it has been suggested that high entropy alloys (HEAs), made of 5 or more different elements, could bring new opportunities in catalysis.[83] A major challenge for HEAs made of PM NPs remains their synthesis and characterization. We here illustrate how the synthesis presented could be relevant to develop multi-metallic samples, being HEAs or multi-metallic composites. When different precursor containing Au, Pd, Pt, Os, Ir and Ru and are added to a solution containing 30 v.% EtOH and 2 mM LiOH, no colloids NPs are obtained (in contrast to the case of Au, Pd or Au_xPd_y NPs) but a black precipitate is obtained. This precipitate can be washed, redispersed and deposited on an electrode for characterization. Our results so far points towards the role of Au as *catalyst*[84] for this reaction (without Au the reaction does not seem to proceed rapidly within 1-2 hour at RT).

Results. In this case, using EtOH or MeOH or different Base/PM ratios does not influence much the resulting materials all in the range of 1.5-2.5 nm. A first interesting feature of the material obtained is that it is formed of ca. 1.5-2.5 nm NPs, with larger structures also observed. *Bulk* EDS characterization confirm the presence of all elements but nearly no Ir. The fact that all elements are present and that the NPs are homogeneous in size strongly suggests a mix of the different elements within the same NPs. However, a definite proof of this is challenging to provide at this stage since STEM-EDS characterization is not trivial to perform on NPs less than 3-4 nm. We then focus in the next section on the sample $Au_{33}Pd_{19}Pt_{18}Os_{20}Ir_1Ru_9$ (#1).

Table S24. Synthesis conditions of the different multi-metallic samples prepared. All samples were prepared with 0.5 mM $HAuCl_4$, 0.5 mM H_2PtCl_6, 0.5 mM $PdCl_2$, 0.5 mM $RuCl_3$, 0.5 mM $OsCl_3$ and 0.5 mM H_2IrCl_6 and using LiOH as base with 30 v.% ROH.

Sample	H_2O v.% *	EtOH v.%*	MeOH v.%*	Base	V mL *	T °C	t h	Base/Au molar ratio	Composition based on EDS
#1	70	25	5	LiOH	4.2	RT	24	4	$Au_{33}Pd_{19}Pt_{18}Os_{20}Ir_1Ru_9$
#2								10	$Au_{28}Pd_{17}Pt_{23}Os_{20}Ir_1Ru_{11}$
#3		-	30					4	$Au_{28}Pd_{16}Pt_{27}Os_{17}Ir_3Ru_9$
#4								10	$Au_{17}Pd_{15}Pt_{25}Os_{23}Ir_4Ru_{16}$
#5		25	5			50-RT	1-23	4	$Au_{31}Pd_{19}Pt_{25}Os_{17}Ir_0Ru_8$
#6								10	$Au_{21}Pd_{14}Pt_{23}Os_{24}Ir_1Ru_{17}$
#7		-	30					4	$Au_{22}Pd_{13}Pt_{20}Os_{26}Ir_2Ru_{17}$
#8								10	$Au_{23}Pd_{16}Pt_{22}Os_{20}Ir_4Ru_{15}$

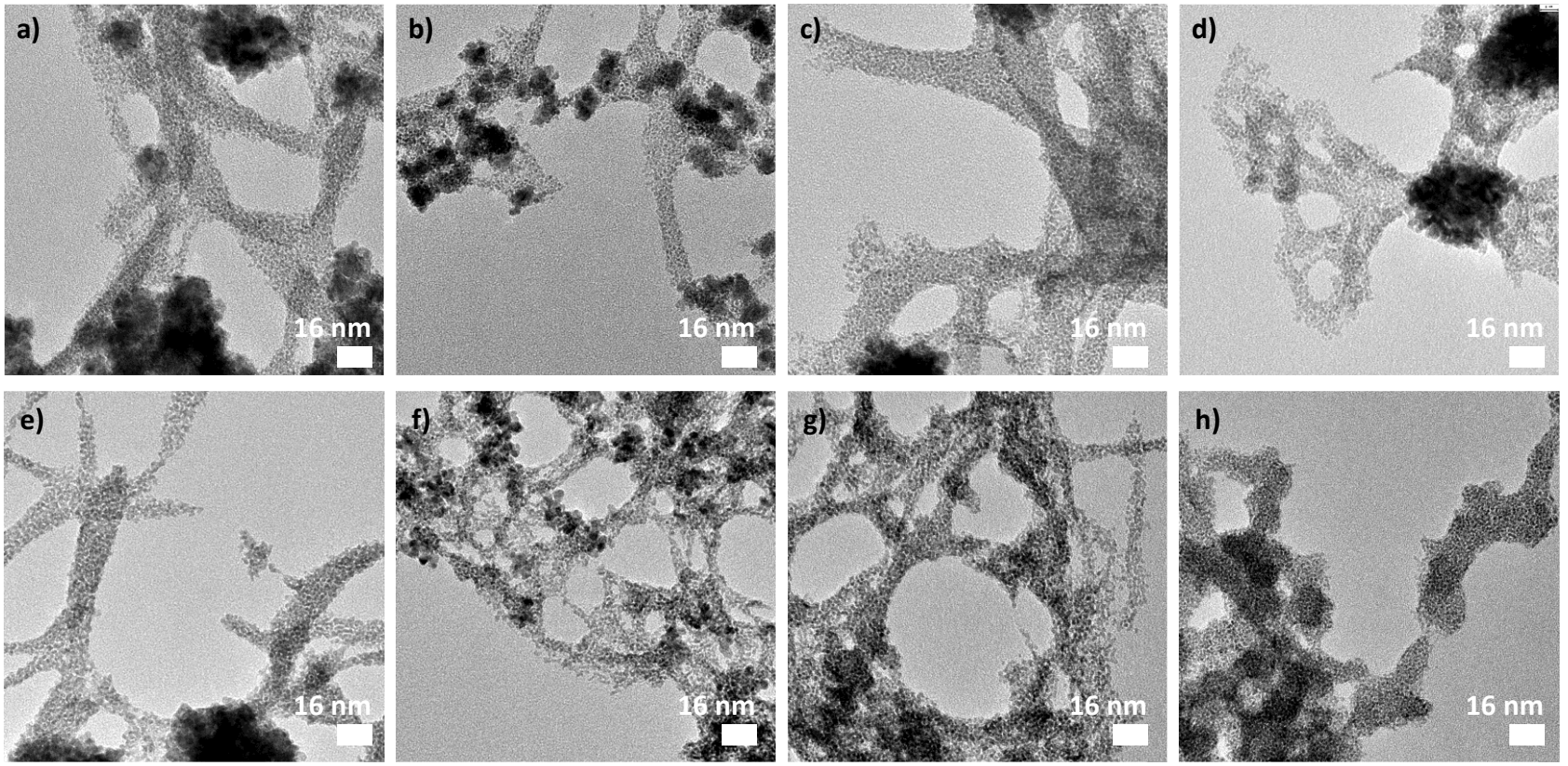

Figure S65. TEM micrographs of samples (a) #1, (b), #2, (c) #3, (d) #4, (e) #5, (f) #6, (g) #7, (h) #8 as defined in **Table S24**.

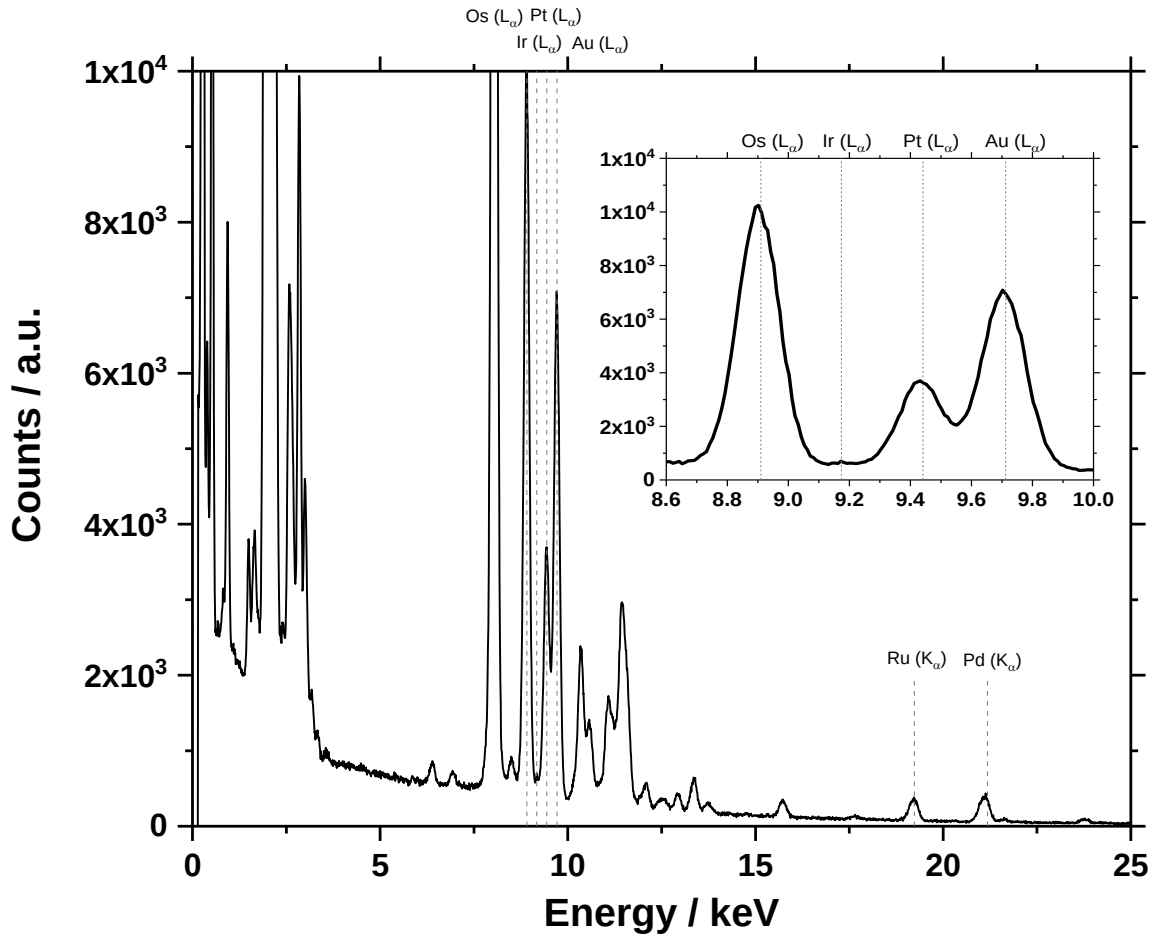

Figure S66. EDS spectrum of sample #1, as defined in **Table S24**.

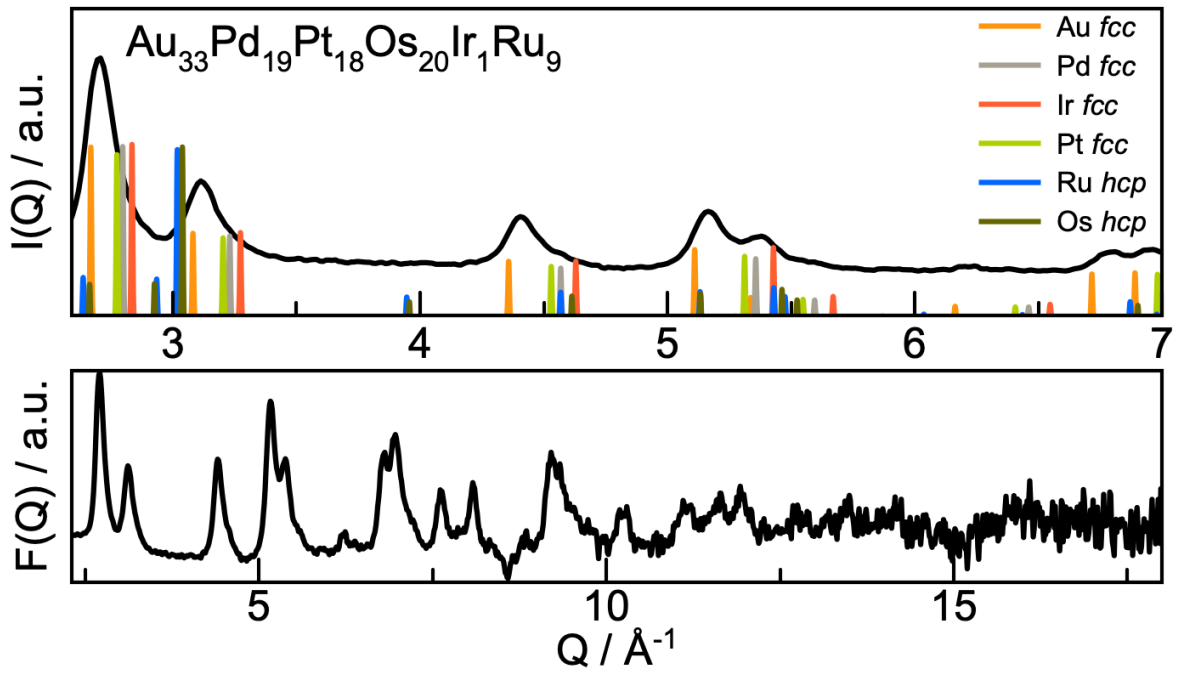

Figure S67. I(Q) and the normalized F(Q) of $Au_{33}Pd_{19}Pt_{18}Os_{20}Ir_1Ru_9$ presented together with the calculated diffraction patterns of the *fcc* or *hcp* structure of the involved elements.

Table S25. Refinement parameters extracted from PDF analysis of X-ray TS for $Au_{33}Pd_{19}Pt_{18}Os_{20}Ir_1Ru_9$. The measurements were performed at P02.1 beamline, DESY.

	$Au_{33}Pd_{19}Pt_{18}Os_{20}$ Ir_1Ru_9
Scale Factor	0.45
Fit range	2.3 Å – 50 Å
Number of refined parameters	5
R_w	0.32
Q_{damp} (Å^{-1})	0.037
Q_{broad} (Å^{-1})	0.001
Q_{max} (Å^{-1})	18.0
U_{iso} (Å^2)	0.0192
Lattice par., *a* (Å)	4.03
δ_2 (Å^2)	5.39
Sp-diameter (Å)	50.0

Structural insight on the $Au_{33}Pd_{19}Pt_{18}Os_{20}Ir_1Ru_9$ sample is revealed through X-ray TS experiments. The Q-space data in **Figure S67** shows symmetric Bragg-peaks at the *fcc* relative Q-positions indicating that one phase *fcc* was formed. Through PDF analysis and real space Rietveld refinement the unit cell parameter of 4.03 Å was extracted being slightly smaller than the Au *fcc* (4.08 Å) which might point towards the contraction of the unit cell as a consequence of the introduction of slightly smaller elements.

We investigated the electrochemical properties of the material $Au_{33}Pd_{19}Pt_{18}Os_{20}Ir_1Ru_9$. An interesting feature is the absence of Au oxide reduction peak in acid, see **Figure S68a**, suggesting that initially there is not much Au exposed on the NM surface. A different feature of this sample compared to Au, Pd, Au_xPd_y or [x Au + y Pd] is a H_{upd} region, highlighted in pink, at low potentials that likely related to Pt species on the surface.

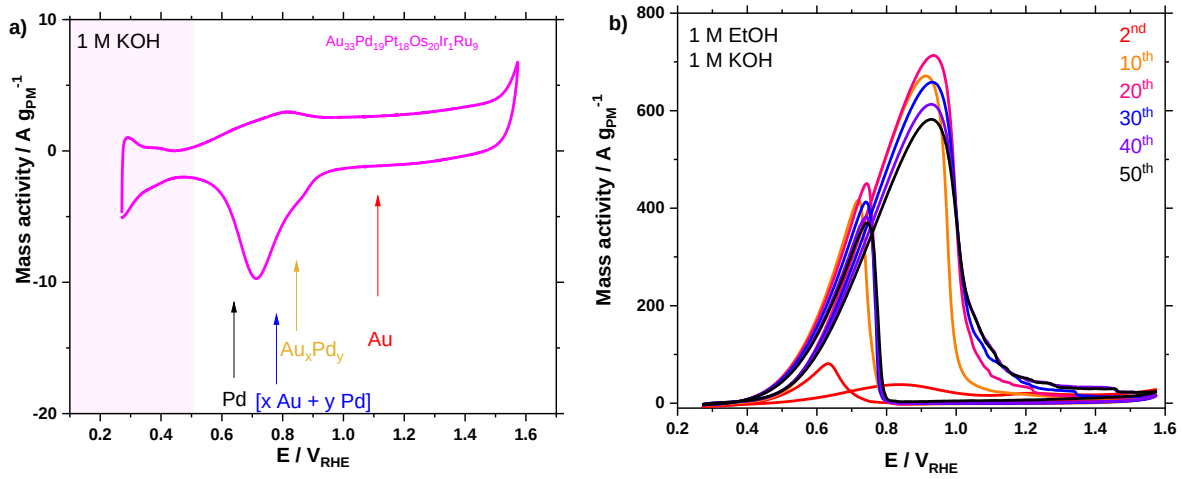

Figure S68. Characteristics of $Au_{33}Pd_{19}Pt_{18}O_{s20}Ir_1Ru_9$ sample prepared at RT using 30 v.% EtOH and 2 mM LiOH. (a) Example of CV in 1 M KOH recorded at 50 mV s^{-1} following the *Protocol A* detailed in **the experimental section of the manuscript**. The expected peaks position for Pd, Au, Au_xPd_y and [x Au + y Pd] samples are indicated with arrows. (b) Successive CVs at 50 mVs^{-1} in 1 M EtOH and 1 M KOH following the *Protocol B* detailed in **the experimental section of the manuscript**.

The sample $Au_{33}Pd_{19}Pt_{18}Os_{20}Ir_1Ru_9$ is readily active for the EOR, **Figure S68b**, however the structure and/or composition of the catalyst is probably changing over time with the number of CVs since a clear activation and then deactivation occurs. A clear feature for the EOR is that the peak ratio between forward and backward scans is relatively high, which is often used as a metric for tolerance to poisoning for EOR catalysts, see **Figure S71c,d**. This is interesting since Au is expected to provide a high ratio to these peaks but is not initially present on the surface, **Figure S68a**.

While the MA is relatively low, this is mainly due to the high amount of PMs used. Different normalization give an averaged MA of ca. 500 A g_{PM}^{-1}, 1480 A g_{Au+Pd}^{-1}, 2280 A g_{Au}^{-1}, 4180 A g_{Pd}^{-1} which indicates a significant improvement of the MA compared to a Au NP catalyst with a MA around ca. 100 A g_{Au}^{-1} or Pd catalyst with a MA around 1520 A g_{Pd}^{-1} (evaluated on the 50th scan for *Protocol B*). As a comparison, the MA of $Au_{65}Pd_{35}$ is ca. 2330 g_{Au+Pd}^{-1}, which is ca. 3000 g_{Au}^{-1} or ca. 10340 g_{Pd}^{-1} whereas the MA of [40 Au + 60 Pd] is ca. 1095 g_{Au+Pd}^{-1} which is ca. 1980 g_{Au}^{-1} or 2440 g_{Pd}^{-1}. These estimations are performed assuming a 100% conversion of all precursors to NPs and so probably under-evaluated (e.g. Ir is probably not present in the multi-metallic samples).

Conclusion. These results show that the synthesis approach proposed is suitable to develop SurFree multi metallic samples structured at the nanoscale for improved catalysts, e.g. for the EOR.

SV. Comparison of different catalysts

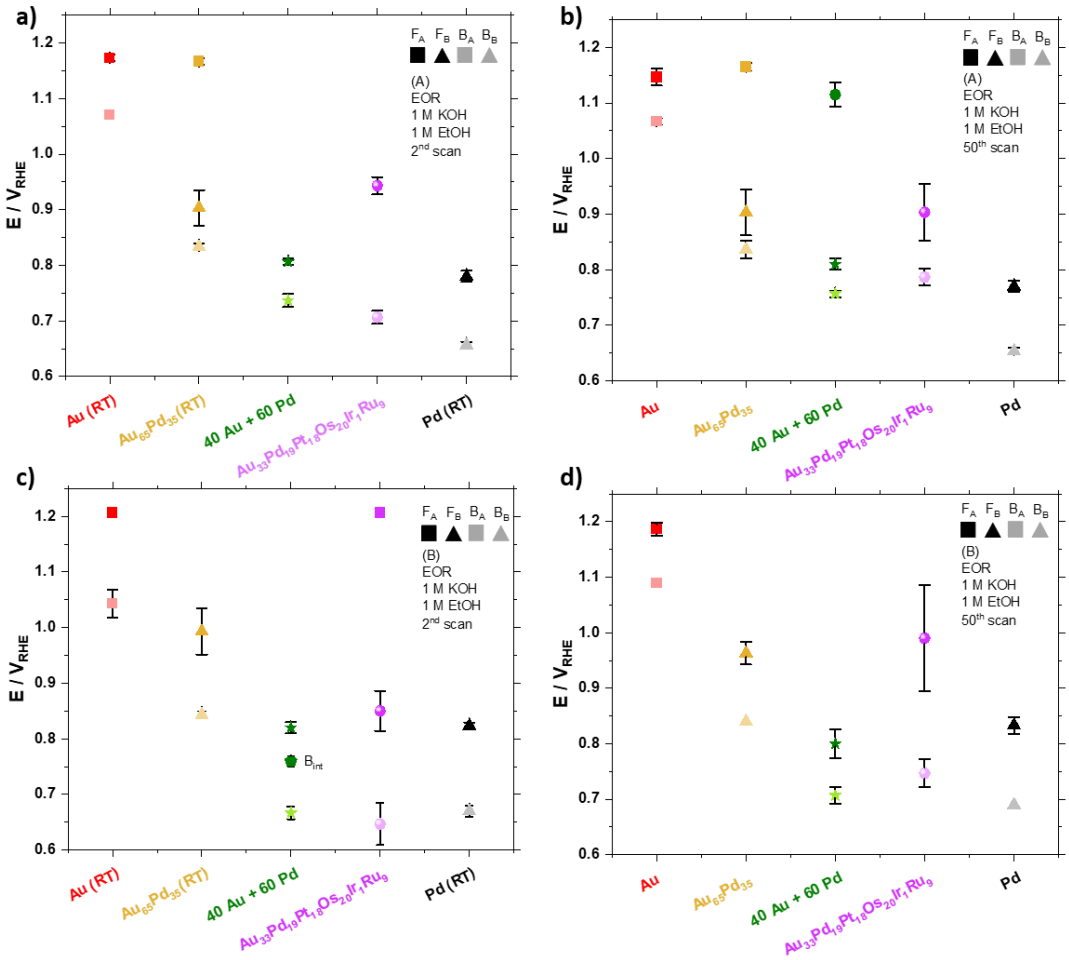

Figure S69. Characteristics of Au, $Au_{65}Pd_{35}$, [40 Au + 60 Pd], $Au_{33}Pd_{19}Pt_{18}O_{s20}Ir_1Ru_9$ and Pd NP samples obtained at RT using 30 v.% EtOH and 2 mM LiOH. (a-d) Peak positions as defined in **Figure S55c** in 1 M EtOH and 1 M KOH (a,c) after 2 scans and (b,d) after 50 scans at 50 mV s^{-1}. The samples were subjected to (a,b) the *Protocol A* and (c,d,) the *Protocol B* detailed in **the experimental section of the manuscript**.

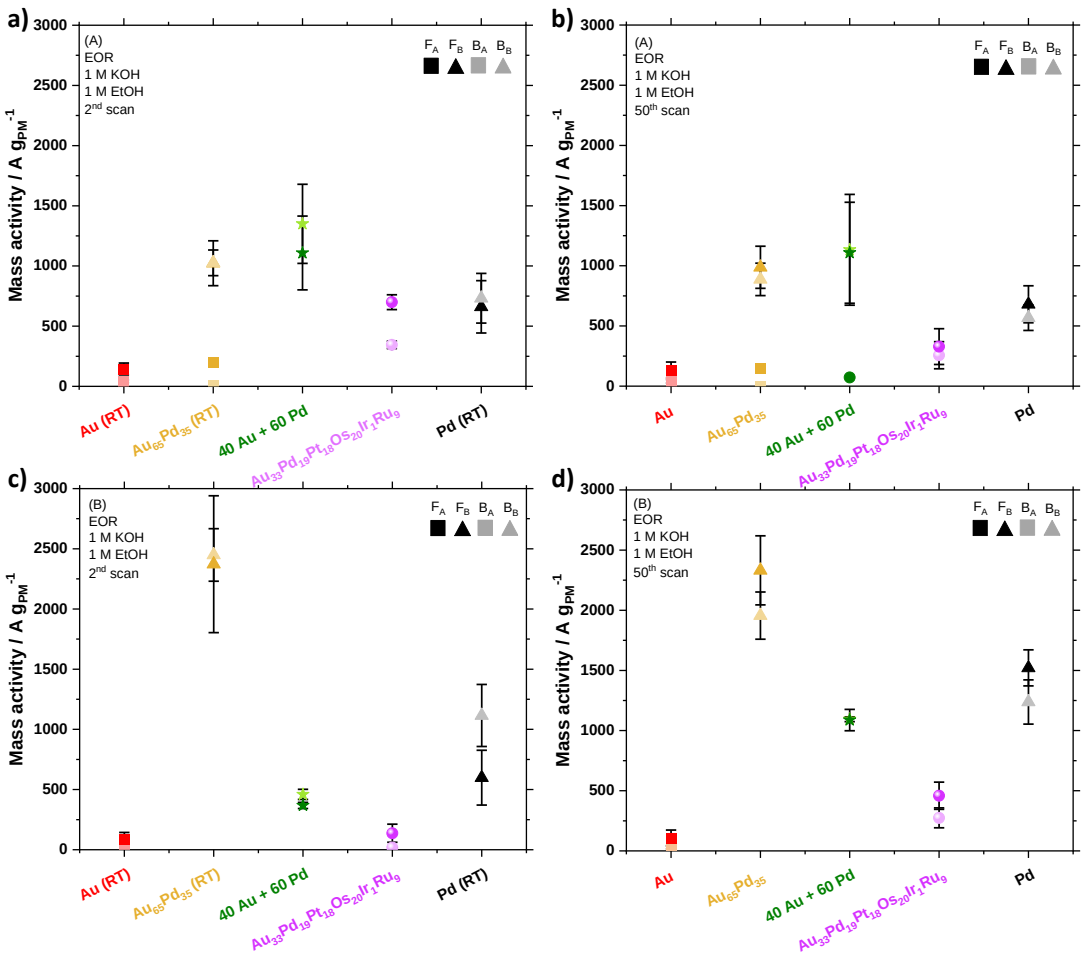

Figure S70. Characteristics of Au, $Au_{65}Pd_{35}$, [40 Au + 60 Pd], $Au_{33}Pd_{19}Pt_{18}O_{s20}Ru_9Ir_1$ and Pd NP samples obtained at RT using 30 v.% EtOH and 2 mM LiOH. (a-d) Mass activities for the EOR in 1 M KOH and 1 M EtOH after (a,c) 2 scans and (b,d) 50 scans at 50 mV s^{-1}. The samples were subjected to (a,b) the *Protocol A* and (c,d) the *Protocol B* detailed in **the experimental section of the manuscript**. The peak positions are defined in **Figure S54c** for the EOR.

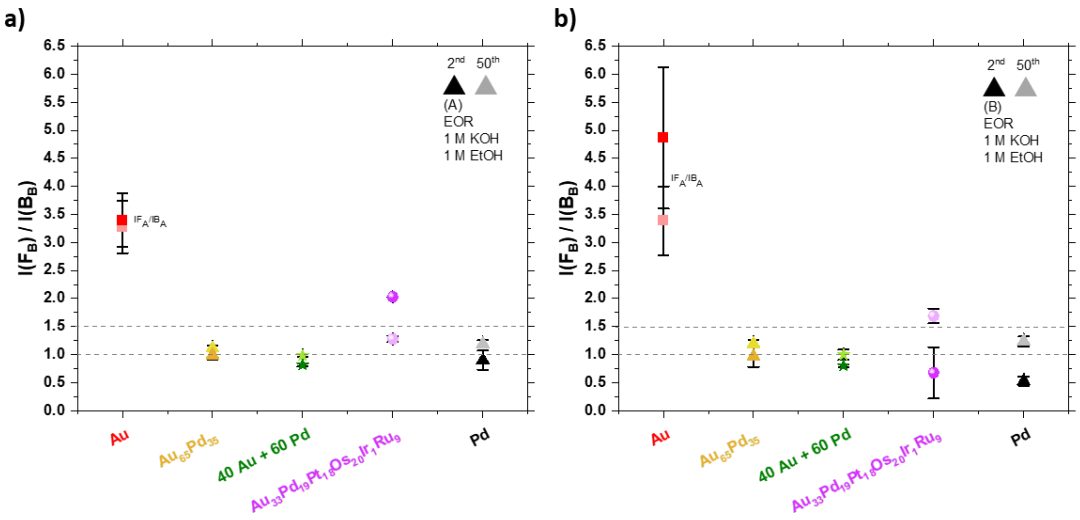

Figure S71. (a,b) Ratios of the intensity of the oxidation peaks observed in the forward (F) and backward (B) scans for the 2nd or 50th scans, as indicated, recorded at 50 mV s^{-1} in 1 M EtOH and 1 M KOH for different Au, $Au_{65}Pd_{35}$, [40 Au + 60 Pd], $Au_{33}Pd_{19}Pt_{18}O_{s20}Ir_1Ru_9$ and Pd NP samples obtained at RT tested following (a) the *Protocol A* and (b) the *Protocol B* detailed in **the experimental section of the manuscript**. The peak positions are as defined in **Figure S54c** for the EOR. Ratio of the forward and backward scan intensity for the highest peak observed in the characterization of the different materials. $I(F_B)/I(B_B)$was used for all materials except for Au NPs where $I(F_A)/I(B_A)$ was used.

A comparison of the different SurFree Au–based catalysts obtained in this study is proposed in **Figure S70**. While Au NPs are relatively poor catalysts for the EOR, they show good poisoning resistance, see **Figure S71**. Pd is a suitable catalyst for the EOR but suffer poisoning and stability issues. An approach to develop improved catalyst is to develop Au_xPd_y NPs and $Au_{65}Pd_{35}$ gives the highest MA. An alternative strategy consists in developing [x Au + y Pd] sample which depending on the protocol used, e.g. *Protocol A*, gives a higher MA than $Au_{65}Pd_{35}$, Au or Pd NPs, probably due to the *in situ* formation of bimetallic. This approach however offers the benefit to start with a well-defined catalyst mixture as opposed to the possibly more complex bimetallic NP characterization. At last, multi metallic structures like $Au_{33}Pd_{19}Pt_{18}O_{s20}Ir_1Ru_9$, while they show a relatively low MA normalized to the total amount of PM used for the synthesis, show an improve tolerance to poisoning and a relatively high MA normalized to Au or Pd.

Conclusion. While these results are preliminary and there is certainly room for improvement, they nevertheless show how the synthesis reported is relevant to study complex systems with the benefits to use a simple RT surfactant-free synthesis in *green* solvent made of water and mono-alcohols like the sustainable EtOH and only a moderate amount of base, i.e. a simple yet scalable synthesis.

SW. References

1 De Souza, C. D., Nogueira, B. R. & Rostelato, M. Review of the methodologies used in the synthesis gold nanoparticles by chemical reduction. *Journal of Alloys and Compounds* 798, 714-740 (**2019**). https://doi.org:10.1016/j.jallcom.2019.05.153

2 Liz-Marzan, L. M., Kagan, C. R. & Millstone, J. E. Reproducibility in Nanocrystal Synthesis? Watch Out for Impurities! *ACS Nano* 14, 6359-6361 (**2020**). https://doi.org:10.1021/acsnano.0c04709

3 Gilbertson, L. M., Zimmerman, J. B., Plata, D. L., Hutchison, J. E. & Anastas, P. T. Designing nanomaterials to maximize performance and minimize undesirable implications guided by the Principles of Green Chemistry. *Chemical Society Reviews* 44, 5758-5777 (**2015**). https://doi.org:10.1039/c4cs00445k

4 Gobelli, D., Correa, N. M., Barroso, M. F., Moyano, F. & Molina, P. G. "Green Electrodes" Modified with Au Nanoparticles Synthesized in Glycerol, as Electrochemical Nitrite Sensor. *Electroanalysis* 27, 1883-1891 (**2015**). https://doi.org:10.1002/elan.201500022

5 Gasparotto, L. H. S., Garcia, A. C., Gomes, J. F. & Tremiliosi-Filho, G. Electrocatalytic performance of environmentally friendly synthesized gold nanoparticles towards the borohydride electro-oxidation reaction. *Journal of Power Sources* 218, 73-78 (**2012**). https://doi.org:10.1016/j.jpowsour.2012.06.064

6 Nalawade, P., Mukherjee, T. & Kapoor, S. Green Synthesis of Gold Nanoparticles Using Glycerol as a Reducing Agent. *Advances in Nanoparticles* 2, 76-86 (**2013**). http://dx.doi.org/10.4236/anp.2013.22014

7 Ferreira, E. B., Gomes, J. F., Tremiliosi-Filho, G. & Gasparotto, L. H. S. One-pot eco-friendly synthesis of gold nanoparticles by glycerol in alkaline medium: Role of synthesis parameters on the nanoparticles characteristics. *Materials Research Bulletin* 55, 131-136 (**2014**). https://doi.org:10.1016/j.materresbull.2014.04.003

8 Parveen, R. & Tremiliosi, G. A step ahead towards the green synthesis of monodisperse gold nanoparticles: the use of crude glycerol as a greener and low-cost reducing agent. *RSC Advances* 6, 95210-95219 (**2016**). https://doi.org:10.1039/c6ra14259a

9 Parveen, R., Ullah, S., Sgarbi, R. & Tremiliosi, G. One-pot ligand-free synthesis of gold nanoparticles: The role of glycerol as reducing-cum-stabilizing agent. *Colloids and Surfaces a-Physicochemical and Engineering Aspects* 565, 162-171 (**2019**). https://doi.org:10.1016/j.colsurfa.2019.01.005

10 Tang, J. Q. & Man, S. Q. Green Synthesis of Colloidal Gold by Ethyl Alcohol and NaOH at Normal Temperature. *Rare Metal Materials and Engineering* 42, 2232-2236 (**2013**). https://doi.org/10.1016/S1875-5372(14)60027-8

11 Piella, J., Bastus, N. G. & Puntes, V. Size-Controlled Synthesis of Sub-10-nanometer Citrate-Stabilized Gold Nanoparticles and Related Optical Properties. *Chemistry of Materials* 28, 1066-1075 (**2016**). https://doi.org:10.1021/acs.chemmater.5b04406

12 Silva, L. S. R. *et al.* AuPd/C core-shell and alloy nanoparticles with enhanced catalytic activity toward the electro-oxidation of ethanol in alkaline media. *Applied Catalysis B-Environmental* 251, 313-325 (**2019**). https://doi.org:10.1016/j.apcatb.2019.03.067

13 Quinn, M. & Mills, G. Surface-mediated formation of gold particles in basic methanol. *Journal of Physical Chemistry* 98, 9840-9844 (**1994**). https://doi.org:10.1021/j100090a018

14 Kwolek, P. & Wojnicki, M. The kinetic study of photoreduction of tetrachloroaurate acid by methanol in acidic media. *Journal of Photochemistry and Photobiology a-Chemistry* 286, 47-54 (**2014**). https://doi.org:10.1016/j.jphotochem.2014.04.018

15 Gomes, J. F. *et al.* New insights into the formation mechanism of Ag, Au and AgAu nanoparticles in aqueous alkaline media: alkoxides from alcohols, aldehydes and ketones as universal reducing agents. *Physical Chemistry Chemical Physics* 17, 21683-21693 (**2015**). https://doi.org:10.1039/c5cp02155c

16 Rodrigues, C. J. *et al.* Nucleation and growth of gold nanoparticles initiated by nanosecond and femtosecond laser irradiation of aqueous AuCl4 (-). *Physical Chemistry Chemical Physics* 20, 28465-28475 (**2018**). https://doi.org:10.1039/c8cp05774e

17 Quinson, J. *et al.* Monovalent Alkali Cations: Simple and Eco-Friendly Stabilizers for Surfactant-Free Precious Metal Nanoparticle Colloids. *ACS Sustainable Chemistry & Engineering* 7, 13680-13686 (**2019**). https://doi.org:10.1021/acssuschemeng.9b00681

18 Harada, M. & Kizaki, S. Formation Mechanism of Gold Nanoparticles Synthesized by Photoreduction in Aqueous Ethanol Solutions of Polymers Using In Situ Quick Scanning X-ray Absorption Fine Structure and Small-Angle X-ray Scattering. *Crystal Growth & Design* 16, 1200-1212 (**2016**). https://doi.org:10.1021/acs.cgd.5b01168

19 Peck, J. A., Tait, C. D., Swanson, B. I. & Brown, G. E. Speciation of aqueous gold (III) chlorides from ultraviolet visible absorption and Raman resonance Raman spectroscopies. *Geochimica Et Cosmochimica Acta* 55, 671-676 (**1991**). https://doi.org:10.1016/0016-7037(91)90332-y

20 Vinnacombe-Willson, G. A., Chiang, N. H., Weiss, P. S., Tolbert, S. H. & Scarabelli, L. Seeded-Growth Experiment Demonstrating Size- and Shape-Dependence on Gold Nanoparticle-Light Interactions. *Journal of Chemical Education* 98, 546-552 (**2021**). https://doi.org:10.1021/acs.jchemed.0c01150

21 Qiao, J. L., Liu, Y. Y., Hong, F. & Zhang, J. J. A review of catalysts for the electroreduction of carbon dioxide to produce low-carbon fuels. *Chemical Society Reviews* 43, 631-675 (**2014**). https://doi.org:10.1039/c3cs60323g

22 Siiman, O. & Hsu, W. P. Surface-enhanced Raman-scaterring (SERS) enhancements and excitation profiles for 3,5-pyridinedicarboxylate and dabsyl aspartate on colloidal gold. *Journal of the Chemical Society-Faraday Transactions I* 82, 851-867 (**1986**). https://doi.org:10.1039/f19868200851

23 Machesky, M. L., Andrade, W. O. & Rose, A. W. Interactions of gold(III) chloride and elemental gold with peat-derived humic substances. *Chemical Geology* 102, 53-71 (**1992**). https://doi.org:10.1016/0009-2541(92)90146-v

24 Durovic, M. D., Puchta, R., Bugarcic, Z. D. & van Eldik, R. Studies on the reactions of AuCl4 (-) with different nucleophiles in aqueous solution. *Dalton Transactions* 43, 8620-8632 (**2014**). https://doi.org:10.1039/c4dt00247d

25 Holade, Y., Hickey, D. P. & Minteer, S. D. Halide-regulated growth of electrocatalytic metal nanoparticles directly onto a carbon paper electrode. *Journal of Materials Chemistry A* 4, 17154-17162 (**2016**). https://doi.org:10.1039/c6ta08288b

26 Rodrigues, T. S. *et al.* Synthesis of Colloidal Metal Nanocrystals: A Comprehensive Review on the Reductants. *Chemistry-a European Journal* 24, 16944-16963 (**2018**). https://doi.org:10.1002/chem.201802194

27 Jimenez-Ruiz, A., Perez-Tejeda, P., Grueso, E., Castillo, P. M. & Prado-Gotor, R. Nonfunctionalized Gold Nanoparticles: Synthetic Routes and Synthesis Condition Dependence. *Chemistry-a European Journal* 21, 9596-9609 (**2015**). https://doi.org:10.1002/chem.201405117

28 Scarabelli, L., Sanchez-Iglesias, A., Perez-Juste, J. & Liz-Marzan, L. M. A "Tips and Tricks" Practical Guide to the Synthesis of Gold Nanorods. *Journal of Physical Chemistry Letters* 6, 4270-4279 (**2015**). https://doi.org:10.1021/acs.jpclett.5b02123

29 Schulz, F. *et al.* Little Adjustments Significantly Improve the Turkevich Synthesis of Gold Nanoparticles. *Langmuir* 30, 10779-10784 (**2014**). https://doi.org:10.1021/la503209b

30 Shi, L., Buhler, E., Boue, F. & Carn, F. How does the size of gold nanoparticles depend on citrate to gold ratio in Turkevich synthesis? Final answer to a debated question. *Journal of Colloid and Interface Science* 492, 191-198 (**2017**). https://doi.org:10.1016/j.jcis.2016.10.065

31 Wuithschick, M. *et al.* Turkevich in New Robes: Key Questions Answered for the Most Common Gold Nanoparticle Synthesis. *ACS Nano* 9, 7052-7071 (**2015**). https://doi.org:10.1021/acsnano.5b01579

32 El Amri, N. & Roger, K. Polyvinylpyrrolidone (PVP) impurities drastically impact the outcome of nanoparticle syntheses. *Journal of Colloid and Interface Science* 576, 435-443 (**2020**). https://doi.org:10.1016/j.jcis.2020.04.113

33 Quinson, J., Simonsen, S. B., Theil Kuhn, L. & Arenz, M. Commercial spirits for surfactant-free syntheses of electro-active platinum nanoparticles. *Sustainable Chemistry 2*, 1-7 (**2021**). https://doi.org:10.3390/suschem2010001

34 Olveira, S., Forster, S. P. & Seeger, S. Nanocatalysis: Academic Discipline and Industrial Realities. *Journal of Nanotechnology* (**2014**). https://doi.org/10.1155/2014/324089

35 A matter of scale. *Nature Nanotechnology* 11, 733-733 (**2016**). https://doi.org:10.1038/nnano.2016.180

36 Ishida, T., Murayama, T., Taketoshi, A. & Haruta, M. Importance of Size and Contact Structure of Gold Nanoparticles for the Genesis of Unique Catalytic Processes. *Chemical Reviews* 120, 464-525 (**2020**). https://doi.org:10.1021/acs.chemrev.9b00551

37 Huang, H. *et al.* Continuous flow synthesis of ultrasmall gold nanoparticles in a microreactor using trisodium citrate and their SERS performance. *Chemical Engineering Science* 189, 422-430 (**2018**). https://doi.org:10.1016/j.ces.2018.06.050

38 Zhao, L. L. *et al.* Tuning the size of gold nanoparticles in the citrate reduction by chloride ions. *Nanoscale* 4, 5071-5076 (**2012**). https://doi.org:10.1039/c2nr30957b

39 Quinson, J. *et al.* Investigating Particle Size Effects in Catalysis by Applying a Size-Controlled and Surfactant-Free Synthesis of Colloidal Nanoparticles in Alkaline Ethylene Glycol: Case Study of the Oxygen Reduction Reaction on Pt. *ACS Catalysis* 8, 6627-6635 (**2018**). https://doi.org:10.1021/acscatal.8b00694

40 Schmidt, J., Marques, M. R. G., Botti, S. & Marques, M. A. L. Recent advances and applications of machine learning in solid-state materials science. *Npj Computational Materials* 5 (**2019**). https://doi.org:10.1038/s41524-019-0221-0

41 Huber, N., Kalidindi, S. R., Klusemann, B. & Cyron, C. J. Editorial: Machine Learning and Data Mining in Materials Science. *Frontiers in Materials* 7 (**2020**). https://doi.org:10.3389/fmats.2020.00051

42 Kalinin, S. V., Sumpter, B. G. & Archibald, R. K. Big-deep-smart data in imaging for guiding materials design. *Nature Materials* 14, 973-980 (**2015**). https://doi.org:10.1038/nmat4395

43 Quinson, J. Surfactant-free precious metal colloidal nanoparticles for catalysis. *Frontiers in Nanotechnology* 3 (**2021**). https://doi.org/10.3389/fnano.2021.770281

44 Merk, V. *et al.* In Situ Non-DLVO Stabilization of Surfactant-Free, Plasmonic Gold Nanoparticles: Effect of Hofmeister's Anions. *Langmuir* 30, 4213-4222 (**2014**). https://doi.org:10.1021/la404556a

45 Perini, N. & Ticianelli, E. A. Oxygen evolution on gold: The effects of alkali-metal cations and iron impurities from alkaline electrolytes. *Journal of Catalysis* 378, 277-282 (**2019**). https://doi.org:10.1016/j.jcat.2019.09.003

46 Ureta-Zanartu, M. S. *et al.* Importance of the electrolyte cation on the non-covalent interactions in the electrooxidation of 1-heptanol on gold in 0.1 M alkali metal hydroxides. *Materials Chemistry and Physics* 246 (**2020**). https://doi.org:10.1016/j.matchemphys.2020.122828

47 Hersbach, T. J. P. *et al.* Alkali Metal Cation Effects in Structuring Pt, Rh, and Au Surfaces through Cathodic Corrosion. *ACS Applied Materials & Interfaces* 10, 39363-39379 (**2018**). https://doi.org:10.1021/acsami.8b13883

48 Strmcnik, D. *et al.* The role of non-covalent interactions in electrocatalytic fuel-cell reactions on platinum. *Nature Chemistry* 1, 466-472 (**2009**). https://doi.org:10.1038/nchem.330

49 Mathiesen, J. K. *et al.* Insights from In Situ Studies on the Early Stages of Platinum Nanoparticle Formation. *Journal of Physical Chemistry Letters* 12, 3224-3231 (**2021**). https://doi.org:10.1021/acs.jpclett.1c00241

50 Grys, D. B. *et al.* Citrate Coordination and Bridging of Gold Nanoparticles: The Role of Gold Adatoms in AuNP Aging. *ACS Nano* 14, 8689-8696 (**2020**). https://doi.org:10.1021/acsnano.0c03050

51 Closson, Andrew B.,Citrate's Counter Ions and pH Effect on Gold Nanoparticle Growth Kinetics (**2016**).Honors College. 374. https://digitalcommons.library.umaine.edu/honors/374

52 Lu, L. F., Zou, S. H. & Fang, B. Z. The Critical Impacts of Ligands on Heterogeneous Nanocatalysis: A Review. *ACS Catalysis* 11, 6020-6058 (**2021**). https://doi.org:10.1021/acscatal.1c00903

53 Quinson, J., Kunz, S. & Arenz, M. Beyond Active Site Design: A Surfactant-Free Toolbox Approach for Optimized Supported Nanoparticle Catalysts. *ChemCatChem* 13, 1692-1705 (**2021**). https://doi.org:10.1002/cctc.202001858

54 Cargnello, M. *et al.* Efficient Removal of Organic Ligands from Supported Nanocrystals by Fast Thermal Annealing Enables Catalytic Studies on Well-Defined Active Phases. *Journal of the American Chemical Society* 137, 6906-6911 (**2015**). https://doi.org:10.1021/jacs.5b03333

55 Li, D. G. *et al.* Surfactant Removal for Colloidal Nanoparticles from Solution Synthesis: The Effect on Catalytic Performance. *ACS Catalysis* 2, 1358-1362 (**2012**). https://doi.org:10.1021/cs300219j

56 Tremiliosi-Filho, G. *et al.* Electro-oxidation of ethanol on gold: analysis of the reaction products and mechanism. *Journal of Electroanalytical Chemistry* 444, 31-39 (**1998**). https://doi.org:10.1016/s0022-0728(97)00536-6

57 Bai, J., Liu, D. Y., Yang, J. & Chen, Y. Nanocatalysts for Electrocatalytic Oxidation of Ethanol. *Chemsuschem* 12, 2117-2132 (**2019**). https://doi.org:10.1002/cssc.201803063

58 Inaba, M., Quinson, J. & Arenz, M. pH matters: The influence of the catalyst ink on the oxygen reduction activity determined in thin film rotating disk electrode measurements. *Journal of Power Sources* 353, 19-27 (**2017**). https://doi.org:10.1016/j.jpowsour.2017.03.140

59 Arminio-Ravelo, J. A. *et al.* Synthesis of Iridium Nanocatalysts for Water Oxidation in Acid: Effect of the Surfactant. *ChemCatChem* 12, 1282-1287 (**2020**). https://doi.org:10.1002/cctc.201902190

60 Ji, X. *et al.* Size control of gold nanocrystals in citrate reduction: The third role of citrate. *Journal of the American Chemical Society* 129, 13939-13948 (**2007**). https://doi.org:10.1021/ja074447k

61 Zaleska-Medynska, A., Marchelek, M., Diak, M. & Grabowska, E. Noble metal-based bimetallic nanoparticles: the effect of the structure on the optical, catalytic and photocatalytic properties. *Advances in Colloid and Interface Science* 229, 80-107 (**2016**). https://doi.org:10.1016/j.cis.2015.12.008

62 Lu, P. Y. *et al.* Gold-based nanoalloys: synthetic methods and catalytic applications. *Journal of Materials Chemistry A* 9, 19025-19053 (**2021**). https://doi.org:10.1039/d1ta03646g

63 Nasrollahzadeh, M., Sajjadi, M., Dadashi, J. & Ghafuri, H. Pd-based nanoparticles: Plant-assisted biosynthesis, characterization, mechanism, stability, catalytic and antimicrobial activities. *Advances in Colloid and Interface Science* 276 (**2020**). https://doi.org:10.1016/j.cis.2020.102103

64 Qazi, F., Hussain, Z. & Tahir, M. N. Advances in biogenic synthesis of palladium nanoparticles. *RSC Advances* 6, 60277-60286 (**2016**). https://doi.org:10.1039/c6ra11695g

65 Favier, I., Pla, D. & Gomez, M. Palladium Nanoparticles in Polyols: Synthesis, Catalytic Couplings, and Hydrogenations. *Chemical Reviews* 120, 1146-1183 (**2020**). https://doi.org:10.1021/acs.chemrev.9b00204

66 Luo, S. H. *et al.* Perspectives on palladium-based nanomaterials: green synthesis, ecotoxicity, and risk assessment. *Environmental Science-Nano* 8, 20-36 (**2021**). https://doi.org:10.1039/d0en01048k

67 Chen, A. & Ostrom, C. Palladium-Based Nanomaterials: Synthesis and Electrochemical Applications. *Chemical Reviews* 115, 11999-12044 (**2015**). https://doi.org:10.1021/acs.chemrev.5b00324

68 Lin, H. H. *et al.* PdAu Alloy Nanoparticles for Ethanol Oxidation in Alkaline Conditions: Enhanced Activity and C1 Pathway Selectivity. *ACS Applied Energy Materials* 2, 8701-8706 (**2019**). https://doi.org:10.1021/acsaem.9b01674

69 Xu, J. B., Zhao, T. S., Shen, S. Y. & Li, Y. S. Stabilization of the palladium electrocatalyst with alloyed gold for ethanol oxidation. *International Journal of Hydrogen Energy* 35, 6490-6500 (**2010**). https://doi.org:10.1016/j.ijhydene.2010.04.016

70 Zhan, G. W. *et al.* Green synthesis of Au-Pd bimetallic nanoparticles: Single-step bioreduction method with plant extract. *Materials Letters* 65, 2989-2991 (**2011**). https://doi.org:10.1016/j.matlet.2011.06.079

71 Lerch, S. *et al.* Robust Colloidal Synthesis of Palladium-Gold Alloy Nanoparticles for Hydrogen Sensing. *ACS Applied Materials & Interfaces* 13, 45758-45767 (**2021**). https://doi.org:10.1021/acsami.1c15315

72 Moulder, J. F. S., William F. Sobol, Peter E. Bombe, Kennetlf D. *Handbook of X-ray Photoelectron Spectroscopy*. (Perkin-Elmer Corporation, **1995**).

73 Ruban, A. V., Skriver, H. L. & Norskov, J. K. Surface segregation energies in transition-metal alloys. *Physical Review B* 59, 15990-16000 (**1999**). https://doi.org:10.1103/PhysRevB.59.15990

74 Farrow, C. L. *et al.* PDFfit2 and PDFgui: computer programs for studying nanostructure in crystals. *Journal of Physics-Condensed Matter* 19 (**2007**). https://doi.org:10.1088/0953-8984/19/33/335219

75 Rodriguezcarvajal, J. Recent advances in magnetic-structure determination by neutron powder diffraction. *Physica B* 192, 55-69 (**1993**). https://doi.org:10.1016/0921-4526(93)90108-i

76 Du, J. *et al.* Bifunctional Pt-IrO_2 Catalysts for the Oxygen Evolution and Oxygen Reduction Reactions: Alloy Nanoparticles versus Nanocomposite Catalysts. *ACS Catalysis* 11, 820-828 (**2021**). https://doi.org:10.1021/acscatal.0c03867

77 Du, J., Quinson, J., Zana, A. & Arenz, M. Elucidating Pt-Based Nanocomposite Catalysts for the Oxygen Reduction Reaction in Rotating Disk Electrode and Gas Diffusion Electrode Measurements. *ACS Catalysis* 11, 7584-7594 (**2021**). https://doi.org:10.1021/acscatal.1c01496

78 Huang, X. Y. *et al.* Au-Pd separation enhances bimetallic catalysis of alcohol oxidation. *Nature* 603, 271–275 (**2022**) https://doi.org:10.1038/s41586-022-04397-7

79 Inaba, M. *et al.* The Oxygen Reduction Reaction on Pt: Why Particle Size and Interparticle Distance Matter. *ACS Catalysis* 11, 7144-7153 (**2021**). https://doi.org:10.1021/acscatal.1c00652

80 Nesselberger, M. *et al.* The effect of particle proximity on the oxygen reduction rate of size-selected platinum clusters. *Nature Materials* 12, 919-924 (**2013**). https://doi.org:10.1038/nmat3712

81 Helveg, S. An industrial perspective of the impact of Haldor Topsoe on (in situ) electron microscopy in catalysis. *Journal of Catalysis* 328, 102-110 (**2015**). https://doi.org:10.1016/j.jcat.2014.12.017

82 Zhang, A. *et al.* Enhanced Electrocatalytic Activities toward the Ethanol Oxidation of Nanoporous Gold Prepared via Solid-Phase Reaction. *ACS Applied Energy Materials* 3, 336-343 (**2020**). https://doi.org:10.1021/acsaem.9b01588

83 Batchelor, T. A. A. *et al.* High-Entropy Alloys as a Discovery Platform for Electrocatalysis. *Joule* 3, 1-12 (**2019**). https://doi.org/10.1016/j.joule.2018.12.015

84 Chen, D., Li, J. Q., Cui, P. L., Liu, H. & Yang, J. Gold-catalyzed formation of core-shell gold-palladium nanoparticles with palladium shells up to three atomic layers. *Journal of Materials Chemistry A* 4, 3813-3821 (**2016**). https://doi.org:10.1039/c5ta10303g